FACULTY OF ENGINEERING AND ARCHITECTURE

Wireless health monitoring for different horse breeds

Jirka Verleysen
Student number: 01704628

Supervisors: Prof. dr. ir. Margot Deruyck, Prof. dr. ir. Wout Joseph

Master's dissertation submitted in order to obtain the academic degree of
Master of Science in de industriële wetenschappen: elektronica-ICT

Academic year 2022-2023

GHENT UNIVERSITY

FACULTY OF ENGINEERING AND ARCHITECTURE

Wireless health monitoring for different horse breeds

Jirka Verleysen
Student number: 01704628

Supervisors: Prof. dr. ir. Margot Deruyck, Prof. dr. ir. Wout Joseph

Master's dissertation submitted in order to obtain the academic degree of
Master of Science in de industriële wetenschappen: elektronica-ICT

Academic year 2022-2023

GHENT UNIVERSITY

Acknowledgment

This dissertation is written to obtain a degree in Master of Science in Electronics and ICT Engineering Technology (Electronics Engineering). I would like to express sincere gratitude to Prof. Dr. Ir. Margot Deruyck, Prof. Dr. Ir. Wout Joseph, and Prof. Dr. Ir. Günter Vermeeren for providing the opportunity to undertake the master's thesis on this subject.

I would like to extend my special thanks to Ir. Jasper Goethals for his dedicated guidance and support throughout the duration of this thesis. His expertise and assistance in both theoretical aspects and simulations have been invaluable.

Finally, I want to thank my parents and friends for their unwavering support throughout this journey. Providing the necessary sounding board that allowed me to gain valuable perspectives and approach challenges from different angles. Their constant encouragement and motivation have been instrumental in my progress and success.

Notes on the master's thesis and oral presentation

This master’s dissertation is part of an exam. Any comments formulated by the assessment committee during the oral presentation of the master’s dissertation are not included in this text.

Abstract English

This dissertation focuses on conducting research on body-mounted Wireless Body Area Networks (WBANs) within the context of different horse breeds. The objective is to study the path loss experienced by antennas placed on various horse breeds and develop a path loss model that encompasses multiple breeds.
The initial part of this dissertation involves a comprehensive literature review, which forms the foundation of the research. Based on this review, a patch antenna with dimensions of 70mm by 70mm and a frequency of 2.4GHz is selected. Three horse models are chosen for simulation: Selveryne, Falabella, and Shetland. While Falabella and Shetland are real horse breeds, Selveryne is a fictional breed specifically created for faster simulations. The antenna locations are carefully selected at specific points on the horse, the poll, wither, sacrum, left front leg, left hind leg, right front leg, and right hind leg. These locations are chosen based on existing systems and practical considerations. The distance between these antennas is utilized to predict the path loss model for both line of sight (LOS) and non-line of sight (NLOS) scenarios.
The simulations are thoroughly discussed, including an examination of the limitations associated with using the Finite-Difference Time-Domain (FDTD) approach for simulation in sim4life. A path loss model is presented for all the chosen points, NLOS and LOS scenarios. Additionally, the model is analysed with an embedded and de-embedded approach, accounting for or disregarding the antenna's gain, respectively.
Future directions are outlined to further test and enhance the path loss model, aiming to refine its accuracy and effectiveness.

Abstract Dutch

Deze thesis richt zich op het uitvoeren van onderzoek naar op het lichaam aangebrachte Wireless Body Area Networks (WBAN's) binnen de context van verschillende paardenrassen. Het doel is het padverlies te bestuderen dat wordt ervaren door antennes geplaatst op verschillende paardenrassen en een padverliesmodel te ontwikkelen dat meerdere rassen omvat. Het eerste deel van dit proefschrift omvat een uitgebreide literatuurstudie, die de basis vormt van het onderzoek. Op basis van dit overzicht wordt een patch antenne geselecteerd met afmetingen van 70mm bij 70mm en een frequentie van 2.4GHz. Voor de simulatie worden drie paardenmodellen gekozen: Selveryne, Falabella en Shetland. Terwijl Falabella en Shetland echte paardenrassen zijn, is Selveryne een fictief ras dat speciaal is gecreëerd voor snellere simulaties. De antennelocaties zijn zorgvuldig gekozen op specifieke punten van het paard, namelijk de poll, de schoft, het sacrum, de linker voorpoot, de linker achterpoot, de rechter voorpoot en de rechter achterpoot. Deze locaties zijn gekozen op basis van bestaande systemen en praktische overwegingen. De afstand tussen deze antennes wordt gebruikt om het padverliesmodel te voorspellen voor zowel line of sight (LOS) als not line of sight (NLOS). De simulaties worden grondig besproken, inclusief een bespreking omrent de beperkingen van het gebruik van de Finite-Difference Time-Domain (FDTD) benadering voor simulatie in sim4life. Er wordt een padverliesmodel gepresenteerd voor alle gekozen punten, NLOS- en LOS-scenario's. Bovendien wordt het model geanalyseerd met een ingebedde en niet-ingebedde benadering, waarbij de versterking van de antenne al dan niet in rekening wordt gebracht. Er worden toekomstige mogelijkheden geschetst om het padverliesmodel verder te testen en te verbeteren, met als doel de nauwkeurigheid en doeltreffendheid ervan te verfijnen.

Wireless health monitoring for different horse breeds

Jirka Verleysen
Supervisor(s): Prof. Dr. Ir. Margot Deruyck, Prof. Dr. Ir. Wout Joseph, Ir. Jasper Goethals, Prof. Dr. Ir. Günter Vermeeren

Abstract - The interest in wireless body area networks (WBANs) have grown significantly. WBANs consist of miniaturized sensors designed to collect and transmit data wirelessly, enabling remote monitoring of human and animal health. This paper begins by discussing the selection of antennas and their placement locations. Subsequently, it focuses on analysing the path loss of a Wireless Body Area Network (WBAN) system designed for monitoring the health of horses. The main objective is to develop a robust path loss model capable of predicting path loss for different horse breeds. To achieve this, three horse breeds, namely Selveryne (created for simulation purposes), Falabella, and Shetland, are chosen as the basis for collecting measurement data. In the simulation, seven locations for antennas were chosen on each horse, and Finite-Difference Time-Domain (FDTD) method was employed using sim4life. Three main models were made for line-of-sight (LOS), non-line-of-sight (NLOS) and all points, as well as the presence or absence of antenna gain, in both embedded and de-embedded scenarios. The resulting path loss models exhibit a path loss exponent ranging from 1.90 to 4.30, depending on the specific scenario. These values can be compared to the path loss exponent ranges typically observed in different environments, such as free space (2) and urban (2.7-3.5) or suburban (3-5) areas when using conventional antennas. This demonstrates that communication is possible in the WBAN system, albeit with some added difficulty.

Index terms: WBAN, FDTD, sim4life, horse, path loss, de-embedded path loss, embedded path loss.

1 Introduction

WBAN networks enable continuous wireless monitoring capabilities, both externally and internally on the body, for extended periods [1]. These networks support several types of traffic, such as real-time monitoring, on-demand services, and emergency communications [2]. However, a major challenge associated with WBANs is power consumption, especially for sensors implanted inside the body, where regular battery replacements are impractical. Path loss, which refers to the loss of signal strength during data transmission due to signal attenuation, significantly contributes to sensor power consumption. Signal attenuation can occur due to numerous factors, including energy absorption, reflection, diffraction, body shadowing, body posture, and multipath effects. Among these factors, body posture and body shadowing are the main concerns when using WBANs [3]– [5]. However, the current simulation does not consider multipath effects. Several types of path loss models exist, including purely theoretical or empirical models, or a combination of both[5]–[7]. Path loss can be calculated separately for each connection, or an averaged path loss can be used, considering all connections[8], [9]. It is important to distinguish between the embedded and de-embedded path loss models. The embedded path loss model includes the gains of the antennas used, which can be effective but not universally applicable as it depends on the specific antenna[7]. Most path loss models are based on the Friis formula, which calculates the received power of an antenna[8]. The path loss exponent is a parameter that allows the formula to adapt easily to the environment. While originally developed to differentiate between free space and (sub)urban areas, it can also account for the influence of the body on path loss[6], [8], [10]. Developing an accurate path loss model can enhance the efficiency of WBAN networks.

In this research, the path loss model used for WBANs is described in paper [7]. This model is chosen because it is based on simulations and measurements conducted on a cow, which shares a similar body structure with a horse. It provides both embedded and de-embedded solutions based on the Friis formula, simulations, and measurements. The objective of this research is to create a path loss model capable of accurately predicting path loss for different horse breeds, considering their unique anatomical structures and varying distances between antennas.

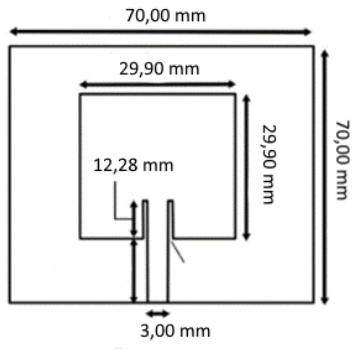

Figure 1 Dimensions patch antenna[11]

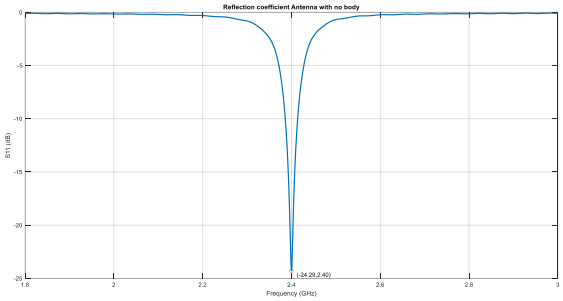

Figure 2 Reflection coefficient without body present

2 Methods

2.1 Choice antenna

The selection of an appropriate antenna is crucial in WBAN applications. As the network needs to be worn, it is important to ensure that the system remains compact and unobtrusive. This applies not only to the sensor but also to the accompanying antenna. Opting for a smaller antenna enhances comfort for the wearer. It is also important to consider the impact of antenna radiation on the body, as excessive exposure should be avoided [12]– [14].

In addition to the antenna's impact on the body, the body itself affects the antenna's performance, leading to variations in input impedance, radiation pattern distortion, frequency shifts, and reduced efficiency [15]. To mitigate these effects, a patch antenna with a ground plane, as presented in paper [11] , is chosen. It has a ground plane which serves as a barrier between the body and the antenna, providing protection to both sides. Figure 1 illustrates the dimensions of the selected antenna.

To ensure the antenna's suitability for the application, simulations are conducted without the presence of a body. The results, depicted in Figure 2 and Figure 3 , demonstrate a

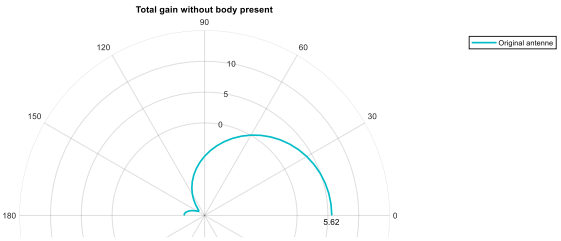

Figure 3 Gain without body present.

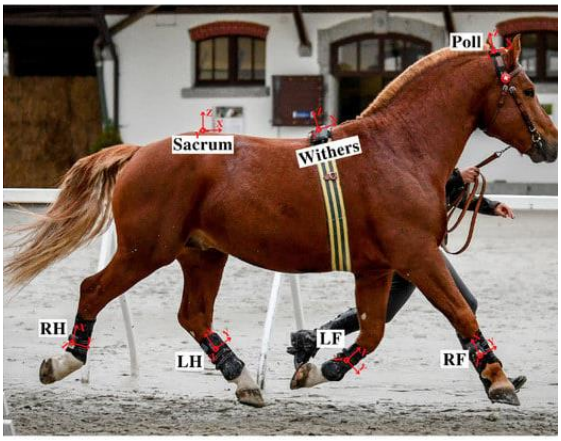

Figure 4 Locations sensor on horse [16]

frequency of 2.4 GHz, an S11 value of -24.29 dB, and a maximum gain of 5.62 dB, which are favourable characteristics for this particular application.

2.2 Antenna locations

The selection of antenna locations is based on practical considerations, focusing on areas that facilitate the measurement of parameters such as heart rate and movement in horses. These locations are determined by considering existing systems available in the market as well as those used in research[16]– [23] . The locations chosen are shown in Figure 4

2.3 Choice horse breeds

Initially, three horse breeds were selected for the study: Shire, Quarter, and Falabella, with Shire being the largest and Falabella being the smallest breed [24]– [27] . The respective heights of these breeds are presented in Table 1. The intention behind this selection was to encompass the complete range of horse sizes to improve the accuracy of the model.

Table 1 Height of the horses [28]– [31]

	Shire horse	Quarter horse	Falabella
Height at the withers (cm)	160-205	145-165	63-86

Table 2 Simulation times larger breeds

Breed	Simulation time per antenna (hours)	Simulation time whole horse
Quarter	16	112 hours (4.6 days)
Shire	20	140 hours (5.83 days)

However, it soon became apparent that simulating the Quarter and Shire horses was impractical due to their large size, as indicated by the simulation times provided in Table 2.
To address this limitation, alternative horse breeds were chosen: Selveryne, Falabella, and Shetland. While Falabella and Shetland are actual horse breeds, Selveryne was created as a fictional breed with a smaller size to expedite the simulations. The heights of these selected models are displayed in Table 3 , and their relative proportions can be observed in Figure 5. The placement of squares on the model ensures optimal antenna positioning for maximum tissue connection.

2.4 Choice path loss model

For the path loss model, a model done in previous work [7] is selected. The rationale behind this choice is that the model was developed based on simulations and measurements conducted on cows, making it more relevant to a horse model than a human-based model. The paper distinguishes between path loss with antenna properties included (2.1) and path loss with antenna properties excluded (2.2) which are embedded and de-embedded models respectively.

$$PL_{embedded} = P_{TX} - P_{RX} \quad (2.1)$$

$$PL = P_{TX} + G_{TXb} + G_{RXb} - P_{RX} \quad (2.2)$$

Table 3 Height horses [29], [30], [32]

	Shetland horse	Falabella	Selveryne
Height at the withers (cm)	71-107	63-86	52.2

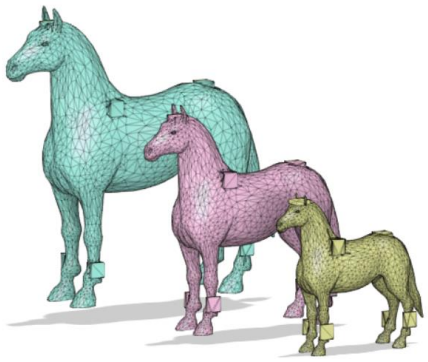

Figure 5 Breeds comparison.

In the model, $PL_{embedded}$ represents the path loss with antenna gains embedded, expressed in dB. PL is the de-embedded path loss in dB. P_{TX} and P_{RX} denote the transmitted and received power, respectively, expressed in dBm. G_{TXb} and G_{RXb} represent the gain from the transmitting and receiving antenna when placed on the body, expressed in dB.
The path loss can be modelled using a reference distance of 10 cm.

$$PL(d) = PL(d_0) + 10n \log\left(\frac{d}{d_0}\right) + X_\sigma \quad (2.3)$$

Where PL represents the path loss in dB, while $PL(d_0)$ represents the path loss between two antennas on the body at the reference distance, also expressed in dB. d represents the distance between the receiver (RX) and the transmitter (TX), expressed in meters. n represents the path loss exponent, and d_0 is the reference distance in meters. X_σ, correspond to a zero-mean Gaussian distribution with a standard deviation σ, both expressed in dB.
By utilizing the simulated data, it is possible to calculate the received power. The transmitted power remains constant at 30 dBm for all scenarios. A fitting process is performed using the least squared error method, which enables the calculation of the standard deviation between the fit and the data points. Based on this information, a suitable path loss exponent can be determined by sweeping through different values of the path loss exponent and selecting the value that best aligns with the fit.

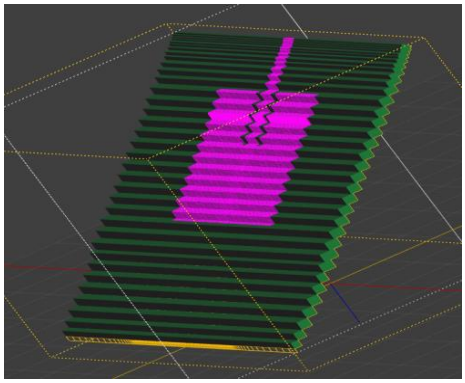

Figure 6 Voxels antenna at 33°

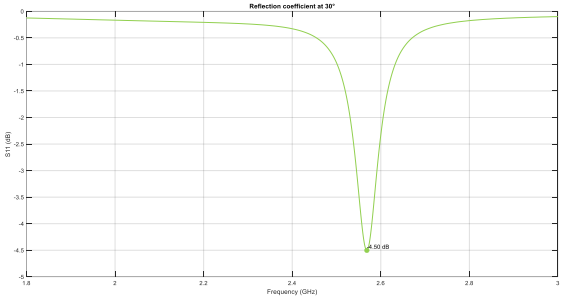

Figure 7 Reflection coefficient at 33°

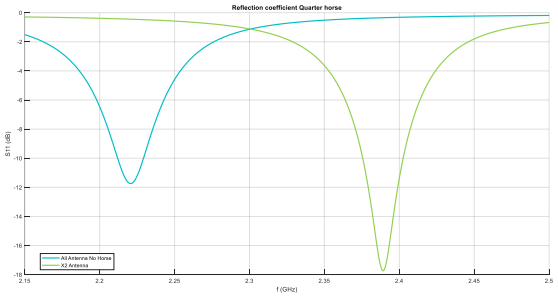

Figure 8 Reflection coefficient Quarter horse with grid problems

2.5 Simulations

Certain choices were made for the simulations to ensure smooth execution. The chosen model was originally designed as a 3D-printed model, containing intricate details that, while not significantly affecting the results, consumed considerable simulation time. To address this, the number of triangles in the model was reduced, resulting in a file size of 2.029 kB instead of the original 392.339 kB.

The angle of the antenna was not arbitrarily chosen but set at multiples of 90°. Although this approach sacrifices some realism, it is necessary to avoid the "staircase problem" that arises when simulating with FDTD. Figure 6 illustrates this issue. If not addressed, this problem would lead to voxelization errors, affecting the accuracy of the antenna's results, as evident from the shift in the S11 value depicted in Figure 7.

Furthermore, when using simulation software, it is crucial to ensure that the grid aligns perfectly. with the patch to avoid any slight misalignment that could alter the antenna's dimensions and consequently, impact its reflection coefficient. This discrepancy is highlighted in Figure 8.

Table 4 Results standard deviation, pathloss exponent and the reference path loss

		σ	n	PL(d_0) (dB)
All points	Embedded	3.63	3.60	28.19
	De-embedded	3.62	3.90	38.56
NLOS	Embedded	3.63	3.00	28.19
	De-embedded	3.62	4.30	38.56
LOS	Embedded	3.81	1.90	28.19
	De-embedded	3.87	3.20	38.26

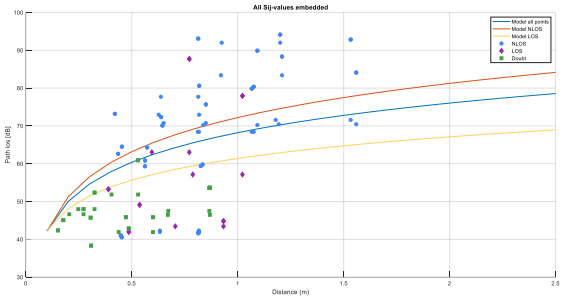

Figure 9 Prediction path loss embedded.

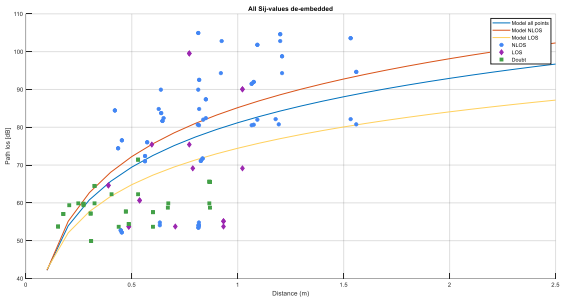

Figure 10 Prediction path loss de-embedded

3 Results

The path loss model is calculated for three scenarios, considering both embedded and de-embedded path loss. These scenarios include all points, only non-line-of-sight (NLOS) points, and

Table 5 Path loss exponent in different environments [33]

Environment	Path loss exponent
Free space	2
Urban area	2.7 – 3.5
Suburban area	3 – 5
Indoor line-of-sight	1.6 – 1.8
Obstructed in building	4-6
Obstructed in factories	2-3

only line-of-sight (LOS) points. The "doubt" points, which do not clearly fall into either LOS or NLOS category, are disregarded in the last two scenarios. The results are presented in Figure 9 and Figure 10. Table 4 displays the path loss exponent, standard deviation, and reference pathloss for each scenario. When comparing these values to the path loss exponent for non-body-worn antennas (Table 5), it can be concluded that the obtained values are reasonable. The LOS scenario consistently exhibits a better path loss exponent compared to the NLOS scenario, with one scenario even surpassing free space conditions. However, the path loss exponent for LOS is still higher than the typical range of 1.6-1.8 observed in normal LOS scenarios.

Various path loss models are determined based on specific situations and connection scenarios. These models align with the findings presented in the referenced paper [7]. The additional de-embedded model facilitates easy comparison irrespective of the antenna used, simplifying system implementation when different antenna types are chosen. The calculated path loss exponent aligns with a best-case scenario resembling free space and a worst-case scenario simulating obstructions within buildings. The average case represents a (sub)urban area. These results are realistic and achievable. The model enables path loss prediction on larger scales without the need for time-consuming simulations. For instance, when considering a Shire horse with a wither height of 2 meters, the de-embedded model predicts a loss of approximately 100 dB, while the embedded model predicts a loss of around 80 dB. This emphasizes the significance of antenna selection in mitigating path loss.

4 Conclusions

In this paper, various path loss models are proposed for WBAN architecture on different horse breeds. The research begins by selecting suitable antennas and antenna locations, considering practical applications such as heart rate and movement monitoring. Simulations are conducted using the FDTD algorithm and then fitted to an existing path loss model. This approach aids in predicting path loss for horse breeds that have not been previously simulated.

5 Further work

Future research could validate the model by measuring it on actual horses. Starting with tests on Falabella or Shetland horses, then moving to larger breeds like Quarters or Shires. Practical challenges may arise due to the antenna size, especially on smaller breeds. The width of the antenna exceeds the legs of small horses, leaving a portion unsupported. This may have a slight practical influence, despite the theoretical separation by the ground plane. Before practical measurements can be done a wireless technology needs to be selected. This along with the antenna can help further mitigate path loss. By comparing measurements to simulations, the model can be refined for implementation across various horse breeds.

A next step would then be to incorporating movement changes into the model. This namely causes doppler effect and shifts in the power needed to send data [34],[35].

6 Acknowledgments

The author expresses sincere gratitude to Prof. Dr. Ir. Margot Deruyck, Prof. Dr. Ir. Wout Joseph, and Prof. Dr. Ir. Günter Vermeeren for providing the opportunity to undertake the master's thesis on this subject. Special thanks are extended to Ir. Jasper Goethals for the dedicated guidance and support throughout the duration of this thesis.

7 References

[1] R. Cavallari, F. Martelli, R. Rosini, C. Buratti, and R. Verdone, “A survey on wireless body area networks: Technologies and design challenges,” *IEEE*

Communications Surveys and Tutorials, vol. 16, no. 3, pp. 1635–1657, 2012, doi: 10.1109/SURV.2014.012214.00007.

[2] Md. T. Arefin, M. H. Ali, A. K. M. F. Haque, Md. T. Arefin, M. H. Ali, and A. K. M. F. Haque, "Wireless Body Area Network: An Overview and Various Applications," *Journal of Computer and Communications*, vol. 5, no. 7, pp. 53–64, May 2017, doi: 10.4236/JCC.2017.57006.

[3] S. L. Cotton, A. Mckernan, A. J. Ali, and W. G. Scanlon, "An Experimental Study on the Impact of Human Body Shadowing in Off-Body Communications Channels at 2.45 GHz," *Proceedings of the 5th European Conference on Antennas and Propagation (EUCAP)*, 2011.

[4] Ł. Januszkiewicz, "Analysis of Human Body Shadowing Effect on Wireless Sensor Networks Operating in the 2.4 GHz Band," *Sensors 2018, Vol. 18, Page 3412*, vol. 18, no. 10, p. 3412, Oct. 2018, doi: 10.3390/S18103412.

[5] S. Kaur and J. Malhotra, "Survey on Empirical Channel Models for WBAN," *International Journal of Future Generation Communication and Networking*, vol. 8, no. 2, pp. 399–410, 2015, doi: 10.14257/ijfgcn.2015.8.2.34.

[6] L. Roelens and L. Martens, "Path loss model for wireless narrowband communication near biological tissue," *6th UGent-FirW Doctoraatssymposium, Interactive poster session, paper nr. 120 (proceedings available on CD-Rom)*, 2005, doi: 1854/4782.

[7] S. Benaissa *et al.*, "Internet of animals: On- and off-body propagation analysis for energy efficient WBAN design for dairy cows," *2017 11th European Conference on Antennas and Propagation, EUCAP 2017*, pp. 298–302, May 2017, doi: 10.23919/EUCAP.2017.7928112.

[8] M. M. Khan, Q. H. Abbasi, A. Alomainy, and C. Parini, "Experimental Investigation of Subject-Specific On-Body Radio Propagation Channels for Body-Centric Wireless Communications," *Electronics 2014, Vol. 3, Pages 26-42*, vol. 3, no. 1, pp. 26–42, Jan. 2014, doi: 10.3390/ELECTRONICS3010026.

[9] E. Reusens, W. Joseph, G. Vermeeren, and L. Martens, "On-body measurements and characterization of wireless communication channel for arm and torso of human," *IFMBE Proc*, vol. 13, pp. 264–269, 2007, doi: 10.1007/978-3-540-70994-7_44.

[10] T. Kumpuniemi, T. Tuovinen, M. Hämäläinen, K. Yekeh Yazdandoost, R. Vuohtoniemi, and J. Iinatti, "Measurement-Based On-Body Path Loss Modelling for UWB WBAN Communications".

[11] "FR4 Dielectric Constant and Material Properties." https://resources.altium.com/p/fr4 (accessed Mar. 28, 2023).

[12] "Cell Phones and Cancer Risk Fact Sheet - NCI." https://www.cancer.gov/about-cancer/causes-prevention/risk/radiation/cell-phones-fact-sheet (accessed May 23, 2023).

[13] M. I. Hossain, M. R. I. Faruque, and M. T. Islam, "Analysis on the effect of the distances and inclination angles between human head and mobile phone on SAR," *Prog Biophys Mol Biol*, vol. 119, no. 2, pp. 103–110, Nov. 2015, doi: 10.1016/J.PBIOMOLBIO.2015.03.008.

[14] V. G. Khurana, C. Teo, M. Kundi, L. Hardell, and M. Carlberg, "Cell phones and brain tumors: a review including the long-term epidemiologic data," *Surg Neurol*, vol. 72, no. 3, pp. 205–214, Sep. 2009, doi: 10.1016/J.SURNEU.2009.01.019.

[15] "Wearable Antennas – Applications, Technologies, and their Impact on Human Body - Mistral Solutions." https://www.mistralsolutions.com/blog/wearable-antennas-applications-technologies-impact-human-body/ (accessed Mar. 09, 2023).

[16] H. Darbandi *et al.*, "Using different combinations of body-mounted IMU sensors to estimate speed of horses-A machine learning approach," *Sensors (Switzerland)*, vol. 21, no. 3, pp. 1–12, Feb. 2021, doi: 10.3390/S21030798.

[17] "How it works - EquiMoves." https://equimoves.nl/system-overview/how-it-works/ (accessed Mar. 28, 2023).

[18] C. J. Thompson, L. M. Luck, J. Keshwani, S. K. Pitla, and L. K. Karr, "Location on the Body of a Wearable Accelerometer Affects Accuracy of Data for Identifying Equine Gaits," *J Equine Vet Sci*, vol. 63, pp.

1–7, Apr. 2018, doi: 10.1016/J.JEVS.2017.12.002.

[19] A. Eerdekens *et al.*, "A framework for energy-efficient equine activity recognition with leg accelerometers," *Comput Electron Agric*, vol. 183, p. 106020, Apr. 2021, doi: 10.1016/J.COMPAG.2021.106020.

[20] C. Hartmann, L. Lidauer, J. Aurich, C. Aurich, and C. Nagel, "Detection of the time of foaling by accelerometer technique in horses (Equus caballus)—a pilot study," *Reproduction in Domestic Animals*, vol. 53, no. 6, pp. 1279–1286, Dec. 2018, doi: 10.1111/RDA.13250.

[21] S. Bosch *et al.*, "EquiMoves: A Wireless Networked Inertial Measurement System for Objective Examination of Horse Gait," 2018, doi: 10.3390/s18030850.

[22] J. W. Kamminga, L. M. Janßen, N. Meratnia, and P. J. M. Havinga, "Horsing Around-A Dataset Comprising Horse Movement," 2019, doi: 10.4121/uuid:2e08745c-4178-4183-8551-f248c992cb14.

[23] J. B. Burla, A. Ostertag, H. Schulze Westerath, and E. Hillmann, "Gait determination and activity measurement in horses using an accelerometer," *Comput Electron Agric*, vol. 102, pp. 127–133, Mar. 2014, doi: 10.1016/J.COMPAG.2014.01.001.

[24] "Shire horses – the world's largest horse breed | gentle giants." https://www.cavalluna.com/en/backstage-more/knowledge-about-horses/horse-breeds/shire-horse (accessed Mar. 28, 2023).

[25] "Breed Standard & Points of the Horse – The Shire Horse Society." https://www.shire-horse.org.uk/about-us/the-shire-horse/breed-standard-points-of-the-horse/ (accessed May 23, 2023).

[26] food and agriculture organization of the united nations, "Falabella pony/argentina (horse)." https://fao-dadis-breed-detail.firebaseapp.com/?country=ARG&specie=Horse&breed=Falabella%20Pony&lang=en (accessed May 23, 2023).

[27] "Fokprogramma 2020 EFS; European Falabella Studbook", Accessed: May 23, 2023. [Online]. Available: www.europeanFalabellastudbook.com

[28] "What are the Most Popular Horse Breeds?" https://www.saddlebox.net/what-are-the-most-popular-horse-breeds/ (accessed Mar. 28, 2023).

[29] food and agriculture organization of the united nations, "Falabella pony/argentina (horse)." https://fao-dadis-breed-detail.firebaseapp.com/?country=ARG&specie=Horse&breed=Falabella%20Pony&lang=en (accessed May 23, 2023).

[30] "Fokprogramma 2020 EFS; European Falabella Studbook", Accessed: May 23, 2023. [Online]. Available: www.europeanFalabellastudbook.com

[31] "Breed Standard & Points of the Horse – The Shire Horse Society." https://www.shire-horse.org.uk/about-us/the-shire-horse/breed-standard-points-of-the-horse/ (accessed May 23, 2023).

[32] "Typische Kenmerken - Belgisch Studbook van de Shetlandpony." http://www.shetlandstudbook.be/typische-kenmerken.html (accessed May 24, 2023).

[33] N. Atina *et al.*, "The Distribution of Path Loss Exponent in 3D Indoor Environment," *International Journal of Applied Engineering Research*, vol. 12, pp. 7154–7161, 2017, Accessed: Mar. 06, 2023. [Online]. Available: http://www.ripublication.com

[34] K. Hasan, K. Biswas, K. Ahmed, N. S. Nafi, and M. S. Islam, "A comprehensive review of wireless body area network," *Journal of Network and Computer Applications*, vol. 143, pp. 178–198, Oct. 2019, doi: 10.1016/J.JNCA.2019.06.016.

[35] M. O. Munoz, R. Foster, and Y. Hao, "Exploring physiological parameters in dynamic WBAN channels," *IEEE Trans Antennas Propag*, vol. 62, no. 10, pp. 5268–5281, Oct. 2014, doi: 10.1109/TAP.2014.2342751.

Draadloze gezondheidsmonitoring voor verschillende paardenrassen

Jirka Verleysen
Begeleider(s): Prof. Dr. Ir. Margot Deruyck, Prof. Dr. Ir. Wout Joseph, Ir. Jasper Goethals, Prof. Dr. Ir. Günter Vermeeren

Abstract - De belangstelling voor draadloze lichaamsnetwerken (WBAN's) is sterk toegenomen. WBAN's bestaan uit geminiaturiseerde sensoren die zijn ontworpen om draadloos gegevens te verzamelen en door te geven, waardoor de gezondheid van mens en dier op afstand kan worden gecontroleerd. Deze paper begint met een bespreking van de selectie van antennes en hun plaatsingslocaties. Vervolgens richt het zich op de analyse van het padverlies van een WBAN systeem dat is ontworpen voor het monitoren van de gezondheid van paarden. Het hoofddoel is de ontwikkeling van een robuust padverliesmodel dat het padverlies voor verschillende paardenrassen kan voorspellen. Daartoe worden drie paardenrassen, namelijk Selveryne (gemaakt voor simulatiedoeleinden), Falabella en Shetland, gekozen als basis voor het verzamelen van meetgegevens. Bij de simulatie zijn op elk paard zeven locaties voor antennes gekozen, en de Finite-Difference Time-Domain (FDTD)-methode is toegepast met behulp van sim4life. Er werden drie hoofdmodellen gemaakt voor line-of-sight (LOS), non-line-of-sight (NLOS) en alle punten, alsook de aan- of afwezigheid van antenneversterking, zowel in ingebedde als niet-ingebedde scenario's. De resulterende padverlies modellen vertonen een padverlies exponent die varieert van 1,90 tot 4,30, afhankelijk van het specifieke scenario. Deze waarden kunnen worden vergeleken met de padverlies exponenten die gewoonlijk worden waargenomen in verschillende omgevingen, zoals de vrije ruimte (2) en stedelijke (2,7-3,5) of sub stedelijke (3-5) gebieden bij gebruik van conventionele antennes. Hieruit blijkt dat communicatie in het WBAN-systeem mogelijk is, zij het met enige extra moeite.

Index termen: WBAN, FDTD, sim4life, paard, padverlies, niet- ingebedde padverlies, ingebedde padverlies

1 Inleiding

WBAN-netwerken maken continue draadloze controle mogelijk, zowel extern als intern op het lichaam, gedurende langere perioden [1]. Deze netwerken ondersteunen verschillende soorten verkeer, zoals real-time monitoring, on-demand diensten en nood communicatie [2]. Een belangrijke uitdaging in verband met WBAN's is echter het stroomverbruik, vooral voor in het lichaam geïmplanteerde sensoren, waar regelmatige vervanging van de batterij onpraktisch is. Padverlies, dat verwijst naar het verlies van signaalsterkte tijdens gegevensoverdracht als gevolg van signaalverzwakking, draagt aanzienlijk bij tot het stroomverbruik van sensoren. Signaalverzwakking kan het gevolg zijn van talrijke factoren, waaronder energieabsorptie, reflectie, diffractie, lichaamsschaduw, lichaamshouding en multipath-effecten. Van deze factoren zijn lichaamshouding en schaduwwerking de belangrijkste aandachtspunten bij het gebruik van WBAN's [3] – [5]. De huidige simulatie houdt echter geen rekening met multipath-effecten. Er bestaan verschillende soorten padverlies modellen, waaronder zuiver theoretische of empirische modellen, of een combinatie van beide [5] – [7]. Padverlies kan voor elke verbinding afzonderlijk worden berekend, of er kan een gemiddeld padverlies worden gebruikt, waarbij alle verbindingen in rekening worden genomen [8], [9]. Het is belangrijk onderscheid te maken tussen het ingebedde en het niet-ingebedde padverliesmodel. Het ingebedde padverliesmodel omvat de versterkingen van de gebruikte antennes, hetgeen doeltreffend kan zijn maar niet universeel toepasbaar, aangezien het afhangt van de specifieke antenne [7]. De meeste padverlies modellen zijn gebaseerd op de formule van Friis, die het ontvangen vermogen van een antenne berekent[8]. De padverlies-exponent is een parameter waarmee de formule gemakkelijk aan de omgeving kan worden aangepast. Hoewel het model oorspronkelijk is ontwikkeld om onderscheid te maken tussen de vrije ruimte en (sub)stedelijke gebieden, kan het ook rekening houden met de invloed van het lichaam op het padverlies [6], [8], [10]. De ontwikkeling van een nauwkeurig padverliesmodel kan de efficiëntie van WBAN-netwerken verbeteren.

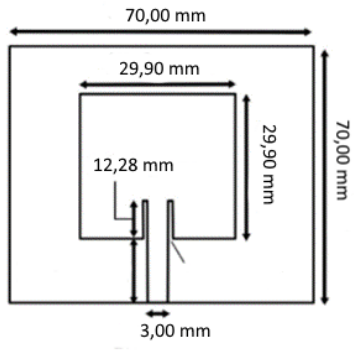

Figuur 1 Dimensies patch antenne [11]

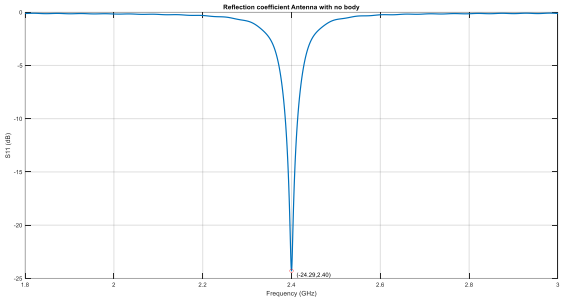

Figuur 2 Reflectiecoëfficiënt zonder een lichaam aanwezig

In dit onderzoek wordt het padverliesmodel dat voor WBAN's gebruikt, zoals beschreven in paper [7]. Dit model is gekozen omdat het gebaseerd is op simulaties en metingen aan een koe, die een vergelijkbare lichaamsstructuur heeft als een paard. Het biedt zowel ingebedde als niet-ingebedde oplossingen op basis van de Friis-formule, simulaties en metingen. Het doel van dit onderzoek is het creëren van een padverliesmodel waarmee het padverlies voor verschillende paardenrassen nauwkeurig kan worden voorspeld, rekening houdend met hun unieke anatomische structuren en variërende afstanden tussen antennes.

2 Methodes

2.1 Keuze antenne

De keuze van een geschikte antenne is van cruciaal belang bij WBAN-toepassingen. Aangezien het netwerk gedragen moet worden, is het belangrijk dat het systeem compact en onopvallend blijft. Dit geldt niet alleen voor de sensor, maar ook voor de bijbehorende antenne. De keuze voor een kleinere antenne verhoogt het comfort voor de drager. Het is ook belangrijk rekening te houden met de impact van de antennestraling op het lichaam, aangezien

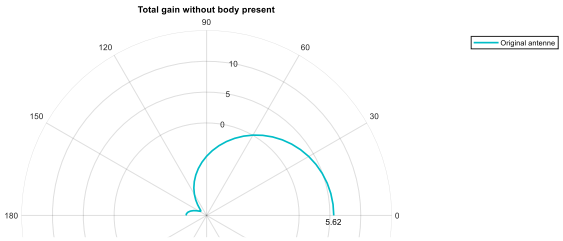

Figuur 3 Gain zonder een lichaam aanwezig

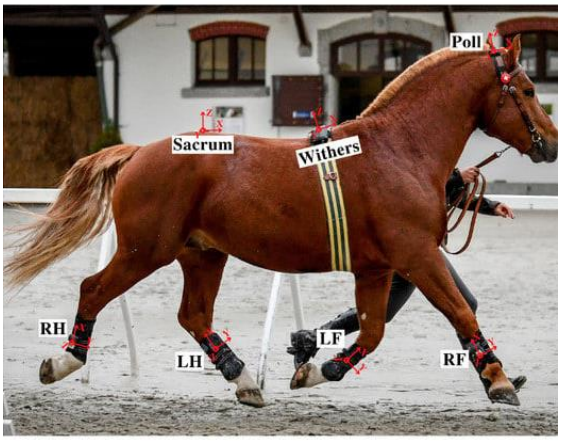

Figuur 4 Locaties sensoren op het paard [16]

overmatige blootstelling moet worden vermeden [12] – [14]. Naast de invloed van de antenne op het lichaam heeft ook het lichaam zelf invloed op de prestaties van de antenne, wat leidt tot variaties in ingangsimpedantie, vervorming van het stralingspatroon, frequentieverschuivingen en verminderde efficiëntie [15]. Om deze effecten te beperken is gekozen voor een patch-antenne met een massaplaat, zoals gepresenteerd in paper [11] . De massaplaat dient als barrière tussen het lichaam en de antenne en biedt bescherming aan beide zijden. Figuur 1 illustreert de afmetingen van de gekozen antenne.
Om de geschiktheid van de antenne voor de toepassing te waarborgen, zijn simulaties uitgevoerd zonder de aanwezigheid van een lichaam. De resultaten, weergegeven in Figuur 2 en Figuur 3, tonen een frequentie van 2,4 GHz, een S11-waarde van -24,29 dB en een maximale versterking van 5,62 dB, wat gunstige eigenschappen zijn voor deze specifieke toepassing.

2.2 Antenne locaties

De keuze van de antennelocaties is gebaseerd op praktische overwegingen, waarbij de nadruk ligt op gebieden die het meten van parameters zoals hartslag en beweging bij paarden vergemakkelijken. Deze locaties worden bepaald aan de hand van bestaande systemen die op de

Tabel 1 Hoogte van de paarden [28] – [31]

	Shire paard	Quarter paard	Falabella
Schofthoogte (cm)	160-205	145-165	63-86

Tabel 2 Simulatie tijden voor de grotere paardenrassen

Ras	Simulatietijd per antenne (uren)	Simulatietijd heel paard
Quarter	16	112 uren (4.6 dagen)
Shire	20	140 uren (5.83 dagen)

markt beschikbaar zijn en van systemen die in onderzoek worden gebruikt.[16] – [23] . De gekozen locaties zijn weergegeven in Figuur 4.

2.3 Keuze paarden rassen

Aanvankelijk werden voor de studie drie paardenrassen geselecteerd: Shire, Quarter en Falabella, waarbij Shire het grootste en Falabella het kleinste ras is [24] – [27] . De respectieve hoogtes van deze rassen zijn weergegeven in Tabel 1. De bedoeling van deze selectie was het volledige scala aan paardenmaten te omvatten om de nauwkeurigheid van het model te verbeteren. Het werd echter al snel duidelijk dat het simuleren van de Quarter en Shire paarden onpraktisch was vanwege hun grote omvang, zoals blijkt uit de simulatietijden in
Tabel 2. Om deze beperking aan te pakken werden alternatieve paardenrassen gekozen: Selveryne, Falabella en Shetland. Falabella en Shetland zijn echte paardenrassen, terwijl Selveryne is gecreëerd als een fictief ras met een kleinere omvang om de simulaties te versnellen. De hoogtes van deze geselecteerde modellen zijn weergegeven in Tabel 3 en hun relatieve verhoudingen zijn te zien in Figuur 5. De plaatsing van de vierkanten op het model zorgt voor een optimale positionering van de antenne voor een maximale weefselverbinding.

2.4 Keuze padverliesmodel

Voor het padverliesmodel is gekozen voor een model uit een eerdere studie[7]. De redenering achter deze keuze is dat het model is ontwikkeld op basis van simulaties en metingen aan koeien, waardoor het relevanter is voor een

Tabel 3 Hoogte van de paarden [29], [30], [32]

	Shetland paard	Falabella	Selveryne
Schofthoogte (cm)	71-107	63-86	52.2

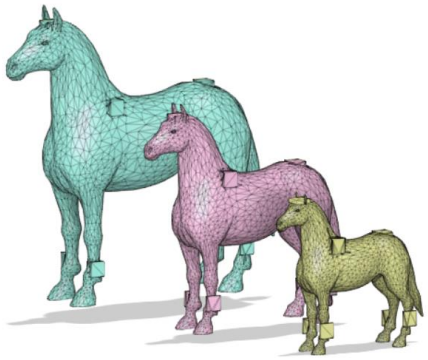

Figuur 5 Vergelijking van de rassen

paardenmodel dan voor een op mensen gebaseerd model. In het document wordt onderscheid gemaakt tussen padverlies met antenne-eigenschappen inbegrepen (2.1) en padverlies met antenne-eigenschappen uitgesloten (2.2) , die respectievelijk ingebedde en niet-ingebedde modellen zijn.

$$PL_{embedded} = P_{TX} - P_{RX} \quad (2.1)$$

$$PL = P_{TX} + G_{TXb} + G_{RXb} - P_{RX} \quad (2.2)$$

In het model staat $PL_{embedded}$ voor het padverlies met geïntegreerde antenneversterking, uitgedrukt in dB. PL is het niet-ingebedde padverlies in dB. P_{TX} en P_{RX} staan respectievelijk voor het uitgezonden en ontvangen vermogen, uitgedrukt in dBm. G_{TXb} en G_{RXb} staan voor de versterking van de zend- en ontvangstantenne bij plaatsing op het lichaam, uitgedrukt in dB.
Het padverlies kan worden gemodelleerd aan de hand van een referentieafstand van 10 cm.

$$PL(d) = PL(d_0) + 10n\log\left(\frac{d}{d_0}\right) + X_\sigma \quad (2.3)$$

Waarbij PL staat voor het padverlies in dB, terwijl $PL(d_0)$ staat voor het padverlies tussen twee antennes op het lichaam op de referentieafstand, eveneens uitgedrukt in dB. d staat voor de afstand tussen de ontvanger (RX) en de zender (TX), uitgedrukt in meters. n staat voor de

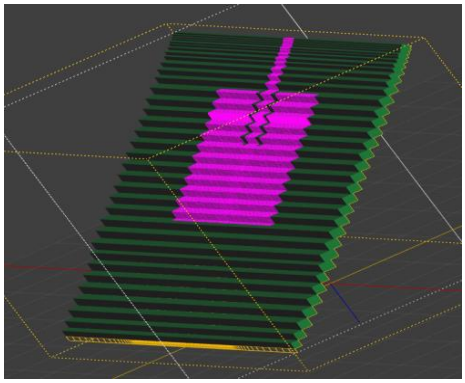

Figuur 6 Voxelisatie van de antenne bij 33° kanteling

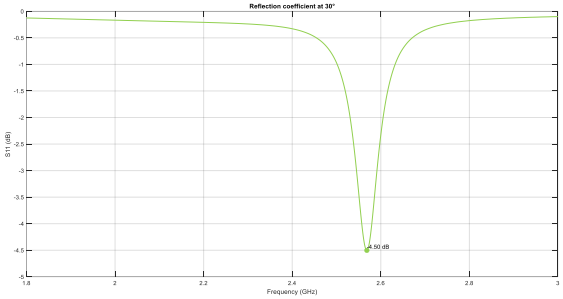

Figuur 7 Reflectiecoëfficiënt bij kanteling van 33°

exponent van het padverlies, en d_0 is de referentieafstand in meters. X_σ, komt overeen met een Gaussische verdeling met nul gemiddelden en een standaardafwijking σ , beide uitgedrukt in dB. Met behulp van de gesimuleerde gegevens kan het ontvangen vermogen worden berekend. Het uitgezonden vermogen blijft voor alle scenario's constant op 30 dBm. Er wordt een fitting uitgevoerd met behulp van de methode van de kleinste gekwadrateerde fout, waarmee de standaardafwijking tussen de fit en de datapunten kan worden berekend. Op basis van deze informatie kan een geschikte exponent van het padverlies worden bepaald door verschillende waarden van de exponent van het padverlies te doorlopen en de waarde te selecteren die het best past.

2.5 Simulaties

Voor de simulaties werden bepaalde keuzes gemaakt om een vlotte uitvoering te garanderen. Het gekozen model voor het paard was oorspronkelijk ontworpen als een 3D-geprint model, met ingewikkelde details die, hoewel ze geen significante invloed hadden op de resultaten, wel veel simulatietijd vergden. Om dit te verhelpen werd het aantal driehoeken in het model verminderd, wat resulteerde in een

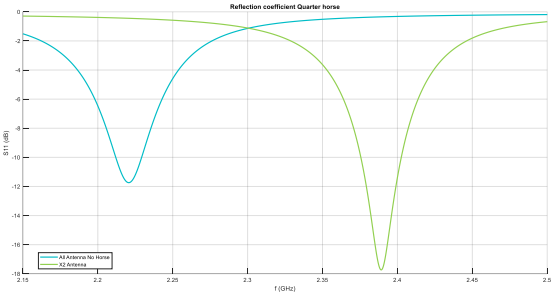

Figuur 8 Reflectie coefficient Quarter paard bij grid problemen

bestandsgrootte van 2,029 kB in plaats van de oorspronkelijke 392,339 kB.

De hoek van de antenne werd niet willekeurig gekozen, maar ingesteld op veelvouden van 90°. Hoewel deze aanpak enig realisme opoffert, is hij noodzakelijk om het "trappenprobleem" te vermijden dat optreedt bij simulatie met FDTD. Figuur 6 illustreert dit probleem. Als dit probleem niet wordt aangepakt, zou dit leiden tot voxelisatie fouten, waardoor de nauwkeurigheid van de resultaten van de antenne zou worden aangetast, zoals blijkt uit de verschuiving van de S11-waarde in Figuur 7. Bovendien is het bij gebruik van simulatiesoftware van cruciaal belang ervoor te zorgen dat het raster perfect uitgelijnd is met de patch om elke kleine scheefstand te vermijden die de afmetingen van de antenne kan veranderen en bijgevolg de reflectiecoëfficiënt kan beïnvloeden. Een voorbeeld hiervan wordt weergegeven in Figuur 8.

3 Resultaten

Het padverliesmodel wordt berekend voor drie scenario's, waarbij zowel ingebedde als niet-ingebedde padverlies in rekening wordt gebracht. Deze scenario's omvatten alle punten, alleen non-line-of-sight (NLOS) punten, en alleen line-of-sight (LOS) punten. De "twijfelpunten", die niet duidelijk in de categorie LOS of NLOS vallen, worden in de laatste twee scenario's buiten beschouwing gelaten. De resultaten zijn weergegeven in Figuur 9 en Figuur 10. Tabel 4 toont de padverlies exponent, standaardafwijking en referentie padverlies voor elk scenario. Bij vergelijking van deze waarden met de padverlies exponent voor niet op het lichaam gedragen antennes (Voorspelling bij embedded pad verlies) kan worden geconcludeerd dat de verkregen waarden acceptabel zijn. Het LOS-scenario

Tabel 4 Resultaten standaard afwijking, padverlies en referentie padverlies

		σ	n	PL (d_0) (dB)
Alle points	Embedded	3.63	3.60	28.19
	De-embedded	3.62	3.90	38.56
NLOS	Embedded	3.63	3.00	28.19
	De-embedded	3.62	4.30	38.56
LOS	Embedded	3.81	1.90	28.19
	De-embedded	3.87	3.20	38.26

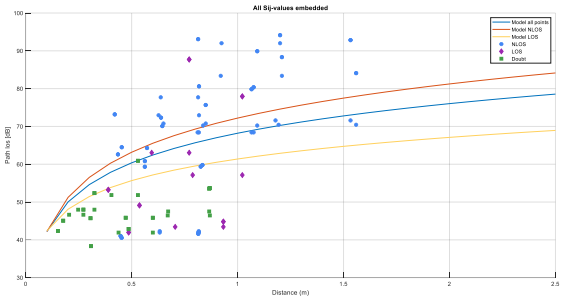

Figuur 9 Voorspelling bij embedded pad verlies

vertoont consequent een betere padverlies exponent dan het NLOS-scenario, waarbij één scenario zelfs de omstandigheden in de vrije ruimte overtreft. Het padverlies exponent voor LOS is echter nog steeds hoger dan het typische bereik van 1,6-1,8 dat in normale LOS-scenario's wordt waargenomen. Op basis van specifieke situaties en verbindingsscenario's zijn verschillende padverlies modellen vastgesteld. Deze modellen komen overeen met de bevindingen in eerdere studies [7]. Het aanvullende de-embedded model maakt een gemakkelijke vergelijking mogelijk, ongeacht de gebruikte antenne, en vereenvoudigt de systeemimplementatie wanneer verschillende antennetypen worden gekozen. De berekende padverlies exponent komt in het beste geval overeen met een scenario dat lijkt op de vrije ruimte en in het slechte geval met obstructies binnen gebouwen. Het gemiddelde geval vertegenwoordigt een (sub)stedelijk gebied. Deze resultaten zijn realistisch en haalbaar. Het model maakt padverlies voorspelling op grotere schaal mogelijk zonder dat tijdrovende simulaties nodig zijn. Wanneer bijvoorbeeld een Shire-paard met een schofthoogte van 2 meter wordt beschouwd, voorspelt het niet-ingebedde model een verlies van ongeveer 100 dB, terwijl het ingebedde model een verlies van ongeveer 80 dB voorspelt.

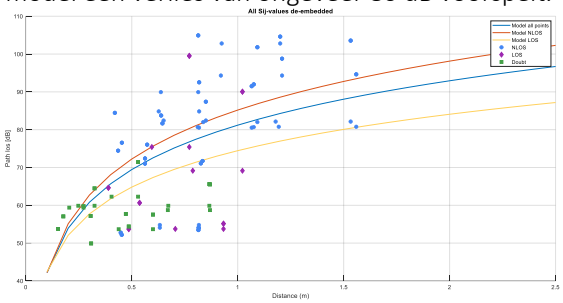

Figuur 10 Voorspelling de-embedded pad verlies

Tabel 5 Pad loss exponent in verschillende omgevingen [33]

Environment	Path loss exponent
Free space	2
Urban area	2.7 – 3.5
Suburban area	3 – 5
Indoor line-of-sight	1.6 – 1.8
Obstructed in building	4-6
Obstructed in factories	2-3

Dit benadrukt het belang van antennekeuze voor het beperken van het padverlies.

4 Conclusie

In dit artikel worden verschillende padverlies modellen voorgesteld voor WBAN-architectuur op verschillende paardenrassen. Het onderzoek begint met het selecteren van geschikte antennes en antennelocaties, rekening houdend met praktische toepassingen zoals hartslag- en bewegingsmonitoring. Simulaties worden uitgevoerd met behulp van het FDTD-algoritme en vervolgens toegepast op een bestaand padverliesmodel. Deze aanpak helpt bij het voorspellen van padverlies voor paardenrassen die nog niet eerder zijn gesimuleerd.

5 Toekomstig onderzoek

Toekomstig onderzoek zou het model kunnen valideren door het te meten op echte paarden. Te beginnen met tests op Falabella- of Shetland paarden, en dan over te gaan naar grotere rassen zoals Quarters of Shires. Praktische problemen kunnen ontstaan door de grootte van de antenne, vooral bij kleinere rassen. De breedte van de antenne is breder dan de poten van de kleinere paarden, waardoor een deel niet wordt

ondersteund. Dit kan een geringe praktische invloed hebben, ondanks de theoretische scheiding door het grondvlak. Voordat praktische metingen kunnen worden verricht, moet een draadloze technologie worden gekozen. Deze kan samen met de antenne helpen het padverlies verder te beperken. Door metingen te vergelijken met simulaties kan het model worden verfijnd voor toepassing in verschillende paardenrassen.
Een volgende stap is dan het opnemen van bewegingsveranderingen in het model. Dit veroorzaakt namelijk een dopplereffect en verschuivingen in het vermogen dat nodig is om gegevens te verzenden [34],[35].

6 Dankwoord

De auteur spreekt haar oprechte dank uit aan Prof. Dr. Ir. Margot Deruyck, Prof. Dr. Ir. Wout Joseph, en Prof. Dr. Ir. Günter Vermeeren voor het bieden van de mogelijkheid om de masterproef over dit onderwerp uit te voeren. Speciale dank gaat uit naar Ir. Jasper Goethals voor de toegewijde begeleiding en ondersteuning tijdens de duur van deze thesis.

7 References

[1] R. Cavallari, F. Martelli, R. Rosini, C. Buratti, and R. Verdone, "A survey on wireless body area networks: Technologies and design challenges," *IEEE Communications Surveys and Tutorials*, vol. 16, no. 3, pp. 1635–1657, 2012, doi: 10.1109/SURV.2014.012214.00007.

[2] Md. T. Arefin, M. H. Ali, A. K. M. F. Haque, Md. T. Arefin, M. H. Ali, and A. K. M. F. Haque, "Wireless Body Area Network: An Overview and Various Applications," *Journal of Computer and Communications*, vol. 5, no. 7, pp. 53–64, May 2017, doi: 10.4236/JCC.2017.57006.

[3] S. L. Cotton, A. Mckernan, A. J. Ali, and W. G. Scanlon, "An Experimental Study on the Impact of Human Body Shadowing in Off-Body Communications Channels at 2.45 GHz," *Proceedings of the 5th European Conference on Antennas and Propagation (EUCAP)*, 2011.

[4] Ł. Januszkiewicz, "Analysis of Human Body Shadowing Effect on Wireless Sensor Networks Operating in the 2.4 GHz Band," *Sensors 2018, Vol. 18, Page 3412*, vol. 18, no. 10, p. 3412, Oct. 2018, doi: 10.3390/S18103412.

[5] S. Kaur and J. Malhotra, "Survey on Empirical Channel Models for WBAN," *International Journal of Future Generation Communication and Networking*, vol. 8, no. 2, pp. 399–410, 2015, doi: 10.14257/ijfgcn.2015.8.2.34.

[6] L. Roelens and L. Martens, "Path loss model for wireless narrowband communication near biological tissue," *6th UGent-FirW Doctoraatssymposium, Interactive poster session, paper nr. 120 (proceedings available on CD-Rom)*, 2005, doi: 1854/4782.

[7] S. Benaissa *et al.*, "Internet of animals: On- and off-body propagation analysis for energy efficient WBAN design for dairy cows," *2017 11th European Conference on Antennas and Propagation, EUCAP 2017*, pp. 298–302, May 2017, doi: 10.23919/EUCAP.2017.7928112.

[8] M. M. Khan, Q. H. Abbasi, A. Alomainy, and C. Parini, "Experimental Investigation of Subject-Specific On-Body Radio Propagation Channels for Body-Centric Wireless Communications," *Electronics 2014, Vol. 3, Pages 26-42*, vol. 3, no. 1, pp. 26–42, Jan. 2014, doi: 10.3390/ELECTRONICS3010026.

[9] E. Reusens, W. Joseph, G. Vermeeren, and L. Martens, "On-body measurements and characterization of wireless communication channel for arm and torso of human," *IFMBE Proc*, vol. 13, pp. 264–269, 2007, doi: 10.1007/978-3-540-70994-7_44.

[10] T. Kumpuniemi, T. Tuovinen, M. Hämäläinen, K. Yekeh Yazdandoost, R. Vuohtoniemi, and J. Iinatti, "Measurement-Based On-Body Path Loss Modelling for UWB WBAN Communications".

[11] "FR4 Dielectric Constant and Material Properties." https://resources.altium.com/p/fr4 (accessed Mar. 28, 2023).

[12] "Cell Phones and Cancer Risk Fact Sheet - NCI." https://www.cancer.gov/about-cancer/causes-prevention/risk/radiation/cell-phones-fact-sheet (accessed May 23, 2023).

[13] M. I. Hossain, M. R. I. Faruque, and M. T. Islam, "Analysis on the effect of the distances and inclination angles between human head and mobile phone on SAR," *Prog Biophys Mol Biol*, vol. 119, no. 2, pp. 103–110, Nov. 2015, doi: 10.1016/J.PBIOMOLBIO.2015.03.008.

[14] V. G. Khurana, C. Teo, M. Kundi, L. Hardell, and M. Carlberg, "Cell phones and brain tumors: a review including the long-term epidemiologic data," *Surg Neurol*, vol. 72, no. 3, pp. 205–214, Sep. 2009, doi: 10.1016/J.SURNEU.2009.01.019.

[15] "Wearable Antennas – Applications, Technologies, and their Impact on Human Body - Mistral Solutions." https://www.mistralsolutions.com/blog/wearable-antennas-applications-technologies-impact-human-body/ (accessed Mar. 09, 2023).

[16] H. Darbandi *et al.*, "Using different combinations of body-mounted IMU sensors to estimate speed of horses-A machine learning approach," *Sensors (Switzerland)*, vol. 21, no. 3, pp. 1–12, Feb. 2021, doi: 10.3390/S21030798.

[17] "How it works - EquiMoves." https://equimoves.nl/system-overview/how-it-works/ (accessed Mar. 28, 2023).

[18] C. J. Thompson, L. M. Luck, J. Keshwani, S. K. Pitla, and L. K. Karr, "Location on the Body of a Wearable Accelerometer Affects Accuracy of Data for Identifying Equine Gaits," *J Equine Vet Sci*, vol. 63, pp. 1–7, Apr. 2018, doi: 10.1016/J.JEVS.2017.12.002.

[19] A. Eerdekens *et al.*, "A framework for energy-efficient equine activity recognition with leg accelerometers," *Comput Electron Agric*, vol. 183, p. 106020, Apr. 2021, doi: 10.1016/J.COMPAG.2021.106020.

[20] C. Hartmann, L. Lidauer, J. Aurich, C. Aurich, and C. Nagel, "Detection of the time of foaling by accelerometer technique in horses (Equus caballus)—a pilot study," *Reproduction in Domestic Animals*, vol. 53, no. 6, pp. 1279–1286, Dec. 2018, doi: 10.1111/RDA.13250.

[21] S. Bosch *et al.*, "EquiMoves: A Wireless Networked Inertial Measurement System for Objective Examination of Horse Gait," 2018, doi: 10.3390/s18030850.

[22] J. W. Kamminga, L. M. Janßen, N. Meratnia, and P. J. M. Havinga, "Horsing Around-A Dataset Comprising Horse Movement," 2019, doi: 10.4121/uuid:2e08745c-4178-4183-8551-f248c992cb14.

[23] J. B. Burla, A. Ostertag, H. Schulze Westerath, and E. Hillmann, "Gait determination and activity measurement in horses using an accelerometer," *Comput Electron Agric*, vol. 102, pp. 127–133, Mar. 2014, doi: 10.1016/J.COMPAG.2014.01.001.

[24] "Shire horses – the world's largest horse breed | gentle giants." https://www.cavalluna.com/en/backstage-more/knowledge-about-horses/horse-breeds/shire-horse (accessed Mar. 28, 2023).

[25] "Breed Standard & Points of the Horse – The Shire Horse Society." https://www.shire-horse.org.uk/about-us/the-shire-horse/breed-standard-points-of-the-horse/ (accessed May 23, 2023).

[26] food and agriculture organization of the united nations, "Falabella pony/argentina (horse)." https://fao-dadis-breed-detail.firebaseapp.com/?country=ARG&specie=Horse&breed=Falabella%20Pony&lang=en (accessed May 23, 2023).

[27] "Fokprogramma 2020 EFS; European Falabella Studbook", Accessed: May 23, 2023. [Online]. Available: www.europeanFalabellastudbook.com

[28] "What are the Most Popular Horse Breeds?" https://www.saddlebox.net/what-are-the-most-popular-horse-breeds/ (accessed Mar. 28, 2023).

[29] food and agriculture organization of the united nations, "Falabella pony/argentina (horse)." https://fao-dadis-breed-detail.firebaseapp.com/?country=ARG&specie=Horse&breed=Falabella%20Pony&lang=en (accessed May 23, 2023).

[30] "Fokprogramma 2020 EFS; European Falabella Studbook", Accessed: May 23, 2023. [Online]. Available: www.europeanFalabellastudbook.com

[31] "Breed Standard & Points of the Horse – The Shire Horse Society." https://www.shire-horse.org.uk/about-us/the-shire-horse/breed-standard-

points-of-the-horse/ (accessed May 23, 2023).
[32] "Typische Kenmerken - Belgisch Studbook van de Shetlandpony." http://www.shetlandstudbook.be/typische-kenmerken.html (accessed May 24, 2023).
[33] N. Atina *et al.*, "The Distribution of Path Loss Exponent in 3D Indoor Environment," *International Journal of Applied Engineering Research*, vol. 12, pp. 7154–7161, 2017, Accessed: Mar. 06, 2023. [Online]. Available: http://www.ripublication.com
[34] K. Hasan, K. Biswas, K. Ahmed, N. S. Nafi, and M. S. Islam, "A comprehensive review of wireless body area network," *Journal of Network and Computer Applications*, vol. 143, pp. 178–198, Oct. 2019, doi: 10.1016/J.JNCA.2019.06.016.
[35] M. O. Munoz, R. Foster, and Y. Hao, "Exploring physiological parameters in dynamic WBAN channels," *IEEE Trans Antennas Propag*, vol. 62, no. 10, pp. 5268–5281, Oct. 2014, doi: 10.1109/TAP.2014.2342751.

Contents

List of figures

List of tables

List of abbreviations

6LoWPAN	IPv6 over Low-Power Wireless Personal Area Network
AES	Advanced encryption standard
AMC	Artificial magnetic conductor
BAN	Body area network
BIPT	Belgian institute for postal services and telecommunications
BLE	Bluetooth low energy
Bps	Bits per second
BSN	Body sensor network
CA	Congestion avoidance
CCS	Cooperative carrier signal
CRC	Cycle redundancy check
CSRK	Connection signature resolving key
DAC	Device access code
DP	Deep neural
DSSS	Direct sequence spread spectrum
E2E	End to end
EALB	Energy aware and load balanced parent selection
EBG	Electromagnetic bandgap
ECG	Electrocardiogram
ECRM	Energy and congestion aware routing metric
ETSI	European telecommunication and standardisation institute
FDTD	Finite-difference time-domain method
FHSS	Frequency hopping spread spectrum
FR4	flame retardant 4
GPRS	General packet radio service
HIS	High impedance surfaces
IETF	Internet engineering task force
IoT	Internet of things
IOT	Internet of things
IPv4	Internet protocol 4
IPv6	Internet protocol 6
ISM	Industrial, science and medical
L2CAP	Logical link control and adaptation protocol
LF	Left front leg
LH	Left hind leg
LHCP	Left hand circular polarization
LOS	Line of sight
MAC	Media access control
ML	Machine learning
NLOS	Not line of sight
NRT	Not real time
PCB	Printed circuit board
PD	Personal device
PHY	Physical layer
QoS	Quality of service
RERBDI	Residual energy ratio
RF	Right front leg
RF	Radio frequency
RH	Right hind leg
RHCP	Right hand circularly polarization
ROEE	Region based

RPL	Routing protocol
RSSI	Received signal strength indicator
RT	Real time
SAFER+	Secure And Fast Encryption Routine
SAR	Specific absorption rate
SNR	Signal to interference plus noise ratio
WBAN	Wireless body area network
WHO	World health organisation
WSN	Wireless sensor

1 Introduction

Wireless Body Area Networks (WBANs) have found applications in various fields such as sports, military, lifestyle, and entertainment. However, their significant contribution lies in the medical domain, where WBANs enable continuous monitoring inside or on the body [1]. WBANs also offer potential benefits in animal healthcare and monitoring of endangered species, with minimal discomfort as the antennas used are often inconspicuous to the animals [2].

This study focuses on utilizing WBAN technologies to monitor the health of horses. Specific equine ailments, such as colic and laminitis, can exhibit symptoms that can be easily monitored using sensors, allowing owners to detect any issues at an early stage [3], [4]. Early detection of illnesses increases the chances of survival for the horses.

The primary objective of this work is to develop a path loss model that can be employed for WBAN systems designed for different horse breeds. To achieve this, FDTD algorithms are utilized in the Sim4Life application. The simulations involve equipping three horse breeds of varying sizes with antennas, and the path loss model suggested in paper [5] is applied for this application.

The first part of this study entails a comprehensive literature review, serving as the foundation for the subsequent simulations. It begins with an exploration of wearable technologies and their impact on WBAN efficiency, examining the latest advancements and their potential benefits in healthcare. Furthermore, the use of WBANs in veterinary medicine, specifically for horses, is thoroughly examined, highlighting the unique challenges and opportunities in equine health monitoring. The effects of antennas on the body and vice versa are discussed. Moreover, the most important antenna properties are analysed to understand their impact on system performance. Various path loss models are then evaluated, considering their advantages and limitations in accurately predicting signal attenuation on a horse's body. Lastly, different types of wearable antennas are reviewed, along with their respective benefits and drawbacks.

The second section focuses on the selected antenna, explaining the rationale behind its choice based on the specific requirements of on body health monitoring. It discusses the unique features and design considerations of the chosen antenna. Furthermore, a detailed simulation is conducted to validate the antenna's effectiveness for the intended application. The section concludes by presenting the simulation results.

In the third section, the optimal locations for the antennas are determined. This choice is mainly based on practicality and the best locations for measurement. Having the antenna near the measure location makes the device smaller which causes the horse less discomfort.

The fourth section involves the selection of three horse breeds on which the simulations will be conducted. The chosen horse breeds represent a diverse range of sizes and body characteristics to capture the variations in signal propagation for different horse breeds. The section provides insights into the selection process. By simulating the WBAN system on these specific horse breeds, the study aims to provide a comprehensive understanding of the system's performance across a wide range of equine profiles.

Section five delves into the simulation progress, highlighting the methodology employed and discussing any challenges and limitations encountered during the simulations. It provides a detailed overview of the simulation setup, including the software tools used, the modelling assumptions made, and the parameters varied. The section presents and analyses the results obtained from the simulations, offering insights into signal propagation characteristics, antenna performance, and the overall feasibility of the WBAN system for horse health monitoring.

Finally, the last section discusses the findings and implications of the study, providing a comprehensive analysis of the simulation results. It addresses the limitations of the research and suggests avenues for further research based on the obtained results.

2 Literary study

This chapter explains the theory used for the simulations. However, it should be noted that most research in this area focuses on humans[6]–[12]. The average human weighs 62.0 kg and has a height of 177.7 cm for a man and 164.7cm for a woman in Belgium, both values vary depending on the country [13], [14]. In contrast, the smallest breed of horses weighs 70kg-80kg and has a height of 70cm-106cm at the wither, while the largest breed weighs 1100 kg and has a height of 178 cm at the wither. This significant difference in body mass could have a considerable impact on the simulations [15]–[17].

2.1 Wearable technology

Wearable technologies are implemented in products that are integrated into or onto the human body in different ways, usually connected to a network. These are products, such as jewellery, glasses, clothing, or any other similar items that include sensors[18].

2.1.1 WSN, BSN BAN en WBAN

The terms body sensor network (BSN), wireless sensor network (WSN), wireless body area network (WBAN), and body area network (BAN) are often used interchangeably when discussing wearable and wireless technology. However, it is important to clarify their distinctions.
A WSN consists of a possibly large number of wireless devices able to take environmental measurements such as temperature, light, sound, and humidity. These sensor readings are transmitted over a wireless channel to a running application that makes decisions based on the sensor readings. These networks have several detection stations, known as sensor nodes, which are small, portable, and lightweight. WSNs have diverse applications in various domains, including IoT, industrial automation and smart homes [19].
A BSN is a special kind of WSN, where the sensors are closer together an attached to a (human) body. This is used to acquire physiological data[20].This placement close to a body is the main difference between WSN and BSN. This brings different challenges when setting up a BSN compared to a WSN (Table 2-1).

Table 2-1 Difference between WSN en BSN [21]

Challenges	WSN	BSN
Scale	As large as the environment being monitored (meters/kilometres)	As large as (human) body parts (millimetres/centimetres)
Node number	Greater number of nodes required for accurate, wide area coverage	Fewer, more accurate sensor nodes required (limited by space and comfort)
Node function	Multiple sensors, each preforming dedicated tasks	Single sensors, each performing multiple tasks
Node accuracy	Large node number compensates for accuracy and allows result validation	Limited node number with each required to be robust and accurate
Node size	Small size preferable but not a major limitation in many cases	Pervasive monitoring and need for miniaturization
Dynamics	Exposed to extreme weather, noise, and asynchrony	Exposed to more predictable environment but motion artefacts are a challenge
Event detection	Early adverse event detection desirable; failure often is reversible	Early adverse events detection vital; human tissue failure is irreversible
Variability	Much more likely to have a fixed or static structure	Biological variation and complexity mean a more variable structure
Data protection	Low level wireless data transfer security required	High level wireless data transfer security required to protect patient information
Power supply	Accessible and likely to be changed more easily and frequently	Inaccessible and difficult to replace in an implantable setting
Power demand	Likely to be greater as power is more easily supplied	Likely to be lower as energy is more difficult to supply
Energy scavenging	Solar and wind power are most likely candidates	Motion (vibration) and thermal (body heat) are most likely candidates
Access	Sensors more easily replaceable or even disposable	Implantable sensor replacement difficult and requires biodegradability
Biocompatibility	Not a consideration in most applications	A must for implantable and some external sensors. Likely to increase cost.
Context awareness	Not so important with static sensors where environments are well defined	Very important because body physiology is very sensitive to context change.
Wireless technology	Bluetooth, Zigbee, GPRS, wireless LAN and RF already offer solutions	Low power wireless required, with signal detection more challenging
Data transfer	Loss of data during wireless transfer is likely to be compensated by the number of sensors used.	Loss of data is more significant and may require additional measures to ensure QoS and real-time data interrogation capabilities.

A BAN network is a specific type of BSN that Is focused on collecting data from a particular area of the body. BANs therefore, are typically used in medical applications, such as monitoring of vital signs or tracking movement. BSN and BANs are often used interchangeable since it is difficult to determine just how big an area is.
An WBAN network can provide continuous monitoring on or inside the body for long periods of time thanks to it being wireless. It also can support transmission of real time traffic to observe the status of vital functionalities [1].It has different applications in the medical field such as remote healthcare monitoring, assisted living and telemedicine. Other application fields include sports, military, lifestyle, and entertainment [1]. The main requirements for a WBAN should be wearability, reliability, security, and interoperability[22]. Figure 2-1 gives an idea of the workflow of a WBAN.

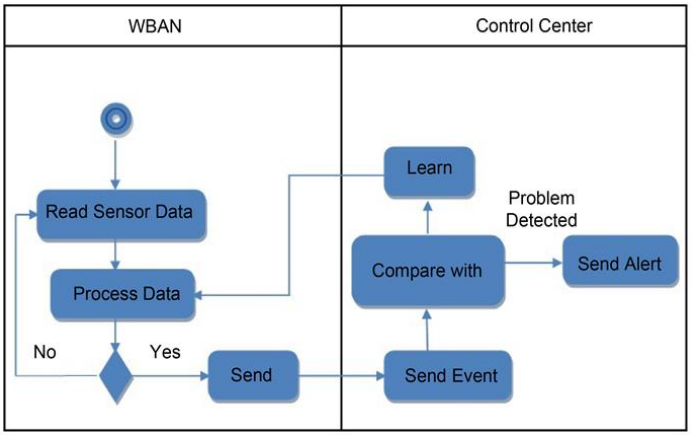

Figure 2-1 Workflow WBAN [22]

Types of sensors

In general, there are 2 types of sensors. The first type only measures data and sends it to the second type. The second type, called actuators, measure, and send data as the first type but can in addition perform an action on the body (e.g., administer medication) based on the collected data[23].

Traffic types

WBAN has three different traffic types. Normal, emergency and on-demand traffic. Normal traffic is the data traffic used to monitor the normal condition of a person without any criticality and on-demand events [22]. On-demand traffic is traffic which is initiated by an (authorized) person to acquire certain information for diagnostic purposes [22]. Emergency traffic is initiated by the nodes when they exceed a predefined threshold or in any situation that is considered an emergency. Such a type of traffic is unpredictable. This is the most difficult one of the traffics since there shouldn't be any delays whatsoever as it is a potential life-threatening situation. There are different ways to label traffic within a network to allow for this speed so in case of emergency other traffic in the network will be delayed instead of this traffic [22], [23].

Privacy and security

WBAN transmits sensitive data, which requires protection to ensure its confidentiality, integrity, and availability. Communication technologies can provide security measures to safeguard the data. Moreover, incorrect data can also pose a threat to a patient's life, emphasizing the importance of preventing any tampering with the data. The primary security requirements for WBAN include availability, confidentiality, authentication, and integrity [23].

Interference

The popularity of WBAN has led to an increase in the number of systems in some areas, which may cause interference with each other or other already existing infrastructure. Such interference can cause an increase in power consumption and in critical situations could cause fatal delays. Interference can be addressed through hardware or software solutions. One effective software solution is to use wireless

technology with a robust encoding scheme to reduce interference and enhance reliability. This approach can help mitigate the risks associated with interference and ensure the effective operation of WBAN systems in critical applications [23].

2.2 Wireless technologies

The impact of wireless technologies on WBANs can be significant. Factors such as their topology and error rate can have a substantial effect on power consumption. Additionally, encryption plays a vital role in ensuring the security of private data and preventing unauthorized tampering. Given the ubiquitous nature of these technologies, there is a possibility of interference between them. Therefore, it is crucial to design a robust system that can effectively mitigate such interference. This section will provide a detailed exploration of these topics.

2.2.1 Parts of a technology

A technology exists out of different aspects. The first one is the topology. This choice has significant impact on the network. A suboptimal topology choice can result in a wastage of time and energy. In the case of a WBAN, there is an additional challenge due to the requirement of wearable devices. Minimizing the number of devices is always desirable for wearer comfort. However, this constraint can limit the available options for choosing a suitable topology. One commonly used topology is the tiered approach. Data collection from the network can be transmitted wirelessly to a medical server for analysis and storage. This approach can be implemented with multiple tiers (minimum being two). Figure 2-2 depicts an example of a three-tier WBAN [23], [24].

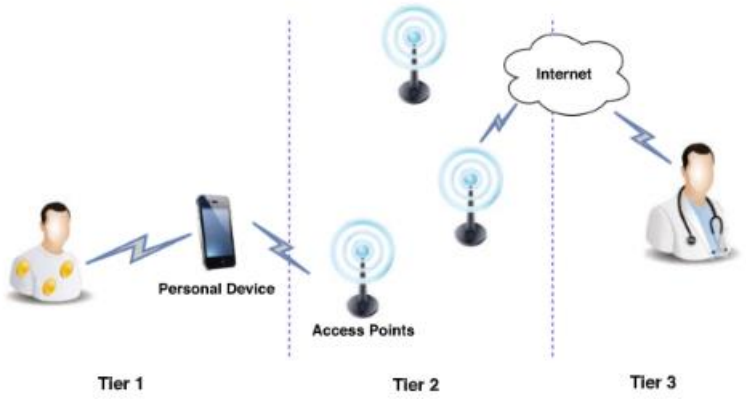

Figure 2-2 Three-tiers WBAN [23]

The topology also influences the power consumption. Power consumption is crucial for WBAN applications. Lower power consumption is preferred to extend battery life. However, WBAN poses additional challenges as it requires small size for comfort, with the sensor antenna and battery being as small as possible, while also lasting a long time. In-body sensors are an extreme case, as they are difficult to replace and should ideally have batteries that allow years of usage.
Efficient sleep modes are also vital in WBAN applications, as many applications only need to transmit/receive data intermittently. Putting the sensors to sleep between transmissions/receptions can significantly save battery power. In addition to the evaluation of power consumption, it is also worthwhile to explore energy harvesting methods that can utilize sources such as heat, vibration, or movement. These alternative approaches can provide intriguing possibilities for generating and harnessing energy. When designing a sensor, it is important to consider peak currents. For instance, if you plan to use a CR2302 button cell, the peak current should be limited to 15mA [23], [24].
The data communication error correction is a significant factor. It enables the correction of corrupted or incorrect data. In most WBAN technologies mistakes are not severe as they result in unrealistic values, which can easily be filtered out. If such value is detected, there are two options: either take no action since measurements occur periodically or request the device to resend the data. In most medical applications, the wireless range for data transmission typically falls within the range of 2 meters to 10 meters. This range

allows multiple devices in the immediate vicinity to send and receive data [11]. It is worth noting that these figures are based on studies conducted on humans. Therefore, the results may vary significantly when applied to other animals such as horses.
The data is communicated wirelessly, a significant drawback for this approach is that it allows unrestricted access to the data due to an absence of a physical barrier. The concerns are even more pronounced in public settings like hospitals. WBAN involves highly private data, necessitating robust protection measures. Encryption and authentication are effective means of safeguarding the data, ensuring that only authorized individuals can access it. Encryption adds an additional layer of security by making it challenging, and ideally impossible, for unauthorized individuals to decipher intercepted wireless transmissions.
The data rate itself depends on the specific use case. Certain measurements like blood pressure, body temperature, breathing speed and pH levels can tolerate a slight delay between measurement, transmission, and reception. On the other hand, measurements such as an electrocardiogram (ECG) demand a high data transmission rate. In medical applications, data transfer rates can range from 10 kbps to 10 Mbps, depending on the type of measurement and data being transmitted[24].

2.2.2 IEEE 802.15.6

IEEE 802.15.6 is a wireless communication standard specifically developed for WBANs. It specifies the physical layer (PHY) and media access control (MAC) layer protocols. Although the focus of the thesis primarily centers around the MAC layer, it is evident that the MAC and PHY layers are closely intertwined and interconnected. This standard serves as the foundation for many of the technologies discussed in section 2.2.3. Table 2-2 presents the key properties determined by IEEE 802.15.6.

Table 2-2 Properties IEEE 802.15.6[24], [25]

Metric	Quantity/description
Data speed	10 kbps-10Mbps depending on the datatype
Number of sensors in a network	Maximum of 256 per network
Network density	2-4 networks per square meter in assumption that one wearer could wear sensors of 2 different networks
Quality of service (QoS)	Medical application: less than 125 ms Non-medical application: less than 250 ms
Security	Data protection, integrity, and authentication are the primary security requirements in healthcare. Medical data is highly sensitive, and any unauthorized access or leakage of patient data is unacceptable.
Mobility	Flexibility should be provided to allow patients to move freely both within and outside the hospital or their home environment.

2.2.3 Technologies

Various technologies can be employed for WBAN applications, with the most common options being Bluetooth, Bluetooth Low Energy (BLE), and technologies based on the IEEE 802.15.4 protocol like ZigBee and 6LoWPAN.

Bluetooth

Bluetooth is an open standard wireless protocol that was originally developed as a variation of the RS-232 protocol. It is defined by IEEE 802.15.1. Bluetooth networks can have different topologies, with piconet and scatternet being the most common. However, scatternet implementations are currently limited due to Bluetooth and MAC address protocol constraints, and ongoing research is exploring this area [26].As a result, piconet, which is a point-to-multipoint connection, is the most frequently used topology. This topology divides the network into piconets, as shown in Figure 2-3. These smaller networks can be used to implement one of the tiers as discussed in section 2.2.1.

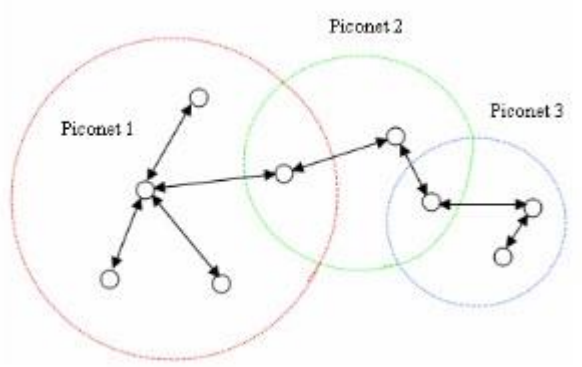

Figure 2-3 Bluetooth topology[27]

In terms of link layer security, Bluetooth employs a standard 16-bit cyclic redundancy check (CRC). For data encryption, it uses an E0 stream encoder that relies on a pre-established 128-bit encryption key derived from the user-entered pin code. However, successful attacks have compromised the 128-bit encryption key, reducing it to a 64-bit encryption key. Additionally, the algorithms based on the SAFER+ algorithm used in Bluetooth have been found to be susceptible to attacks.

Within a piconet, the Bluetooth devices' access code (DAC) addresses are limited to only 3 bits, which restricts the maximum number of devices that can actively communicate with the master node to 8. However, there can be more devices in the piconet, but they will have to wait their turn to communicate with the master node, resulting in unwanted delays. Moreover, Bluetooth has a relatively slow wake-up delay of approximately 3 seconds, which may present challenges in certain applications.

For a comprehensive overview of the key properties of Bluetooth, see Table 2-3 [26]–[28].

Table 2-3 Properties of Bluetooth[24], [27]

Metric	Quantity/description
Average consumption	100 mW
Peak current	Unknown
Data speed	24 Mbps
Frequency band	2.4-2.48 GHz
Range	10m

Bluetooth low energy

Bluetooth Low Energy (BLE) is the energy-efficient version of Bluetooth. It achieves this by using a lighter version of the Logical Link Control and Adaptation Protocol (L2CAP). This protocol makes a best effort to send data at the next hop without requiring the retransmission or flow control mechanisms commonly used in Bluetooth applications. The star topology of BLE is depicted in Figure 2-4.BLE operates with devices that have specific functions such as advertisers and initiators.[27].

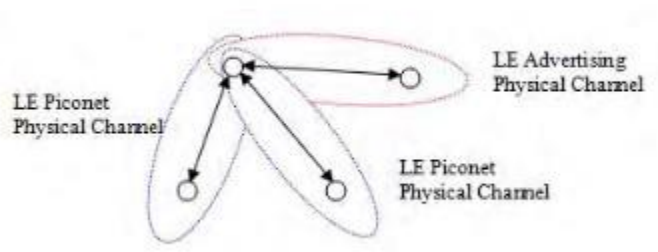

Figure 2-4 BLE topology [27]

A dual-mode implementation is employed to achieve an ultra-low power consumption level by reusing the Bluetooth radio frequency (RF). This results in a power reduction of up to 90% compared to traditional Bluetooth. BLE utilizes a 24-bit CRC for the link layer and employs the advanced encryption standard (AES) with a 128-bit key for data encryption. Additionally, BLE supports the transmission of authenticated data over a non-encrypted channel between two devices that have prior knowledge of each other. This is accomplished using a 128-bit Connection Signature Resolving Key (CSRK). The range of BLE is typically like that of Bluetooth. Table 2-4 shows the key properties of BLE [27].

Table 2-4 Properties BLE[24], [27]

Metric	Quantity/description
Average consumption	10 mW
Peak current	12-15mA
Data speed	1 Mbps
Frequency band	2.4 GHz
Range	10m

Zigbee

Zigbee utilizes the IEEE 802.15.4 protocol, which provides the foundation for its functionality. A typical Zigbee network consists of one or more coordinators, one or more end devices, and optionally one or more routers. See Figure 2-5 for the topology. The range of Zigbee is approximately 100m due to the layout of the network. Zigbee was developed as a low-power alternative to Bluetooth, achieving a power consumption of around 30mW compared to the 100mW of regular Bluetooth.

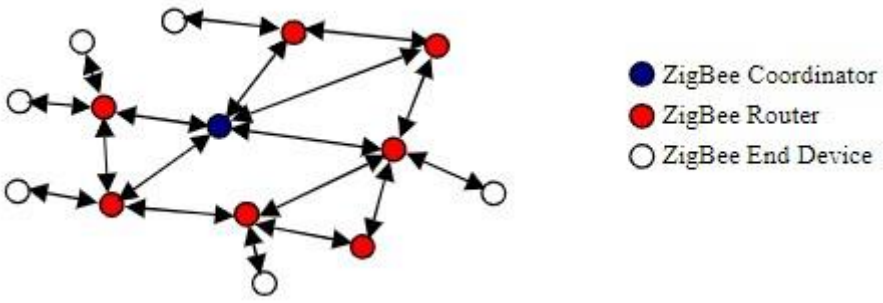

Figure 2-5 Zigbee topology[27]

For error control, Zigbee employs a 16-bit CRC on the link layer. Its security is based on the security specifications established in the IEEE 802.15.4 protocol, utilizing the AES algorithm with a 128-bit key. AES can be used in various Zigbee modes to enhance data privacy, data integrity, and authentication. Refer to Table 2-5 for the key properties of Zigbee[27], [29].

Table 2-5 Properties Zigbee[27], [29]

Metric	Quantity/description
Average consumption	30 mW
Peak current	29 mA
Data speed	250 kbps
Frequency band	868 MHz, 902-928 MHz, 2.4-2.48 GHz
Range	100m

6LoWPAN

To understand the need for 6LoWPAN, let's first examine the use of IPv4 and IPv6 in WBAN applications. One advantage of using IPv4 or IPv6 is that the infrastructure is already established in most locations, making implementation easier. However, there are significant drawbacks. IPv4, for example, has a limited number of addresses. When sensor addresses are needed, they must be chosen from a limited pool shared with other infrastructure. Additionally, traditional encryption technologies and network redundancy are not ideal for WBAN applications.

IPv6 addresses some of these issues by providing a significantly larger address space (2^{128}addresses), more than sufficient for infrastructure and sensors. It also offers higher QoS and improved security capabilities. However, IPv6 does not consider low power consumption, which poses challenges for directly using it as a WBAN technology[29].

Table 2-6 Properties 6LoWPAN

Metric	Quantity/description
Average consumption	30 mW
Peak current	29 mA
Data speed	250 kbps
Frequency band	868 MHz,902-928 MHz,2.4-2.48 GHz
range	200m

This is where IPv6 over Low-Power Wireless Personal Area Network (6LoWPAN) comes into play. It leverages the advantages of IPv6 while mitigating the disadvantages. 6LoWPAN is an international open standard developed by the Internet Engineering Task Force (IETF) for communication within Internet of Things (IoT) applications. It enables small devices with limited computing power to transmit information using the internet protocol. The basic requirements for 6LoWPAN are that devices have a sleeping mode to support power limitations, minimal memory, and reduced routing overhead compared to IPv6[30]. One of the benefits of this technology is its simplicity in communication with other protocols if both can use the internet. It also utilizes the IEEE 802.15.4 protocol, like Zigbee, which simplifies communication between these protocols. However, 6LoWPAN consumes more power to communicate with the internet and lacks as deep sleeping modes as Zigbee. The main advantage of 6LoWPAN is its direct association with IoT applications. This means that it can directly leverage the benefits of IoT, including interoperability, the use of existing infrastructure, cloud storage, readily available tools for remote management, and assistance with diagnosing IP-based networks. IP technology is also more widely known among a broader audience.

Key properties of 6LoWPAN include efficient header compression, automatic network configuration using neighbourhood discovery, support for unicast/multicast/broadcast, fragmentation, and IP routing using the Routing Protocol for Low-Power and Lossy Networks. There is room for improvement within these properties, such as the possibility of further header compression algorithms to reduce header size. The

sending and receiving of packages consume the most power, so a shorter package length can enhance network efficiency by lowering the loss rate and average delay rate. Research has shown potential improvements within the current technology [29]. The most important properties of 6LoWPAN are summarized in Table 2-6. It's worth noting that the security of 6LoWPAN is less robust than Zigbee[29], [30].

2.2.4 Wi-Fi interference

Most technologies operate in the Industrial, Scientific, and Medical (ISM) band, which is available for free use. Wi-Fi, for example, operates within this frequency range and is widely deployed. Consequently, it is important to consider how different technologies, discussed in section 2.2.3, handle interference in this crowded spectrum.

Bluetooth and BLE employ frequency hopping spread spectrum (FHSS) to mitigate interference. Zigbee and 6LoWPAN, on the other hand, use direct sequence spread spectrum (DSSS). However, these methods can introduce delays for WBAN data when internet traffic is high. Since WBAN devices typically have lower transmission power, they can easily get overshadowed by Wi-Fi. The allowed power limits for Wi-Fi are determined by the European Telecommunications and Standardization Institute (ETSI), as shown in Table 2-7(specific to European use).

Table 2-7 Wi-Fi transmission power limits[31]–[33]

Frequency	2.4GHz		5GHz		
	modulation		Channel		
	DSSS/CCK modulation	OFDM modulation	36-64	100-140	155-171
	63 mW	100 mW	200 mW	1000 mW	4000 mW

In emergency or real-time monitoring scenarios, delays caused by interference are unacceptable and can pose serious risks. To address this issue, algorithms can be developed. One option is to have Zigbee technologies transmit over less-utilized Wi-Fi channels. However, Wi-Fi dynamically changes channels based on traffic, requiring Zigbee nodes to keep up with the shifting pattern, consuming significant power, and time. Additionally, this approach limits the available channels for Zigbee. Another option is to use a cooperative carrier signal (CCS) algorithm, which involves an additional sensor that emits a carrier signal to indicate network activity. While effective in practice, this solution requires an extra node, which may not be ideal for wearer comfort in WBAN applications. Several algorithms have been proposed to reduce interference between Wi-Fi and Zigbee when they share the same channel. However, these algorithms often overlook typical WBAN properties such as the star topology, fast emergency transmission, device limitations, and wearer mobility. As a result, the authors of paper [29] suggest developing a different algorithm that distinguishes between emergency data and non-emergency data. According to TG6 technical requirement document, emergency data should be transmitted within one second[34]. Wi-Fi data can be categorized into non-real-time data (NRT) and real-time data (RT). The algorithm only affects NRT data. Simulations show that the algorithm achieves delays below 0.1 second, well below the suggested one-second threshold, ensuring maximum acceptable delay. It also has a minimal impact on NRT connections. Therefore, there is an influence on existing traffic, but it remains within acceptable limits [29].

6LoWPAN is particularly sensitive to interference since it utilizes the data link and physical layers specified in the IEEE 802.15.4 standard for communication. In paper [35], the authors propose a neural network-based routing algorithm to enhance network lifetime, delay, jitter, and signal-to-interference-plus-noise ratio (SNR) to mitigate interference. Table 2-8 presents a comprehensive comparison of different research efforts and their impact on network lifetime[35] .

Table 2-8 Comparison between existing research[35]

Proposed protocol/ year/ reference	year	Packet size	Network size	Method	Network lifetime improvement	E2E delay improvement
Energy aware and load balanced parent selection (EALB)	2015	100 bytes	144 nodes	Dynamic parent selection based on energy (RSSI level), load and MAC super frame distance	On an average by 8.5% for two different mechanisms than standard RPL	On average by 24% for one mechanism whereas degraded for other mechanisms
Energy and congestion aware routing metric (ECRM)	2017	46 bytes	20 to 100 nodes	Dynamic parent selection based on energy and queue usage	Improved regarding EALB	/
Deep neural RPL (DP-RPL)	2020	125 bytes	20 to 100 nodes	Deep nets-based routing (parent selection based on minimum distance, high link quality, maximum energy level of each node)	On average by >50%	On average by >40%
Machine learning RPL (ML-RPL)	2020	125 bytes	20 to 100 nodes	Machine learning based routing (parent selection based on minimum distance, high link quality, maximum energy level of each node)	On average by > 29%	On average by >26%
Based on residual energy ratio (RERBDI)	2016	100 bytes	31 nodes	Objective function with RER-BDI	Yes, in terms of numbers of nodes alive & in terms of higher percentage of battery power remaining in a greater number of nodes	/
Region based (ROEE)	2013	/	31 nodes	RPL with and without resource availability	Yes, in terms of nodes alive	/
Congestion avoidance (CA)	2016	/	10 to 60 nodes	Congestion aware, load balancing, multipath routing	/	Improvement by 30%

Bluetooth, including BLE, is considered the most effective technology for handling interference from other technologies in the ISM band. This is primarily because Bluetooth utilizes FHSS. With the introduction of IEEE 802.15.4e, channel hopping is integrated, further enhancing network robustness in the presence of interference [1]. The main topic of discussion revolves around Wi-Fi, as it is currently prevalent. However, if different systems are employed, they can also create interference among themselves. This study aims to establish a WBAN network specifically for a horse. Nevertheless, horses often find themselves near other horses, resulting in overlapping WBAN networks. Consequently, interference between these networks is inevitable, even if alternative technologies are utilized on different horses. This factor has not been accounted for in the simulations conducted for this research, as the antennas are situated on one horse and are thus part of the same network.

2.3 Applications for animals

WBAN holds various potential applications for animals. One significant aspect is animal health, which plays a vital role in providing essential resources like milk, eggs, and meat. Additionally, WBAN technology can aid in monitoring endangered animal species, enabling us to track their well-being and locations. Furthermore, considering our deep connection and enjoyment of animals' companionship, their health becomes a major concern. WBAN offers a promising solution for monitoring their well-being without causing discomfort, as the sensors attached are hardly noticeable to them [2].

2.3.1 Horses

In this work, we focus on multiple horse breeds. With approximately 60 million horses worldwide, North America has about one-third of the horse population, where horses are mainly kept for sport. These sporting events attract millions of people throughout the year. In Belgium, there were around 303 077 equidae (horses, ponies, donkeys, and zebras) in 2020, often used for recreational, sporting, or professional purposes [36], [37]. Horses are expensive to maintain and require a lot of care. Horses are also among the most searched pets online, with people often trying to find out which breeds are best suited for their needs[38] . Whether or not you have a fondness for horses, it's clear that their population is increasing, and this requires proper care, health tracking, and performance monitoring.
For instance, horses can experience a condition known as laminitis, which can lead to lameness and affect their gait. They may exhibit symptoms such as weight shifting (paddling), increased digital pulses (bounding), and heat around the hoof wall. Other signs include changes in cardiovascular health, loss of appetite (anorexia), trembling muscles, elevated respiration and pulse rates, and fluctuating body temperature[4]. Colic is another serious and potentially deadly disease that commonly affects domesticated horses. In 2001, the insurance expenses for treating this illness surpassed $115 million. Horses suffering from colic display various symptoms, including excessive pawing, or scraping at the ground, frequent stretching, and urination, closely watching their flanks, biting at their stomach, repeatedly lying down, and getting up, rolling, groaning, loss of appetite, increased heart rate caused by pain and decreased circulation, and even absence of gut sounds[3]. Early detection of any disease can significantly improve the chances of a cure. A WBAN system could be employed to monitor the symptoms mentioned above and alert caretakers without disturbing the horse, enabling them to intervene promptly and prevent severe health consequences.

2.4 Antennas and a (human) body

This section explores the impact of a (human) body on the functionality of an antenna, as well as the influence of the antenna on the (human) body. The goal is to gain a better understanding of the precautions that should be considered when selecting an antenna to ensure optimal performance and minimize any potential effects on the (human) body.

2.4.1 Off, on or in body communication

Body communication can be classified into three types: off-body, on-body, and in-body communication [39]. Off-body communication refers to scenarios where only a few antennas are located on the body, while the majority are situated in the surrounding area. On-body communication, on the other hand, involves most of the antennas being on the body, with only a few located in the surrounding area. In-body communication is primarily used in the medical field, where an antenna is implanted inside the body.

2.4.2 Effects of antennas on the (human) body

Radiation

Antennas are typically designed to operate within the unlicensed and freely available Industrial, Scientific, and Medical (ISM) band. However, it is crucial to monitor radiation levels as the frequencies in this band possess sufficient energy to induce cellular movement and raise cell temperatures. The increase in temperature is particularly significant as it can potentially lead to harmful effects on human tissues. This temperature rise is partly attributed to the absorption of radiation by human tissue, which can be measured

using Specific Absorption Rate (SAR). The penetration of radiation into body tissue can contribute to serious health hazards. The World Health Organization (WHO) has reported that radio frequency electromagnetic waves have become a major source of pollution, posing potential threats to human health. Excessive exposure to electromagnetic waves has been linked to brain tumours, cancer, sister chromatid exchange, and other health issues. However, the existence of conclusive evidence remains a subject of debate, with some studies supporting these claims and others finding no correlation. Regardless, it is essential to minimize the associated risks when designing antenna's for WBAN [40]–[42].

Specific absorption rate (SAR)

To be able to measure the heating effect of radiation on tissue the federal communication commission (FCC) introduced specific absorption rate (SAR) limits for wireless devices to ensure acceptable radiation levels in the human body. These limits differ between the US and Europe. The US limit is 1,6W/kg averaged over one gram) where the Europe limit is 2,0W/kg averaging over ten grams. The US specifications are harder to achieve so in general if a device meets US specifications it will typically meet European specs[12].The SAR parameter is used to measure the rate at which radiofrequency energy is absorbed by human tissues. The formula for SAR is given in equation (2.1) : [12], [43]

$$\mathrm{SAR} = \int_{sample} \frac{\sigma(r)|E(r)|^2}{\phi(r)} dr \qquad (2.1)$$

In which:

SAR: specific absorption rate [W/kg]
$\sigma(r)$: electrical conductivity [S/m]
E(r): induced E-field from radiated energy [V/m]
$\rho(\mathrm{r})$: mass density of the tissue [kg/m^2]

SAR reduction

A first method of reducing SAR is by adding a ground plane to an antenna. This is because the SAR for on-body antennas relies on the near-field coupling to the body. Therefore, methods to reduce SAR include modifying the ground plane to use electromagnetic bandgap (EBG) structures or periodic conductive structures which filters electromagnetic waves at certain frequency bands. An additional method to improve SAR is using high-impedance surfaces (HIS) to help block electromagnetic waves within a certain frequency band and allow for an increase in front to back ratio which reduces the SAR in the body. HIS also prevents propagating surface waves and reflects electromagnetic waves with no phase reversal.
Integrating an artificial magnetic conductor (AMC) into the ground plane is another effective method as the AMC serves as an isolator. Other frequently used methods are ferrite sheets and metamaterials. The SAR value can be influenced by the position of the antenna [41] and depends on the type of tissue located beneath it. Different tissues, such as bone and fat, have varying degrees of radiation absorption. In mobile phones for example, the antenna is typically placed at the bottom to keep it away from the brain. Additionally, adjusting the impedance match and utilizing parasitic resonators can disrupt the antenna's radiation pattern, potentially leading to a reduction in SAR levels [44].

2.4.3 Effects of the (human) body on antenna

The dielectric constant of the human body is shown in Table 2-9. These lossy and high dielectric constants result in a variety of input impedance, fragmentation of the radiation pattern, impedance variations, frequency shift and reduced efficiency of the antenna [45].

Table 2-9 Dielectric properties of different tissues at 2,45 GHz[46]

Tissues	Thickness (mm)	ε_r	σ (S/m)
Skin	4	38,0	1,46
Fat	4	5,28	0,1
Muscle	50	52,7	1,74

2.5 Antenna properties

In this chapter, we will examine the antenna the tools needed to accurately help develop and choose a WBAN antenna. Such properties include but are not limited to frequency, S-parameters, field regions and link budget.

2.5.1 Frequency

Frequency is defined as how often a complete cycle of the signal is complete in one second.
The frequency in antenna's can theoretically be chosen freely. However as discussed in section 2.4.2 the frequency needs to be chosen carefully to reduce the SAR value. Lower frequencies travel further but have a larger wavelength, this will cause the antenna to have a larger dimension which is not useful in wearable applications. Aside from these restrictions there are rules and regulations when it comes to the use of a certain frequency. Within Belgium the organization BIPT (Belgian institute for postal services and telecommunications) can give out licensing for certain frequencies(band).
For research purposes there is a special frequency band, the ISM-band (industrial science and medical) this band of frequencies is defined from 6765 MHz to 246 GHz which are free of use.[47]

2.5.2 Received power/ Friis equation.

The power received at the receiving antenna can easily be expressed by formula (2.2) also known as the Friis formula. However, this is only true if the path loss exponent has a value of two meaning free space. More on this in section 2.6. How good this holds up in this application is one of the things that will be measured [44].

$$P_r = \frac{P_T G_T G_R \lambda^2}{(4\pi d)^2} = \frac{P_T G_T G_R}{L} \qquad (2.2)$$

In which:

- P_r: power received [W]
- P_T: power transmitted [W]
- G_T: gain transmitting antenna [dB]
- G_R: gain receiving antenna [dB]
- L: path loss

2.5.3 Link budget

The link budget gives an idea of the gains and losses the transmitting power has before getting to the receiving antenna. Gains mostly come from the antenna design while losses could have different causes such as weather, multipath, diffraction and shadowing to name a few. Formula (2.3) gives an approach to link budget.

$$P_r = P_t + \mathrm{G} - \mathrm{L} \qquad (2.3)$$

In which

P_r: power received [W]
P_T: power transmitted [W]
G: gain [dB]
L: losses [dB]

2.5.4 S-Parameters

Scattering parameters are a versatile representation method for characterizing networks, applicable to both high and low frequency circuits. However, they are primarily used in high-frequency circuits due to the challenges in accurately defining impedance and admittance parameters at higher frequencies. This limitation arises from three key factors. Firstly, it may not always be possible to uniquely define appropriate voltages or currents for a network. Secondly, direct measurements of voltage, current, impedance, and admittance can be impractical. Lastly, measurements of impedance and admittance would ideally require short circuit and open circuit conditions, which are difficult to achieve in practice at high frequencies as they can lead to circuit oscillations.
In the presented circuit diagram (Figure 2-6), a circuit with N ports is depicted. The parameters are denoted with indices "ii" or "ij". When referring to S_{ii}, it is often called the reflection coefficient, as it represents the ratio of the reflected wave to the incident wave for port i, assuming all other ports are matched and terminated. On the other hand, the scattering parameter S_{ij} represents the ratio of the amplitude of the wave transmitted through port i to the amplitude of the incident wave on port j, assuming all ports except the jth port are terminated[48].

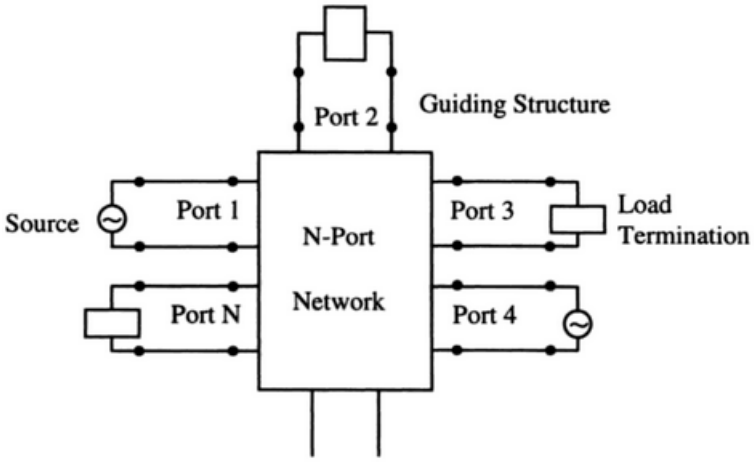

Figure 2-6 N-port network[48]

2.5.5 Field regions

Around the antenna, three primary regions exist: the reactive near field, radiative near field, and far field. These fields play crucial roles in understanding the propagation and interaction of electromagnetic waves around the antenna. This section explores these fields in more detail.

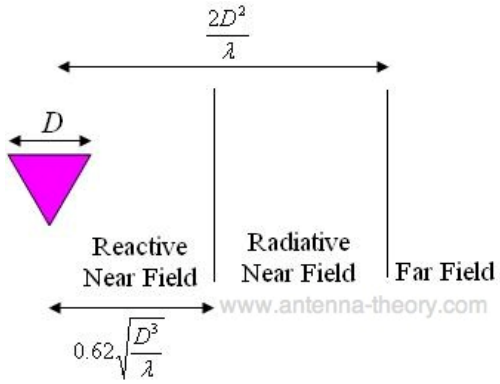

Figure 2-7 Illustration of the field regions for an antenna of maximum linear dimension D [44]

Far-field or Fraunhofer region

This is the field furthest away from the antenna. In this field, the radiation doesn't change shape with distance R. The E- and H-fields do still die off as does the power density. The far field is dominated by radiated fields where E- and H-fields are orthogonal to each other and the direction of propagation. [44]
The far field is defined by 3 equations:[44]

$$\mathrm{R} > \frac{2D^2}{\lambda} \tag{2.4}$$

$$R \gg D \tag{2.5}$$

$$R \gg \lambda \tag{2.6}$$

In which:

R: distance [m]
D: maximum linear dimension of antenna [m]
λ: wavelength [m]

Equation (2.4) and (2.5) ensure that the power radiated in each direction from distinct parts of the antenna are approximately parallel. This ensures that fields in the far-field region behave like plane waves. Equation (2.6) ensure that near field is gone.[44]

Reactive near field

In this region the fields are predominately reactive fields. This means that the E- and H-field are out of phase by 90 degrees to each other. Due to these problems like deflection back into source feeding of the antenna can occur [44].
This zone is roughly defined by.

$$R < 0{,}62\sqrt{\frac{D^3}{\lambda}} \tag{2.7}$$

In which:

R: distance [m]
D: maximum linear dimension of antenna [m]
λ: wavelength [m]

Radiating near field or Fresnel region

Is defined as the region between near and far field. In this region the reactive fields are not dominant, and the radiating fields begin to emerge. The radiation pattern may vary depending on distance.
The region is commonly described by formula (2.8) [44]:

$$0{,}62\sqrt{\frac{D^3}{\lambda}} < \mathrm{R} < \frac{2D^2}{\lambda}$$

(2.8)

In which:

R: distance [m]

D: maximum linear dimension of antenna [m]

λ: wavelength [m]

Depending on the values of D and wavelength this region might not exist at all.[44]

2.5.6 Radiation pattern

A radiation pattern defines the variation of the power radiated by an antenna as a function of the direction away from the antenna. This power variation is observed in the far field. This will often be plotted in dB. This can be plotted in 3D or 2D where the 2D represents a "slice" of the 3D model. Two angles are used to represent this. The elevation angle θ measured of the Z-axis and the azimuth angle ϕ measured counterclockwise of the x-axis[44] .

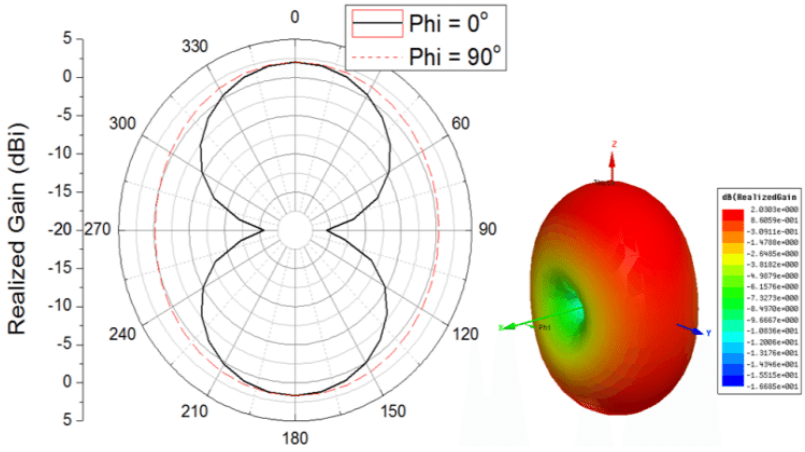

Figure 2-8 Radiation pattern in (a) a 2D view and (b) a 3D view [49]

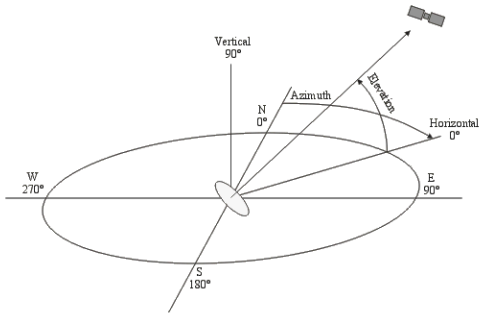

Figure 2-9 Azimuth and elevation

2.5.7 Directivity

Directivity is a measure of how directional an antenna's radiation pattern is. An isotropic antenna (radiates equally in all directions) will have zero directionality and the directivity would be 1 (or 0dB)[44]

Directivity can be defined for every angle but when spoken about the directivity the peak directivity is meant[44]

2.5.8 Antenna efficiency

The antenna's radiation efficiency is the ratio of power delivered to the antenna relative to the power radiated from the antenna. A high radiation efficiency means that most of the power present at the antenna's input is radiated away. If the antenna radiation efficiency is low this means part of the power is lost in e.g., impendency mismatch. The antenna radiation efficiency is not influenced by the fact that the antenna is a receiving or transmitting antenna.
The radiation efficiency can also be expressed by formula (2.9) [44]

$$\epsilon_r = \frac{P_{radiated}}{P_{input}} \quad (2.9)$$

With:

ϵ_r: ratio between 0 en 1
$P_{radiated}$: power radiated from antenna [W]
P_{input} : power on input antenna [W]

Another way of calculating the efficiency of an antenna is using the total efficiency, this is the radiation efficiency multiplied by the impedance mismatch loss of the antenna when connected to a transmission line or receiver.
It can be represented by formula (2.10)[44] :

$$\epsilon_T = M_L . \epsilon_r \quad (2.10)$$

In which:

ϵ_T: total efficiency
M_L = antenna's loss due to impedance mismatch
ϵ_r: ratio between 0 en 1

For the continuation of this paper antenna efficiency refers to the total efficiency.

2.5.9 Antenna gain

The antenna gain describes how much power is transmitted in the direction of peak radiation compared to that of an isotropic source. When antenna gain is discussed in function of the angle this is essentially the same as the radiation pattern as explained in section 2.5.6. If a single number is mentioned, it refers to the maximum gain of all the directions.
The directivity and gain of an antenna can be used to calculate gain[44]

$$\mathrm{G} = \epsilon_R \mathrm{D} \quad (2.11)$$

In which:

G: gain[dB]
ϵ_r: antenna efficiency
D: directivity

2.5.10 Impedance of an antenna

Impedance relates the voltage and current at the input to the antenna. The real part pf the antenna impedance represents power that is radiated away or absorbed within the antenna. The imaginary part of the impedance represents the power that is stored in the near field of the antenna. This is the non-radiated power. If the input impedance is real (imaginary part is 0) the antenna is resonant. However, an antenna can be resonant in one frequency and not on another because impedance depends on the frequency.
It's important to match the antenna impedance to that of the transmission line. This will minimize the losses and power being reflected to the generator. This loss of power is known as an impedance mismatch[44]. In general, the impedance of an antenna is taken at 50 Ω.[50]

VSWR

The voltage standing wave ratio gives a measure of how well matched the antenna is to the transmission line or receiver. This number is always greater than or equal to 1. Where 1 indicated that there is no mismatch loss[44]

$$\mathrm{VSWR} = \frac{1 + |\Gamma|}{1 - |\Gamma|} \qquad (2.12)$$

In which:

Γ : reflection coefficient also known as S11.

To have an idea what VSWR values mean Table 2-10 can be used. It also shows that VSWR is not a linear function.[44]

Table 2-10 VSWR and reflected power[44]

VSWR	Γ (s11)	Reflected Power (%)	Reflected Power (dB)
1.0	0.000	0.00	-∞
1.5	0.200	4.0	-14.0
2.0	0.333	11.1	-9.55
2.5	0.429	18.4	-7.36
3.0	0.500	25.0	-6.00
3.5	0.556	30.9	-5.10
4.0	0.600	36.0	-4.44
5.0	0.667	44.0	-3.52
6.0	0.714	51.0	-2.92
7.0	0.750	56.3	-2.50
8.0	0.778	60.5	-2.18
9.0	0.800	64.0	-1.94
10.0	0.818	66.9	-1.74
15.0	0.875	76.6	-1.16
20.0	0.905	81.9	-0.87

2.5.11 Bandwidth

The bandwidth of an antenna refers to the frequency range in which it can efficiently transmit or receive energy. This bandwidth is often specified in terms of VSWR, indicating that the antenna's VSWR remains below a certain level within a particular frequency range. While changes in radiation pattern may occur at different frequencies, they are typically not significant.

2.5.12 Polarization

The polarization of the antenna is the polarization of the radiated fields produced by an antenna evaluated in the far field.[44]
there are 3 kinds of polarization[51]

Linear polarization

There is only one immutable direction of polarization. The surface of the earth is used as reference. A vertical polarization is when the electrical field is perpendicular to the earth's surface and a horizontal polarization is when the electromagnetic field is parallel to the earth's surface.

Elliptical polarization

This is when the electrical field vector turns in the polarization plane in function of time. The electrical field is not constant which gives the ellipse shape in the polarization field.

Circular polarization

The electrical field is constant when the electrical field vector turns in the polarization plane in function of the time. Often there is a distinction between RHCP (right hand circularly polarized) and LHCP (left hand circularly polarized). Meaning they turn clock or counterclockwise respectively when looking away from the source.

Polarization is an important property to consider when working with LOS antennas. Only when sending and receiving antenna have the same polarization can an optimal power transmission be achieved. The losses due to a miss polarization are called polarization loss. Figure 2-10 gives an idea of polarization losses between antenna's[51]. Note that the polarization loss between a linear and a circular polarization is always 3dB. This is because a circular polarization is really two orthogonal linear polarized waves 90 degrees out of phase. Therefore, the linear polarized antenna will pick up the in-phase component of the circularly polarized wave.[44]
The polarization loss is sometimes referred to as polarization efficiency, antenna mismatch factor or antenna receiving factor. All these names refer to the same concept.[44]

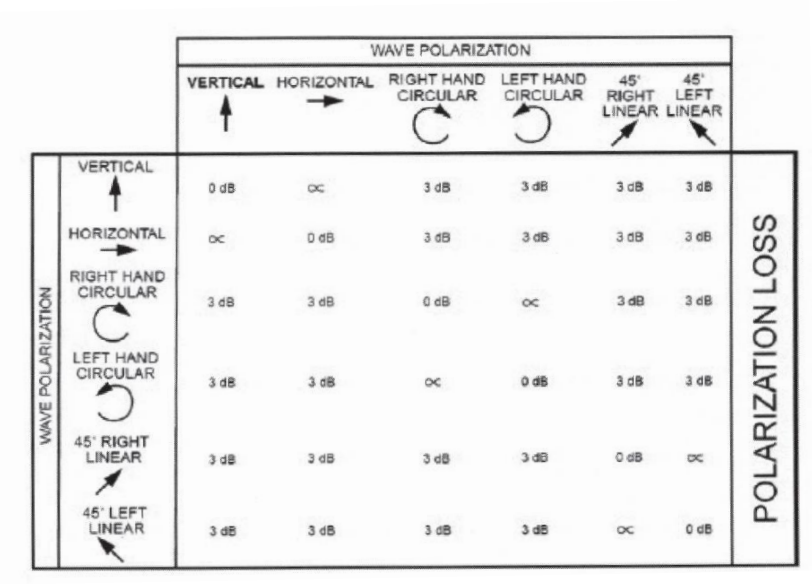

Figure 2-10 Overview if polarization loss between 2 antennas [51]

In practice is a perfect polarization (almost) impossible. Therefore, it's important to mention cross-polarization. This gives a measure of how well an antenna can receive/send signals that aren't correctly polarized. [51]
When working in NLOS polarization is not as important since the environment is responsible for depolarization. For example, a RHCP wave will become a LHCP wave.[51] This can be used in LOS applications too since a RHCP expecting a RHCP can safely ignore LHCP signals since they are most likely not the direct signal but rather signals that have reflected of something. This principle is used in GPS[44].

2.5.13 Received power / Friis equation.

To calculate the received power by an antenna the Friis transmission formula is used.

$$P_R = \frac{P_T G_T G_R \lambda^2}{(4\,\pi\, R)^2} \qquad (2.13)$$

In which:

P_R: power received by antenna [W]
P_T : power delivered to transmitting antenna [W]
$\mathrm{G_T}$: antaanna gain in the direction of the receiving antenna [dB]
G_R: antanna gain of the receiving antenna [dB]
R : distance between the two antennas [m]
λ: wavelength [m]

2.6 Path loss

Path loss is determined by several factors. For this study it will be assumed that the body does not move. However, postural body movement and node mobility cannot be ignored if this application is used outside of the experimental environment. There would also be an additional doppler effect in the case of movement of the body.
Path loss can be expressed as (2.14) or (2.15). which shows clearly that path loss is dependent on distance and frequency[28].
The path loss exponent is chosen depending on the situation in which the communication takes place as shown in Table 2-11

$$\mathrm{L}(d) = \left(\frac{4\pi}{\lambda}\right)^2 d^n \qquad (2.14)$$

$$L_{dB} = 21{,}98\mathrm{dB} - 20\log\lambda + 10\mathrm{n}\log d \qquad (2.15)$$

In which:

L: path loss
λ: wavelength [m]
d: distance [m]
n: path loss exponent as shown in Table 2-11.

Table 2-11 path loss exponent based on different environments [52]

Environment	Path loss exponent
Free space	2
Urban area	2.7 – 3.5
Suburban area	3 – 5
Indoor line-of-sight	1.6 – 1.8
Obstructed in building	4-6
Obstructed in factories	2-3

However, this is not a completely realistic approach as other effects also have an influence on the pathloss. Figure 2-11 gives a realistic approach to path loss. Effects such as (body) shadowing can be partially

simulated. Some effects such as multipath however cannot be simulated that easily and might cause difference between simulation and real-life implementation. These effects will be discussed in the following sections.

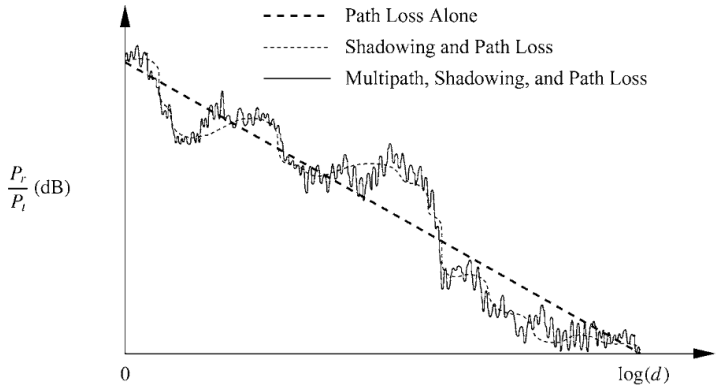

Figure 2-11 Path loss, shadowing and multipath versus distance[53]

2.6.1 Fading marge

Fading can happen for a variety of reasons, including energy absorption, reflection, diffraction, body shadowing, body posture, and multipath. There are two categories of fading: small scale and large-scale fading.
Small scale fading refers to rapid fluctuations in amplitude and phase of the received signal over a small local area and short period. This type of fading occurs due to small changes in the nodes' location on the body or body posture.
On the other hand, large-scale fading occurs due to signal attenuation resulting from mobility over large areas. It is caused by variations in the signal's distance between the antenna on the body and the external node, often resulting from diffraction by large surrounding objects.
To incorporate a certain level of fading into the system's design, a fading margin is set. This ensures that even if fading occurs, the system remains operational [54].
Some of the effects causing fading are discussed below.

Shadowing

Shadowing is caused by obstacles between the transmitter and receiver that attenuate the signal power through absorption, reflection, scattering and diffraction. When the attenuation is strong the signal can even be blocked.[53]
Shadowing can be divided into different categories namely position-depended shadowing caused by obstacles in the environment and orientation depended on shadowing caused by movements of the body and which the antennas are attached. [55]

Body shadowing

Body shadowing is the effects a living organism’s body has on the working of an antenna. A body is a complex object that can scatter, absorb, and reflect waves, therefore causing significant variations in signal strength. In Figure 2-12 a simplified scenario is shown in which wireless transmission between sensors occurs with and without human body shadowing. In the first case Figure 2-12(a) there is no obstacle between the transmitting node 1 and receiving node 2. This assumes signal attenuation in an open environment and there will be a successful transmission. In the second case Figure 2-12(b) the presence of the body in the transmission path between the nodes will cause additional attenuation of the wireless link and body shadowing occurs. If there is a low fading margin this may lead to a loss of packets or even break the wireless link. [6]

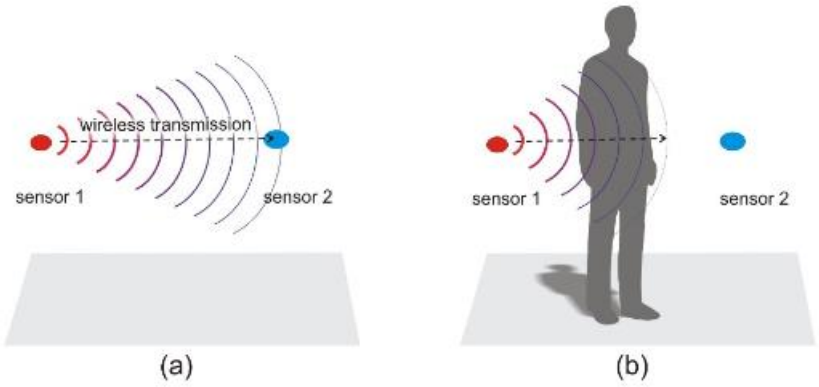

Figure 2-12 influence of body shadowing on wireless transmission between sensors: (a) No shadowing, successful transmission; (b) body shadowing that affects transmission [6]

Figure 2-13 gives an idea of the attenuation. It shows an experiment where a body that has a flexible patch antenna is rotated in an anechoic chamber to see what the maximum attenuation is caused by body shadowing. The body doesn't change positions in this scenario, this could possibly add even more attenuation.[9]

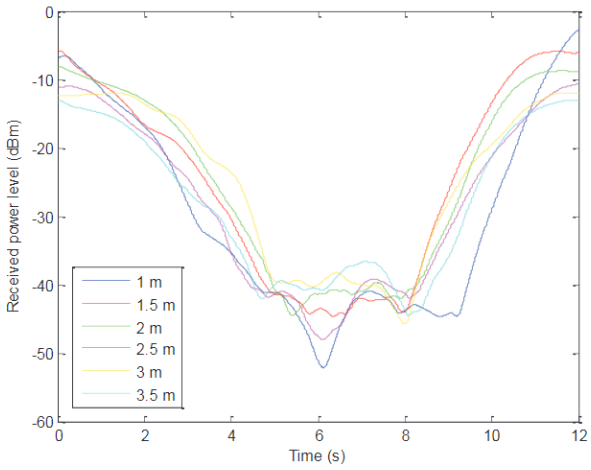

Figure 2-13 Body shadowing for rotation of body at distance points from 1m to 3,5m calculated using a moving window of 1000 samples [9]

When there is a line of sight between the antenna the path loss can be calculated using the log-distance path loss equations (such as equation (2.15)), however, if there are obstruction factors such as respiration and body movement will have noticeable effects on the received signal characteristics. [9]

Multipath

Multipath is when a signal can take multiple paths from transmitter to receiver. These paths are often created due to reflection, refraction, or diffraction. Multipath can lead to distortion, signal interference and fading which all are bad for communication. However multipath isn't always a bad thing. Due to the relative locations of some antennas and body shadowing some antennas would be unreachable. Multipath can help mitigate the effects of body shadowing.

2.6.2 Path loss model

Path loss is the attenuation of an electromagnetic wave as it propagates through space. A path loss model is a mathematical model that describes the attenuation of an electromagnetic wave as it propagates through the medium. The focus of this thesis is on the influence of a body on the pathloss. Therefore, this subject is explored more extensively. There are different kinds of path loss models for WBAN applications. They are often included in a channel model which envelops the gains and losses of the used channel.

Types of models

There are different types of models to create the path loss model namely the theoretical model and the empirical model. Most models won't be purely theoretical or purely empirical but rather a combination of both, often starting with a theoretical approach and adjusting parameters based on experimental measurements. Often models will consider the gain of an antenna. However, when this is not the case for a model it is called an antenna de-embedded model.

Theoretical model

A theoretical model is based on fundamental principles of electromagnetic propagation and will permit precise modelling of a specific situation. It requires a detailed description of the propagation environment and is therefore not suitable for macro environments [54].

Empirical model

An empirical model is a mathematical or statistical model that is based on observed data rather than a theoretical consideration [54]. An empirical model is often used because the (human)body has a complex shape and internal structure which makes it hard to render a simple path loss model [56]. The empirical model is intended to provide a convenient basis for the statistical modelling of the channel. Compared to the theoretical model this model will use a greatly simplified description of the environment making it more stable for macro environments [54].

Antenna de-embedding propagation models / true path loss/antenna-independent path loss model

Path loss models often consider antenna gain. To separate the antenna from the underlying channel "antenna de-embedding propagation" models exist [57]. It is then possible to add G_{TX} and G_{RX} which are the gains and transmitting or receiving antenna gets in the environment of a body [57]. In literature [57] is mentioned when excluding gain, the deviation between measured and simulated path loss decreases. Another advantage of this model is that it is less dependent on the type of antenna, giving it a wider field of application [57].

Channel models

Models based on Friis formula.

A formula often used in research is (2.18) based on the Friis formula (2.16) [56],[58]-[7]. This is a semi-empirical formula [58].

$$P_R = \frac{P_T G_T G_R}{L} \tag{2.16}$$

$$L = \left(\frac{4\pi}{\lambda} d^n\right) \tag{2.17}$$

$$P_L(d) = PL(d_o) + 10.n.log\left(\frac{d}{d_0}\right) + X_\sigma \tag{2.18}$$

In which:

- P_R: power received [W]
- G_T: gain transmitted [dB]
- G_R : gain received [dB]
- L: loss expressed as in (2.17) []
- n: path loss exponent []
- d: propagation distance between 2 antennas [m]
- d_0: reference distance [m]
- X_σ : gaussian zero-mean random variable with standard deviation σ []

Path loss exponent

The path loss exponent (n in (2.18)) indicates the rate at which the path loss increases with distance [58]. It can be chosen to fit the measurements that are known so to best fit a certain environment or body [56],[59],[60]. The path loss exponent is 2 in free space but can have different values as shown in Table 2-12. For the human torso and arm it's around 3,3 as shown in Table 2-13 [7]. The path loss exponent gives an easy and accessible variable to make the formula fit best with measurements and therefore predict unknown new situations.

Table 2-12 path loss exponent based on different environments [52]

Environment	Path loss exponent
Free space	2
Urban area	2.7 – 3.5
Suburban area	3 – 5
Indoor line-of-sight	1.6 – 1.8
Obstructed in building	4-6
Obstructed in factories	2-3

Table 2-13 Parameter values of the path loss models for the arm and torso [7]

parameter	arm	torso	arm + torso
d_0 [cm]	10	10	10
$P_{0,dB}$ [dB]	32.2	41.2	35.7
n [-]	3.35	3.23	3.38
σ [dB]	4.1	6.1	6.2

Adding attenuation

The human body is a complex medium and can be described using permittivity ϵ_r, dielectric constant (κ), conductivity σ and characteristic impedance Z_0 as shown in Figure 2-14. These cause electromagnetic effects such as energy absorption, reflection, diffraction, and shadowing.

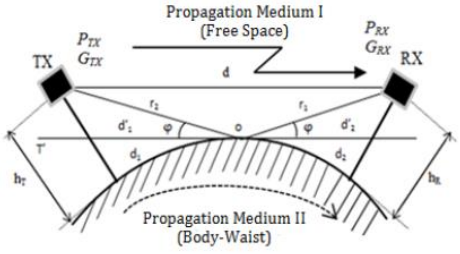

Figure 2-14 On-body communications details [61]

Research [61] looks specifically at the body waist and proposes to take the Friis equation (2.16) in free space (path loss exponent = 2) and add an attenuation α_B written in $\frac{Np}{m}$ as shown in (2.19) or in dB such as shown in (2.20).

$$\alpha_B\left(\frac{Np}{m}\right) \approx \frac{\sigma}{2}\sqrt{\frac{\mu_0}{\epsilon_0\epsilon_r}} \quad (2.19)$$

$$\alpha_B(dB) \approx \frac{520{,}8\pi\sigma}{\sqrt{\epsilon_r}} \quad (2.20)$$

In which:

σ: conductivity $[\frac{S}{m}]$

μ_0 : permeability in vacuum []

ϵ_0: vacuum permittivity []

ϵ_r: relative permittivity []

In the paper [61], the distance between the Tx and Rx is 25cm on the human waist giving an attenuation of approximately 100dB. When the antennas are aligned Figure 2-15 shows the difference between the free space path loss and the total path loss with α_b. This formula is an example of a non-empirical model. This means the results that are presented assume that the human waist is a PEC cylinder with a complex material at 2,4GHz.

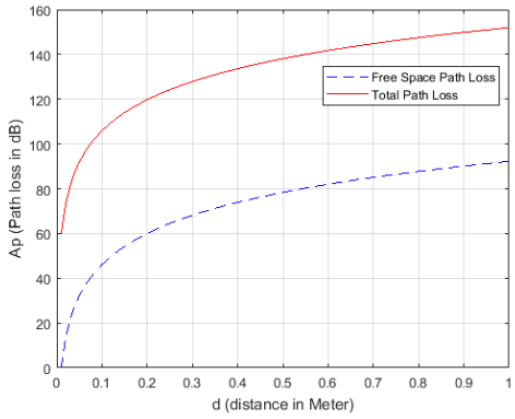

Figure 2-15 Path loss variations [61]

Further testing on this model is done in research [62] where for each point a total of 50 measurements were recorded for a time-varying electrical field and the average received power was calculated for a fixed 2,4GHz frequency. The results of this are shown in Figure 2-16. There is a good match for distances less than 40 cm but at 35 cm an abrupt change of channel is noticed.

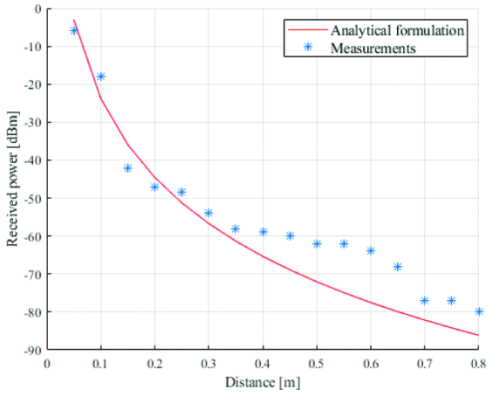

Figure 2-16 Analytical and measured received power on the human body at 2,4GHz [62]

Averaged path loss model

An alternative approach to understanding the path loss model involves examining various measurements and determining the most suitable formula for each measurement. This would entail different formulas for different locations on the body and even for different body types. However, this approach is not very practical. Therefore, it is more realistic to use an average path loss model that can be applied to a general body/scenario. This model can be derived by fitting all known measured data, employing methods such as least-square error fitting, and thereby facilitating predictions for future setups [58].

These diverse measurements could encompass different body parts [7] or comparisons between different body types [58]. The advantage of utilizing an averaged path loss model is that it reduces the likelihood of issues such as those illustrated in Figure 2-17. In Figure 2-17, various measurements on different male bodies result in different path losses due to variations in their physical characteristics. The maximum variation observed is 12.03 dB, primarily attributed to differences in trunk size, which leads to distinct path loss coefficients as depicted in Figure 2-18. A smaller trunk size corresponds to reduced non-line-of-sight (NLOS) propagation and fewer obstructions, resulting in lower path loss values. For ankle channels, the subject's height plays a significant role. The numbers relate specifically to narrowband (as used in this paper), but similar conclusions can be drawn for ultra-wideband (UWB). The narrowband path loss exponent exhibits a maximum variation of 0.85, whereas for UWB, the maximum variation is 1.115. However, UWB generally has a lower overall path loss exponent. This is because UWB encounters additional effects such as reflection, diffraction, and scattering, unlike narrowband, and UWB is highly resilient to multipath interference, all contributing to the lower path loss exponent [58].

If a model were to be constructed using only one male body as a reference, the path loss exponent would not accurately represent other individuals. An averaged path loss model helps alleviate this issue by incorporating values from multiple sources, making it a better fit for the average male body.

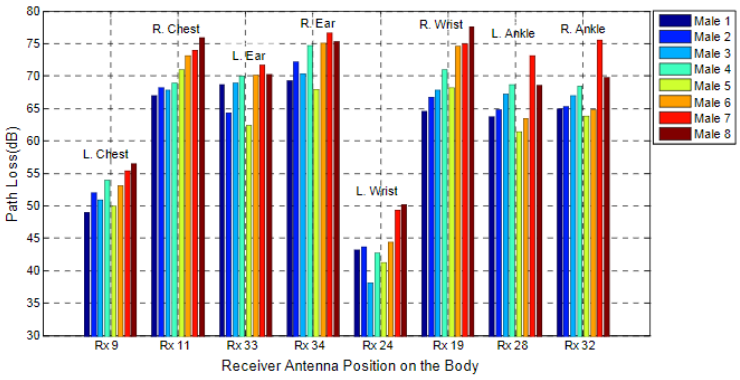

Figure 2-17 The variation of path loss for eight different narrowband on-body radio propagation channels for different human test objects [58]

Dimensions and path loss exponents	Male 1	Male 2	Male 3	Male 4	Male 5	Male 6	Male 7	Male 8
Height (cm)	182	181	186	178	169	168	188	180
Chest circumference (cm)	87	91	92	93	94	114	124	136
Waist circumference (cm)	79	81	82	86	89	96	130	140
Weight (kg)	70	73	74	78	68	91	120	128
Path loss exponents (γ) for the narrowband system at 2.45 GHz	3.20	3.25	3.31	3.39	3.48	3.71	3.85	4.05
Path loss exponents (γ) for the UWB system at 3–10 GHz	1.91	2.0	2.08	2.19	2.33	2.62	2.8	3.06

Figure 2-18 The dimensions (height, shapes, size) and narrowband and UWB path loss exponents (γ) of the eight test subjects [58]

2.7 Wearable antenna technologies

Wearable technologies can incorporate different types of antennas, each with its own unique specifications, advantages, and disadvantages. In the following section, we will explore these various antennas and discuss the reasons behind their selection or exclusion for this application.

2.7.1 Printed dipole antennas.

Shown in Figure 2-19 dipole antenna is popular due to its low profile, ease of production and low cost. It also has wide frequency coverage. Dipoles, however, are large which makes it harder to use them in space-restricted applications.[45]

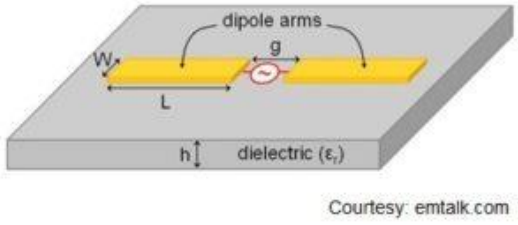

Figure 2-19 Printed dipole [45]

2.7.2 Monopole antennas

Monopole antennas are half the size of dipoles and are mostly mounted above the ground plane. They have a good radiation performance if placed above a high impedance surface (HIS). They are low profile, low cost and easy to fabricate. They are ideal to integrate into clothing[45]

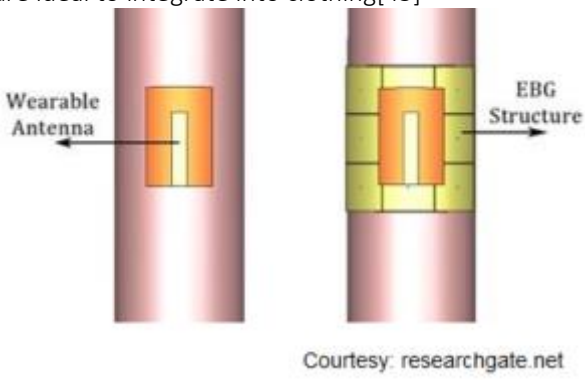

Figure 2-20 Monopole antenna[45]

2.7.3 Printed loop antennas.

The printed loop antenna can be made from single or multiple loops in different closed geometric shapes. The dimension of a loop antenna I less than a wavelength, this ensures that the current throughout the loop remains in phase. These antennas are light in weight and have a simple and compact structure. However, they have relatively poor efficiency which results in power loss in the form of heat. There are two main forms of antennas the large loop which is used for both transmission and reception and the small loop which is used for reception. These antennas are ideal for small radio devices and body-worn communication systems suitable for military applications.[45]

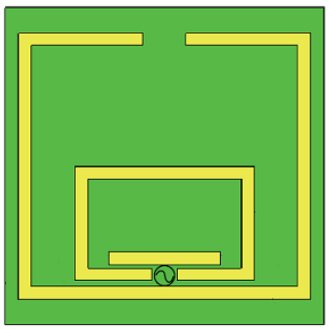

Figure 2-21 Printed loop antenna[45]

2.7.4 Slot antennas

The slot antenna is a flat metal surface with fine narrow slots. They are very versatile and are used typically at frequencies between 300MHz and 24 GHz. It has an omnidirectional radiation pattern and linear polarization. The operation characteristics are determined by the slot size, shape, and material characteristics of the antenna. The simple structure and flexible nature make it suitable for small form-factor wearable applications. It can easily be implemented on flexible surfaces such as denim making it ideal for medical and military applications. The antenna will have an effective transmission even if the (human) posture changes[45]

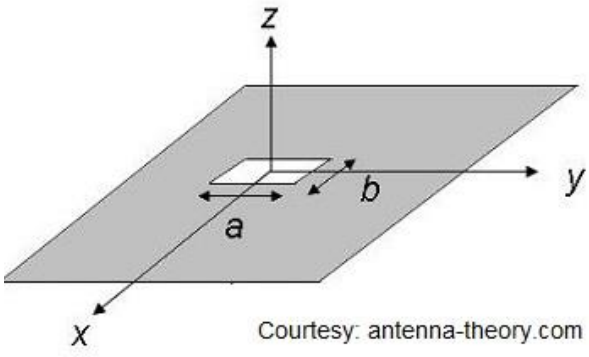

Figure 2-22 slot antenna[45]

2.7.5 Planar inverted-F antennas (PIFA)

This antenna is used in portable smart devices. They resemble an inverted f which gives them their name. They have a low profile and are omnidirectional which makes them popular with wearable product developers. They can be printed on substrates or circuit boards making them easy to make. They have good on-body results and good SAR values making them ideal for body-worn electronic devices.[45]

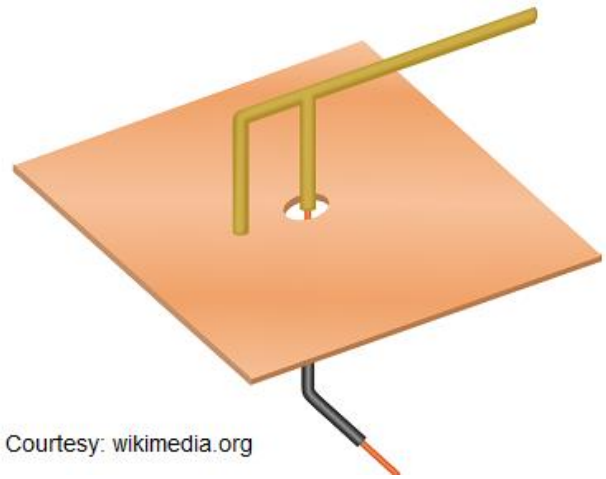

Figure 2-23 Planar inverted - F antenna[45]

2.7.6 Microstrip antenna /patch antenna

Microstrip antennas are metallic strips or patches mounted on a substrate. They are simple to design and inexpensive to manufacture due to their two-dimensional structure. The antenna allows linear or circular polarization. They are easily mounted on rigid surfaces. They are available in different geometrical forms. Their downside is a small frequency band. They are used by most GPS devices.
Due to its ease of production and a substrate that can help reduce the SAR in the body this kind of antenna is chosen for this thesis. Therefore, a more in-depth look is given in section 3[63].

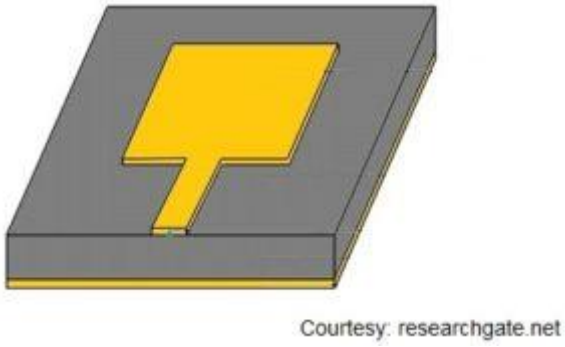

Figure 2-24 Microstrip antenna[45]

2.7.7 Textile wearable antenna's

Textile wearable antennas have the added advantage that they are comfortable to wear since they can be added to clothes such as jeans. They can have different shapes compared to the ones mentioned above, each with a different main aim. In Figure 2-25 the slots are designed to attain adequate bandwidth, high gain, and a minimum variation of the antenna parameters when in a close proximation of the human body. A dipole antenna implementation is shown on Figure 2-26 where the diamond shapes allow a better bandwidth and efficiency compared to the standard dipole. Because there are two diamond shapes this allows for dual band use and increases the bandwidth further. A slot antenna design is shown in Figure 2-27 and is an attempt to reduce the patch area.[63]

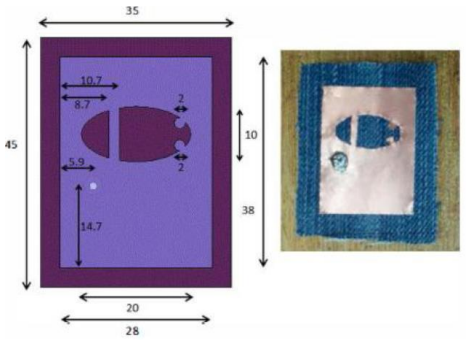

Figure 2-25 Antenna on jeans [63]

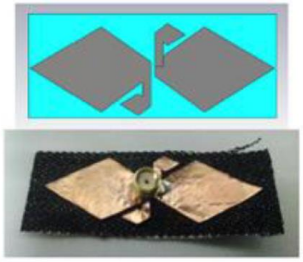

Figure 2-26 Diamond shaped dipole antenna on denim [63]

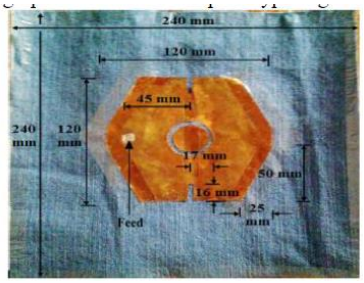

Figure 2-27 Polygon-shaped slotted dual-band antenna [63]

Besides the variation in shapes there is also the possibility to use metamaterials for substrate. These are synthetic materials which have unique electromagnetic properties which don't occur in nature. Examples of this are high impendence surface, electromagnetic bandgap, or artificial magnetic conductor. The advantage of these is that they improve radiation while reducing the SAR. [63]

3 Choice antenna

For this application, a microstrip antenna was chosen. This is due to the fact it is easy to fabricate, cost-efficient and has a substrate by design which separates the human body from the antenna reducing the effects of the body on the antenna. The downside of this antenna is the fact it has a small bandwidth. [44], [63]

3.1 Design antenna

3.1.1 Frequency

The frequency chosen in this paper is the 2,4 GHz band. This is an often-used frequency in WBAN applications because of several reasons. First because of regulatory approval, the 2,4GHz frequency is part of the ISM band (see section 0) this means no licensing is needed to use this band. Compatibility is also an important factor since many existing wireless standards (such as Bluetooth and Wi-Fi) already exist making it easier to integrate the antenna into a WBAN application. Another popular frequency is the 5GHz frequency. However, for WBAN applications this isn't ideal due to its higher attenuation through the (human) body and in general leading to a limited range.

The centre frequency of a patch antenna can be determined by the formula (3.1). This can be the same as the resonance frequency which is given in formula (3.2). From this, it can be derived that the frequency is mostly influenced by the length of the patch [44].

$$f \approx \frac{c}{2L\sqrt{\varepsilon_r}} = \frac{1}{2L\sqrt{\varepsilon_0 \varepsilon_r \mu_0}} \quad (3.1)$$

In which:

f_c : centre frequency [Hz]
L: length as shown in Figure 3-2 [m]
c: speed of light [m/s]
ε_r: permittivity of substrate [F/m]
ε_0: permittivity of the vacuum [F/m]
μ_0: magnetic permittivity of the vacuum [N/A^2]

$$f_{res} = \frac{c}{\lambda_{res}} = \frac{c}{2 * L_{res}} \qquad (3.2)$$

In which:

f_{res}: resonance frequency [Hz]
λ_{res} : resonancy wavelength [m]
L_{res} : length as shown in Figure 3-2 [m]

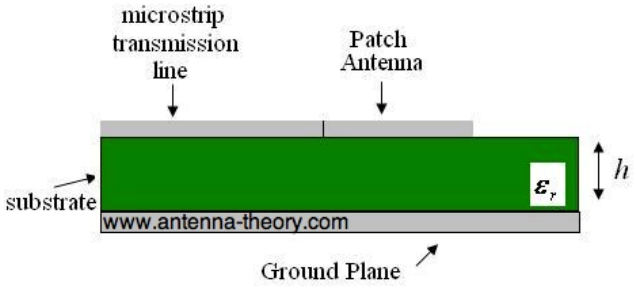

Figure 3-1 Side view of patch antenna[44]

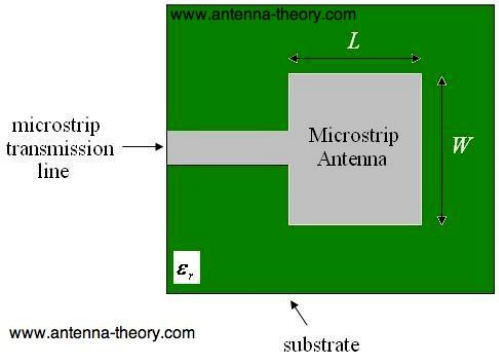

Figure 3-2 Top view patch antenna [44]

3.1.2 Production

As mentioned, the patch antenna can be produced directly on a PCB making experimenting easy. The thickness of the ground plane is not very influential but is typically smaller than the wavelength (but not smaller than $\frac{1}{40}$ th of the wavelength since this would influence the efficiency.

3.1.3 Length of a patch antenna

The length (L) of the patch antenna as defined in Figure 3-2. Formula (3.1) determines its value.

3.1.4 Bandwidth

The bandwidth of the patch antenna is given by formula (3.3). The width, length of the antenna and the height of the substrate play a critical role.

$$b \propto \frac{\varepsilon_r - W}{\varepsilon_r^2 L} h$$

(3.3)

In which:

B: bandwidth [Hz]
ε_r: permittivity of substrate [F/m]
W: width as shown in Figure 3-2 [m]
L: length as shown in Figure 3-2 [m]
H: height of substrate as shown in Figure 3-1 [m]

3.1.5 Input impedance

The input impedance is controlled by the width of the microstrip. However, these withs can quickly become too big for on-body application therefore different impedance matching techniques are possible [44]. The first approach is called insert feed and is used the most often of the shown techniques. As can be seen in Figure 3-3 the feeding patch is closer to the centre and therefore lowers the input impedance. The formula for this impedance match is shown in (3.4) [44].

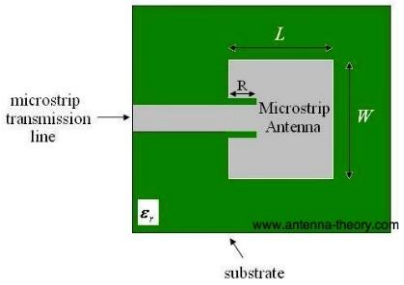

Figure 3-3 Insert feed [44]

$$Z_{in}(R) = \cos^2\left(\frac{\pi R}{L}\right) Z_{in}(0)$$

(3.4)

Another approach is the quarter wavelength transmission line where the parameter Z_1 can be altered by changing the width of the quarter wavelength strip as is shown in Figure 3-4. The formula for this is shown in (3.5) [44].

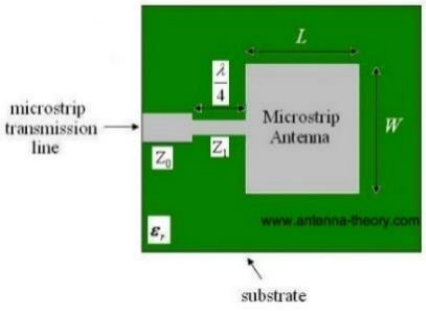

Figure 3-4 Quarter wavelength transmission [44]

$$Z_{in} = Z_0 = \frac{Z_1^2}{Z_A}$$

(3.5)

Coaxial cable probe feeding is an approach which uses the outer conductor of the coaxial cable and connects this to the ground plane. The centre conductor is extended up the patch antenna as shown in Figure 3-5. In this scenario the position of the feed will control the input impedance [44].

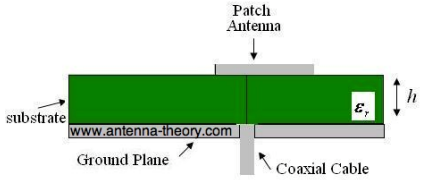

Figure 3-5 Coaxial cable probe feeding [44]

A different approach is using a coupled (indirect) feed. The main advantage of this technique is that it adds an extra degree of freedom to the design. The gap introduces a capacitance that cancels out the inductance added by the probe feed. The setup is shown in Figure 3-6 [44].

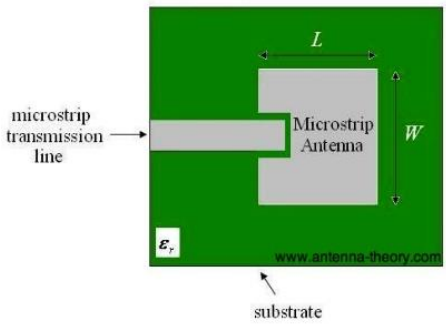

Figure 3-6 Coupled (indirect) feed [44]

The last technique discussed is the aperture feed. Shown in Figure 3-7 the feed circuitry is shielded from the antenna by a conducting plane with a hole. The main disadvantage of this technique is the difficulty to produce it [44].

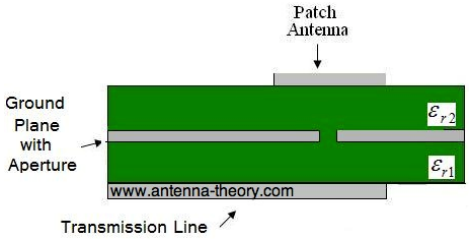

Figure 3-7 Aperture feed [44]

3.1.6 Substrate

The substrate of the patch has different functionalities. For one it shields the body from part of the radiation lowering the SAR value.
The permittivity of the substrate influences the frequency as shown in equation (3.1). it also controls the fringing fields determining values such as radiation, bandwidth (equation(3.3)), efficiency and even the size of the patch antenna (equation (3.1)).[44]
The height of the substrate will also control the bandwidth as is clear from equation (3.3).

3.2 Patch antenna used in paper.

The antenna used in this paper is based on the design used in[11]. Modified further to work within sim4life. The dimensions are shown in Figure 3-8. The dielectric constant is chosen at 4,25 based on the values for FR4 (most often used for PCB)[64]. The thickness of the substrate is chosen at 1,52 mm with a ground plane underneath. These values were first calculated and then fine-tuned using the simulation software.

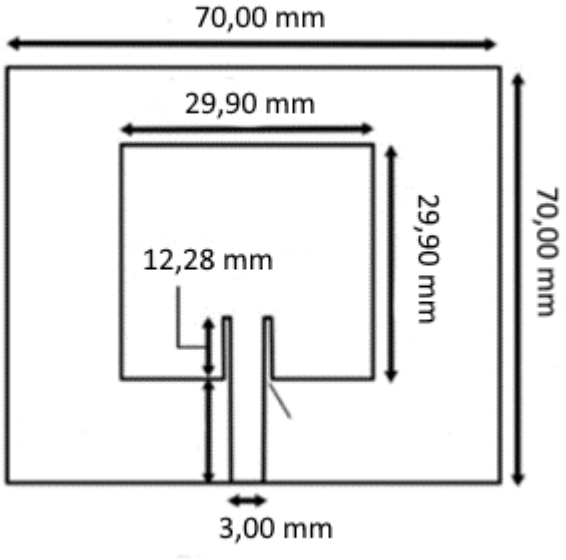

Figure 3-8 Dimensions patch antenna [11]

These settings give an 2,4 GHz antenna as is shown in Figure 3-9. With gain values as shown in Figure 3-10.

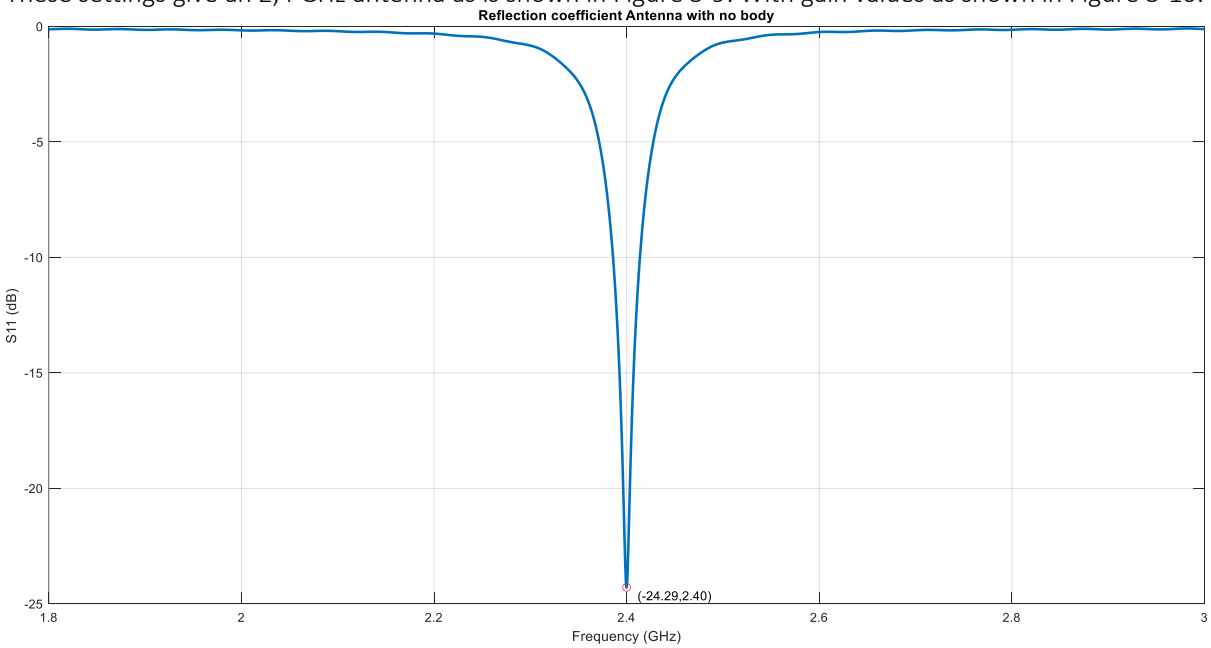

Figure 3-9 reflection coefficient antenna without body present

Figure 3-10 Total gain without body present

4 Location

Location is important for the efficiency of the antenna. However, the focus when choosing the location of the antenna in this paper is the functionality. For horses the locations most often used are the poll, withers, sacrum, RH (right hind leg), RF (right front leg), LF (left front leg), LH (left hind leg) and poll. These locations are shown on Figure 4-1[65]–[72] .

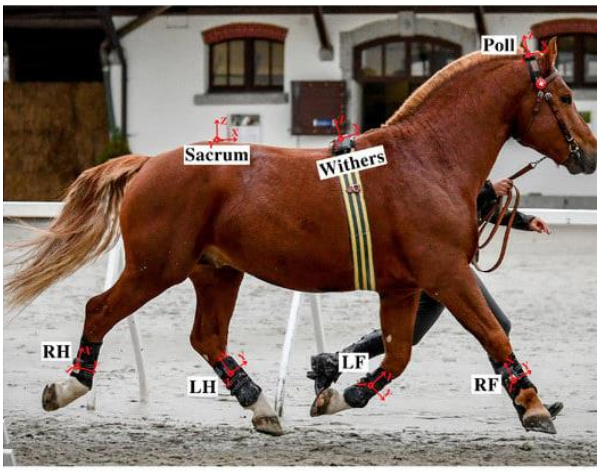

Figure 4-1 Locations sensor on horse[65]

5 Breeds

The purpose of this chapter is to elaborate on the reasons why particular horse breeds were selected.

5.1 First choice of breeds

The breed of horses is chosen by their height and build. The first simulations are based on three different breeds the Shire horse, Falabella pony and the Quarter Horse. The largest, smallest, and most common horse respectively[15], [17], [73].

Table 5-1 shows the average height measured at the withers as is shown in Figure 5-1.

Table 5-1 Height of the horses [15]–[17], [73]

	Shire horse	Quarter horse	Falabella
Height at the withers (cm)	160-205	145-165	63-86

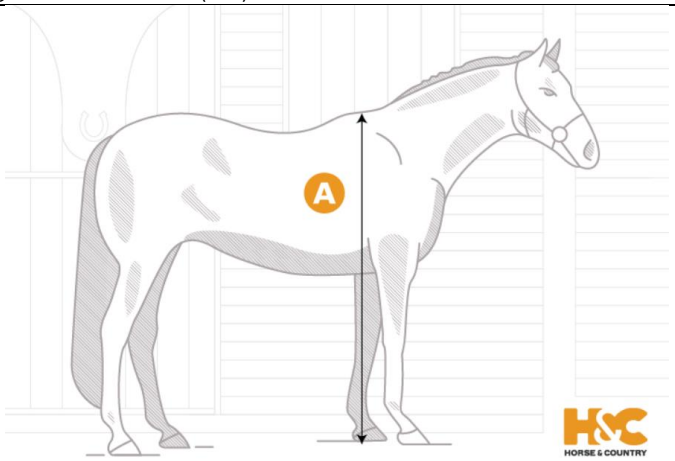

Figure 5-1 Measuring height horse at withers [74]

5.2 Final breeds

Due to the problems explained in section 6.2.4 three new breeds are chosen. The Falabella breed is kept this time as the middle breed. The largest breed is the Shetland, and a smaller imaginary breed is created called Selveryne for the rest of this thesis.
Their height is shown in Table 5-2.

Table 5-2 Height horses [15], [16], [75]

	Shetland horse	Falabella	Selveryne
Height at the withers (cm)	71-107	63-86	52.2

The heights chosen for the models are shown in Table 5-3. The height is chosen so that the percentual difference between Falabella and Shetland $\approx 30\%$ and Fabella and Selveryne $\approx 30\%$. Figure 5-2 shows their height in ratio of each other.

Table 5-3 height chosen models.

	Shetland horse	Falabella	Selveryne
Height at the withers (cm)	96.8	74.5	52.2

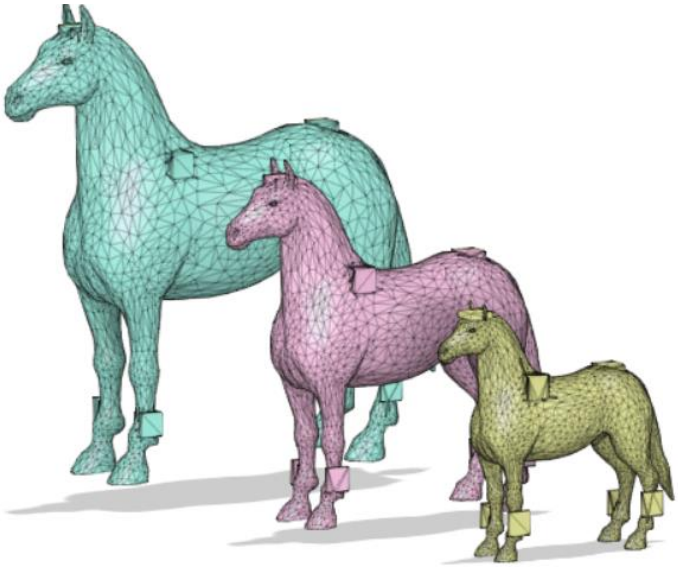

Figure 5-2 Horses comparison

6 Simulation

This chapter delves into the process of creating the simulations, including any difficulties that were encountered, and presents the results.

6.1 Choice of the model

The models used will be homogeneous, therefore it's important to choose the right makeup for this model. In general muscle accounts for 50% of body weight in most athletic horses and 45% in non-athletic horses[76], [77]. This is based on weight and muscle weights more than fat; therefore, this can give a misleading idea. However, the maximum fat percentage of a (healthy) horse is 24,5 %[76] this percentage is for the Percheron breed shown on Figure 6-1.
The distinction between muscle tissue and fat tissue is an important one since muscle tissue exists mostly with water (80%) while fat has little water (16%). Therefore, muscle tissue is a good conductor and fat tissue has isolator characteristics. [76]. The tissue chosen in this thesis is muscle tissue.

Figure 6-1 Percheron[78]

The 3D model is shown in Figure 6-2. This is a model originally used for 3D printing which explains its original sizing [79]. Horses size is most often expressed in wither height as discussed in section 5 .
On the 3D model the height of the withers is measured and used to size the model for the horse breeds chosen as shown in Table 6-1. The length and width of the horse scale together with the height of the model.

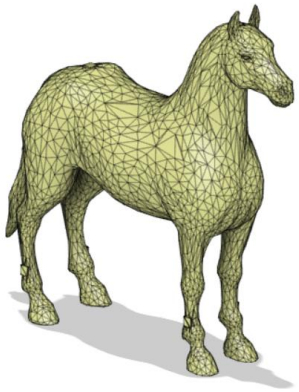

Figure 6-2 3D model horse

Table 6-1 Height of models

	Original	Selveryne	Falabella	Shetland
height at the withers (mm)	13,00	522	745,00	968
total height (mm)	19,19	769	1099,00	1429

To ensure consistent antenna placement and proper connections, cubes are incorporated into the horse to facilitate optimal connectivity for all models as is shown seen in Figure 6-2 and Figure 5-2.

6.2 Simulation issues

This chapter will shortly discuss some of the problems which arose simulating the horse models using FDTD in sim4life.

6.2.1 Reducing size

The horse model was initially intended for 3D printing, which led to its high level of detail. 3D models are composed of mesh triangles, with more triangles generally resulting in increased detail, as demonstrated in Figure 6-3. However, in this case, such detail is not necessarily desirable since it would lengthen the simulation time and increase file sizes, without significantly impacting the outcome.

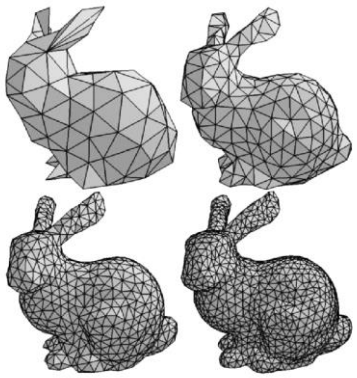

Figure 6-3 3D mesh triangles with different resolutions[80]

To accelerate the simulation process, an initial measure was to decrease the number of triangles in the model. Nevertheless, this approach has its limitations since reducing the triangle count too much may result

in the creation of holes in the model, which leads to unwanted side effects. As demonstrated in Table 6-2, the file size is notably decreased as a result. However, once the model is adjusted to accommodate larger breeds, its size will increase, while the triangle count remains unchanged.

Table 6-2 Effects of reducing the amount of triangle in a model.

Model	STL file size
Original	392.339 kB
Reduced model	2.029 kB

6.2.2 Angle of the antenna

The horse's antennas are aligned at multiples of 90° angles, despite this not being as realistic as other angles could be. Any angle deviation from the 90° multiples will result in voxelization issues, as illustrated in Figure 6-4 which leads to an inaccurate reflection coefficient as shown in Figure 6-5.This voxelization effect, also known as staircasing, occurs due to the FDTD's working principle. It is crucial to align with the x, y and z axis of the grid when using FDTD to achieve accurate results [81], [82].Although higher-order FDTD algorithms or adaptive sub-meshes can mitigate these effects, using multiples of 90° angles, in this situation, can solve the problem without adding too much simulation time.[82]

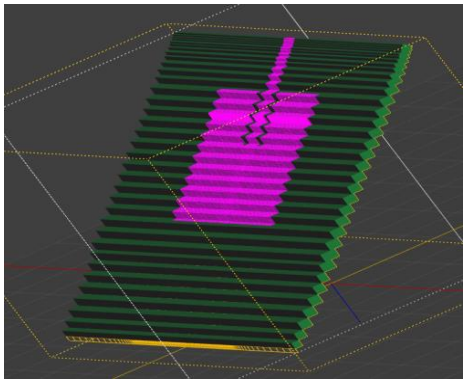

Figure 6-4 Voxels antenna at 33 °

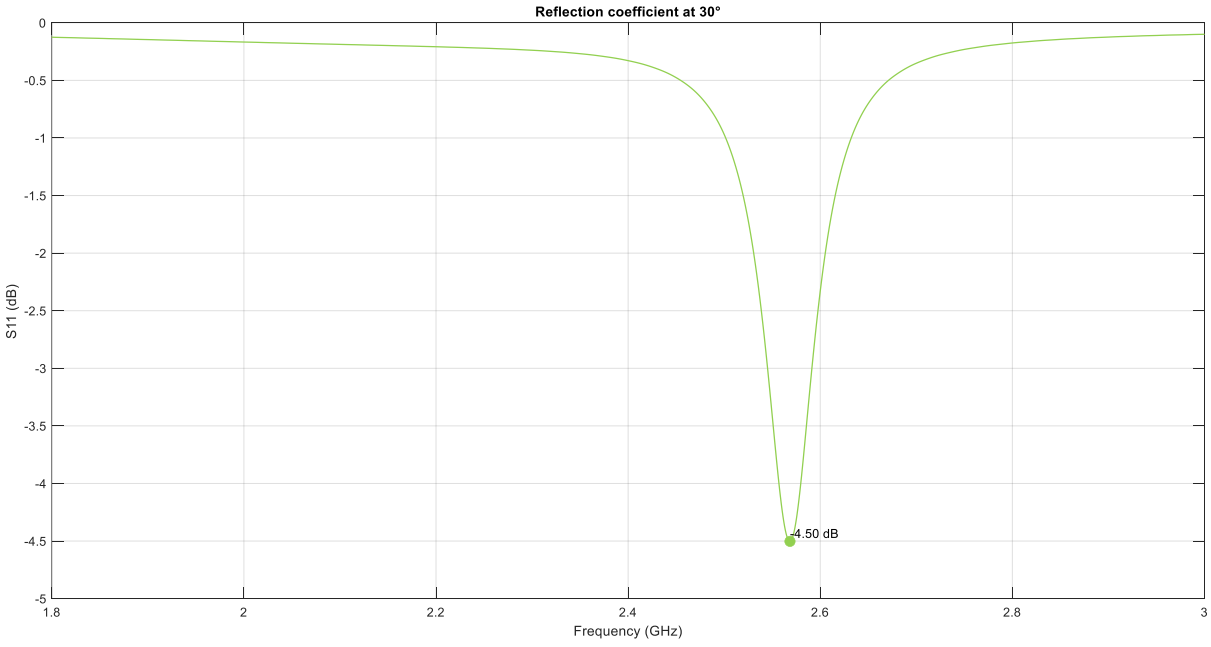

Figure 6-5 Reflection coefficient at 33° angle

6.2.3 Grid

During the initial simulations, an unusual effect was observed where all antennas had a varying frequency shift away from the expected 2.4GHz. However, when only simulating two antennas, this effect was less severe. Figure 6-6 displays the difference between two antennas and all antennas. The body of the horse was not included in the simulation at this stage, so it could not have caused the shift. Additionally, this effect was much greater than what theoretical studies predicted. Although a slight shift is possible, it should not be as severe as observed here.

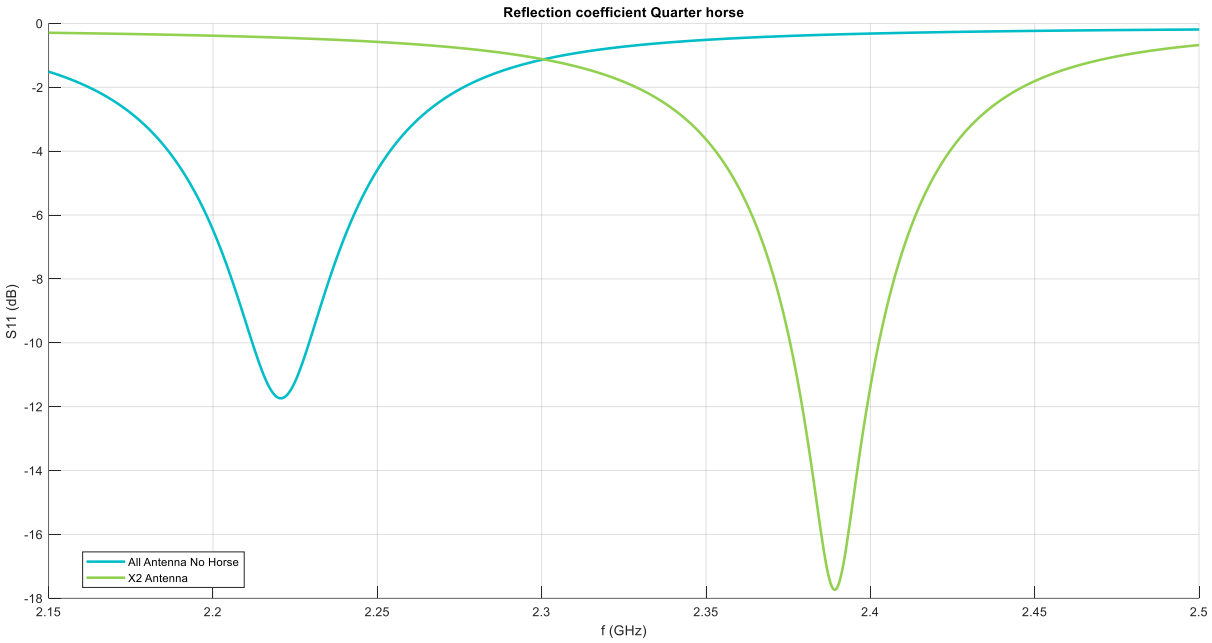

Figure 6-6 Reflection coefficient Quarter with grid problems

The problem was discovered to be in the grid configuration. Specifically, the antenna was being rounded to the nearest grid, resulting in different patch dimensions and, therefore, different reflection frequencies. This problem is illustrated in Figure 6-7 .

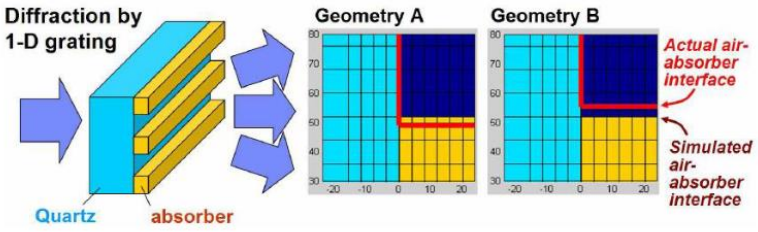

Figure 6-7 Example of error introduced when mask geometries are discretized by coarse grid[81]

Figure 6-8 depicts an incorrect grid setup where no line passes the left side of the patch, causing the patch antenna to be shortened or lengthened along the blue or yellow arrows, respectively. Thus, it is important

that grid lines fall on the patch lines, which can be achieved by adjusting the geometry resolution setting to 0 to preserve all geometrical shapes. A well-configured grid is demonstrated in Figure 6-9.

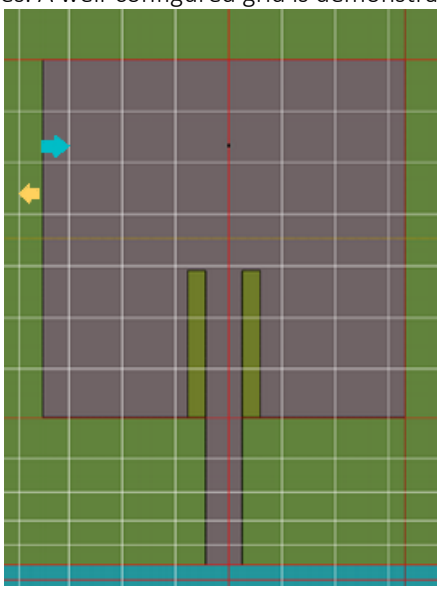

Figure 6-8 Wrong grid line-up

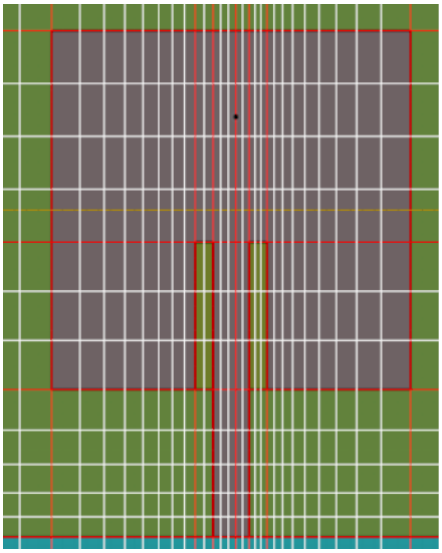

Figure 6-9 Correct grid line-up.

The grid values are specified in Table 6-3. Additionally, it is important to allocate a subset of the grid to each antenna to avoid excessive voxelization in fine grid instances. The provided grid values are for an antenna at 0° with respect to the x, y, and z axes. If the antenna is rotated, the max step of the grid must also be adjusted accordingly.

Table 6-3 Values used for grid.

Part	Grid
Patch	Max step: [0.3; 0.3; 2.7] Geometry resolution: [0.6;1;1]
Enclosure (fabric), substrate, source, ground	Fine grid
Horse	Very coarse

6.2.4 Simulation time

It became evident that simulating the Quarter and Shire horses properly was unfeasible due to their large size. The simulation times are presented in Table 6-4. To address this issue, alternative breeds were selected as outlined in section 5.2.

Table 6-4 Simulation time large breeds

Breed	Simulation time per antenna (hours)	Simulation time whole horse
Quarter	16	112 hours (4.6 days)
Shire	20	140 hours (5.83 days)

6.3 Tissue

The tissues tested are tissue, water, muscle, and fat. These are chosen since they are the main tissues that make up a body. The values are used which are provided in sim4life and shown in Table 6-5these values are specific for the frequency of 2.4GHz.[83]

Table 6-5 Dielectric properties materials [83]

Body	Mass density [kg/m³]	Electrical conductivity [S/m]	Relative permittivity []
tissue	1026.50	1.64402	43.2097
water	994.04	0.00162	83.4085
fat	911.00	0.26148	10.8357
muscle	1090.40	1.70508	52.7909

6.3.1 Distance between tissue and antenna

The easiest way to monitor the influence of tissue is to place the antenna at different distances from the tissue. Then the influence of the distance and the tissue can easily be monitored. In this simulation a 130mm X 130mm X 130mm cube is used for the tissue as shown in Figure 6-10.

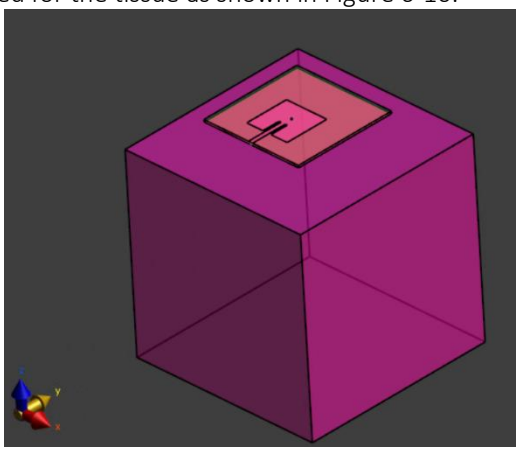

Figure 6-10 Simulation tissue and distance

The results are shown in Figure 6-11.

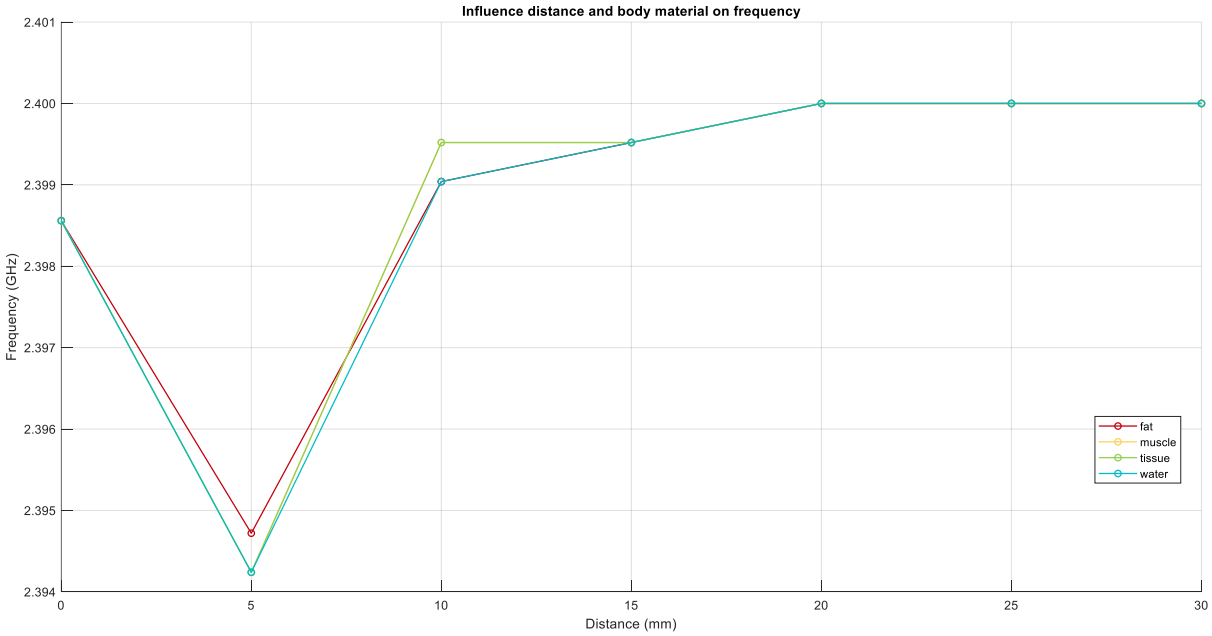

Figure 6-11 Influence of the distance and body material on frequency

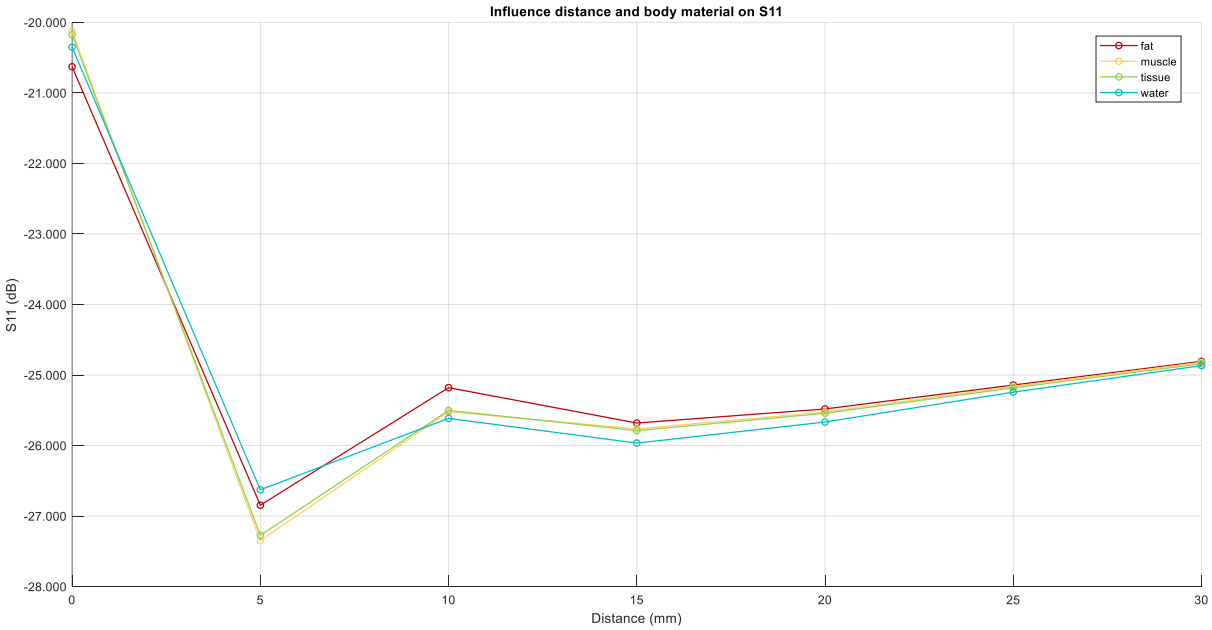

Figure 6-12 Influence of the distance and body material on S11 (taken at the frequency as is shown in Figure 6-11)

As seen in Figure 3-9 the S11 on 2.4 GHz for an antenna without body is -24.29 dB. Figure 6-12 show that S11 gets better when the there is a small distance between the body and the antenna. This is because the body will reflect part of the radiation from the antenna back to the antenna therefore making S11 better. Figure shows the influence the body has on the frequency. This shift is completely gone by 20 mm.

The influence on gain is shown in Figure 6-13. The gain of the original antenna is shown in Figure 3-10 to be 5.62 dB. The gain has a serious drop when the antenna is 5mm from the body. Depending on what the body

is, it is possible for the gain to get better. This difference is due to their dielectric properties as shown in Table 6-5

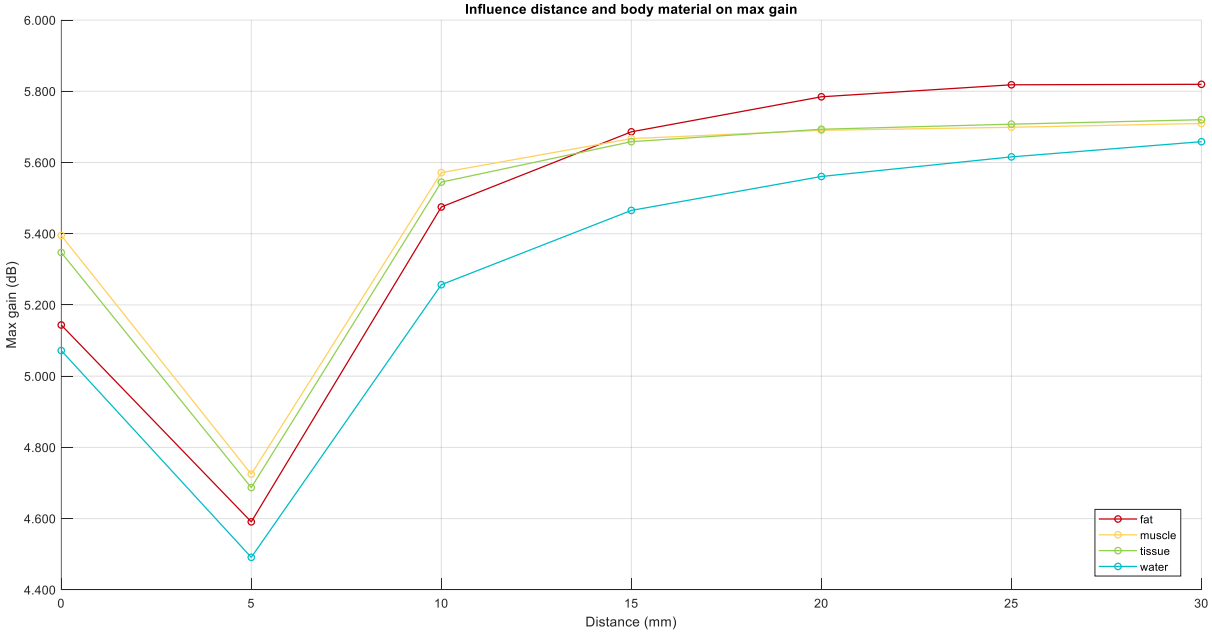

Figure 6-13 Influence body on max gain

These results are not unexpected since other studies such as [84]have found similar results. It's in general clear that the detuning effects are going to be higher when te separation distance between an antenna and an object is lower. This is because the object significantly changes the near field distribution.

6.3.2 Influence thickness tissue

Figure 6-14 shows the influence of the thickness of the tissue and the kind of tissue on the gain. The water tissue will cause great differences in gain, where the muscle is more constant. However, for thin tissues the gain increases compared to the example without thickness changes. This shouldn't be allowed due to the ground plane. Consequently, if the body would consist of water, it is necessary to make the ground plane thicker.

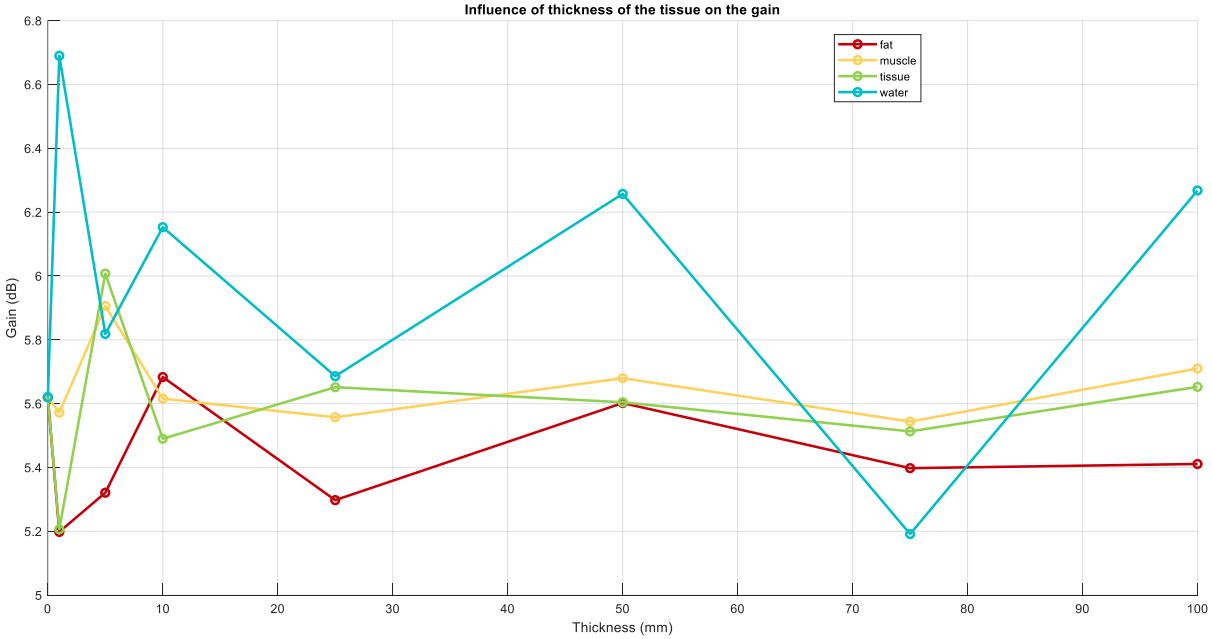

Figure 6-14 Influence thickness on gain.

6.4 Fabric

To add realism to the antenna a fabric is added between the antenna and the tissue. The fabric has a relative permittivity between 1 and 2, therefore 1.5 has been chosen in this simulation.[85]

To see the effect of the fabric on the antenne 5 measurements are done at different fabric thicknesses. The setup is shown in Figure 6-15.

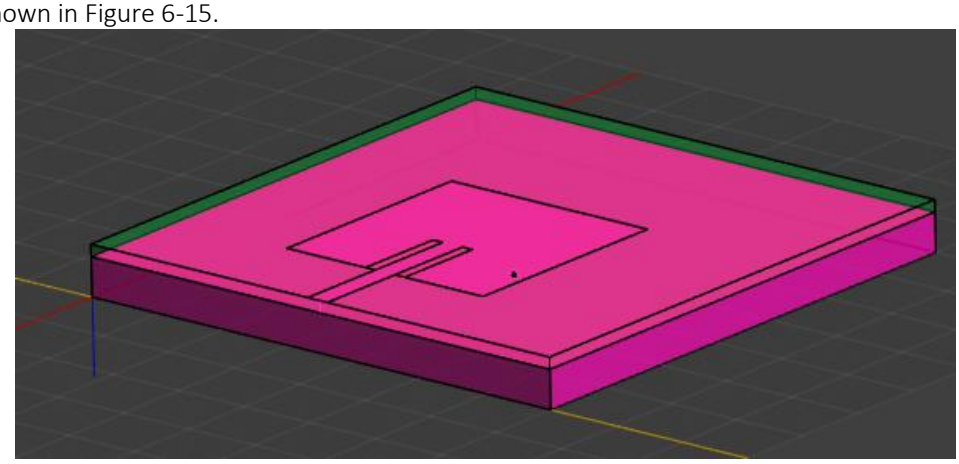

Figure 6-15 Antenna with substrate

Figure 6-16 shows that there is no noticeable difference in the resonant frequency. Table 6-6 shows the variance in the magnitude of S11, improving when there is a fabric underneath the antenna. This improvement is likely because the fabric absorbs some of the energy reflected from the antenna, reducing the amount of energy reflected towards the antenna. In addition, using an extra fabric outside the simulation could provide isolation from nearby objects, reducing their interference and improving S11. However, when adding fabric, it's clear from Figure 6-16 that the S11 is not as stable in other frequencies compared to no or little fabric.

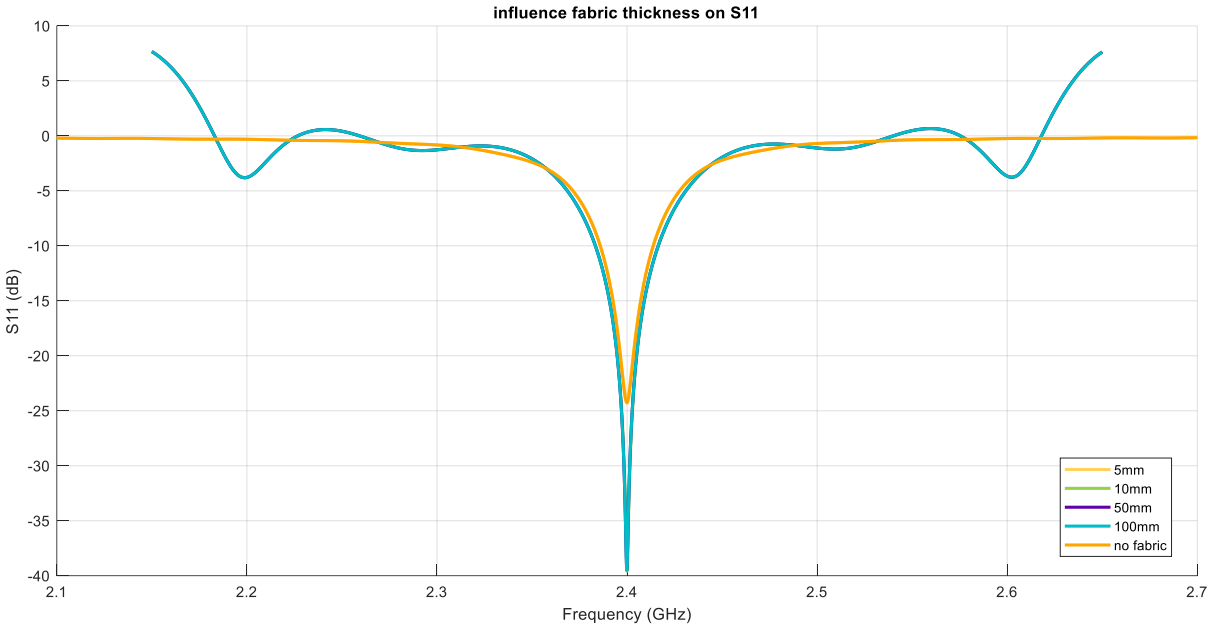

Figure 6-16 Influence fabric thickness on S11.

Table 6-6 Influence fabric on S11

Fabric thickness (mm)	S11 (dB)
0	-24.289
5	-23.802
10	-39.585
50	-39.232
100	-39.354

The gain and directivity will also be influenced by the fabric thickness. Figure 6-17 shows the general radiation of the antenne for different thicknesses of fabric. The form of radiation doesn't change but there is a notable difference in max gain. This is shown even better in

where a thicker fabric will cause considerable gain loss.

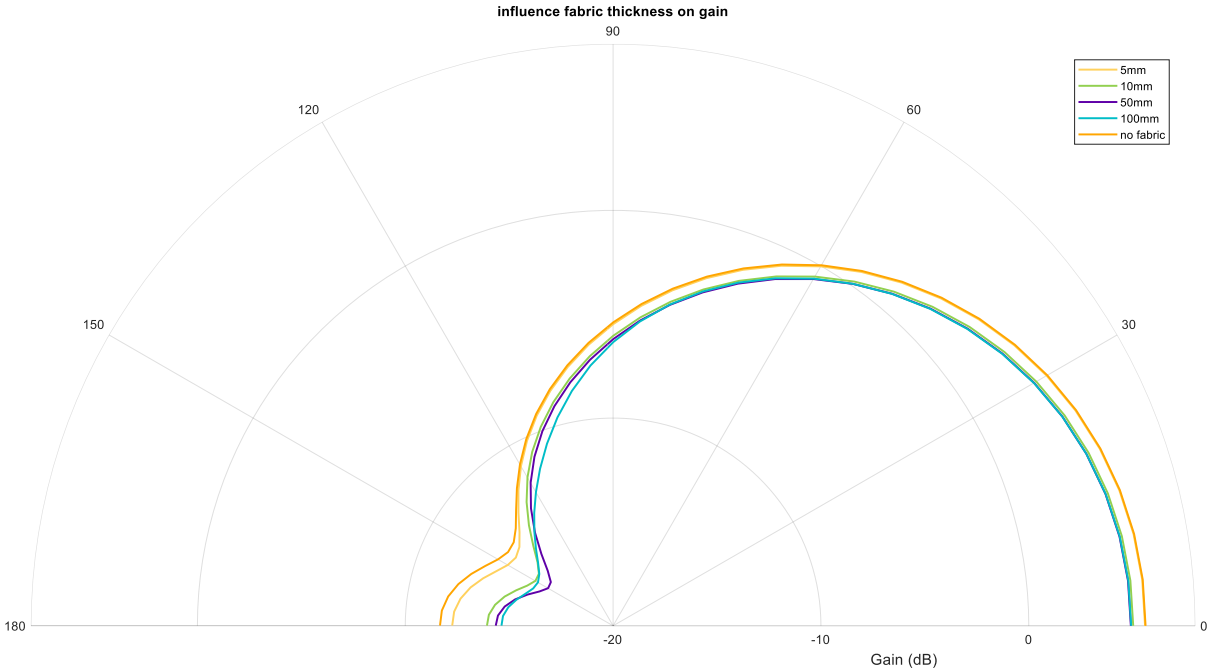

Figure 6-17 Influence fabric on gain

Because of the little frequency shift but considerable gain lost a fabric of 5mm is chosen. This could be made thicker in case this should be needed to temper the influence of the horse's body on the antenna.

6.5 Simulation on horse

The simulation is always done twice. First time with the horse second time without the horse but with the orientation and distance as on the horse. This gives 2 values that can be compared to see the influence of the horse on the measurement since this is the only difference between the two measurements.

6.5.1 Gain

The influence of the body on gain depends on the structure and amount of body underneath the antenna. The full table can be found in the appendix section I. Table 6-7 shows a summary of these values. The average distance between the gain with or without the horse present is minimal and gets even smaller for a bigger horse.

Table 6-7 Summary gain values

difference no horse and horse	Selveryne		Falabella		Shetland	
	value	location	value	location	value	location
min	0.11	Poll	-0.09	Withers	0.01	LF
max	0.54	RF	1.29	Poll	1.21	Poll
median	0.12	/	-0.19	/	-0.05	/

6.5.2 Path loss

There are different ways to calculate a path loss as discussed in section 2.6. For this work the model from paper [5] was chosen. The reason for this choice is that it was developed based on simulations and measurements conducted on a cow, making it more closely aligned with a horse model than a human model would be.
The paper makes a difference between path loss including the antenna properties (6.1) and excluding the antenna properties (6.2).

$$PL_{embedded} = P_{TX} - P_{RX} \quad (6.1)$$

$$PL = P_{TX} + G_{TXb} + G_{RXb} - P_{RX} \quad (6.2)$$

In which:

$PL_{embedded}$: path loss with antenna gains imbedded [dB]
PL: path loss [dB]
P_{TX} : power transmitted [dBm]
P_{RX}: power received [dBm]
G_{TXb}: antenna gain transmitter near horse's body [dB]
G_{RXb}: antenna gain receiver near horse's body [dB]

The path loss can then be modelled using with a reference distance of 10 cm:

$$PL(d) = PL(d_0) + 10logn\left(\frac{d}{d_0}\right) + X_\sigma \quad (6.3)$$

In which:

$PL(d)$: path loss [dB]
$PL(d_0)$: path loss at reference [dB]
d: current distance between RX and TX [m]
n: path loss exponent
d_0: reference distance [m]
X_σ : zero-mean gaussian distributed variable [dB]
σ: standard diviation [dB]

The simulation data obtained from sim4life includes the gains, S-parameters, and distance between the antennas. By analysing the S-parameters, we can determine the received power. The transmitted power remains constant at 30 dBm for all scenarios. To achieve a good fit, a least square error approach is employed. The standard deviation between the data points and the fit is then calculated. Using this information along with the path loss model, a suitable path loss exponent can be determined by sweeping through different values of "n" and selecting the one that closely aligns with the fit. The results for "n" are presented in Table 6-8, while the graphs for (de-)embedded scenarios are shown in Figure 6-18 and Figure 6-19.

The initial fit is performed on all points, including those that do not clearly fall into the categories of NLOS (non-line-of-sight) or LOS (line-of-sight) (refer to appendix 0). However, when fitting for NLOS and LOS, these ambiguous points are disregarded.

Upon comparing the obtained path loss exponents with those presented in Table 2-13, it is evident that most of the calculated values fall within the range expected for an urban area. Interestingly, when examining the LOS in an embedded environment, it performs slightly better than free space. This can be attributed to the fact that indoor LOS typically has a path loss exponent of 1.6-1.8. It is noteworthy that the embedded path LOS consistently outperforms the de-embedded path LOS, which is logical since the embedded calculation considers the gains from the antenna. This provides an indication of the antenna's effectiveness.

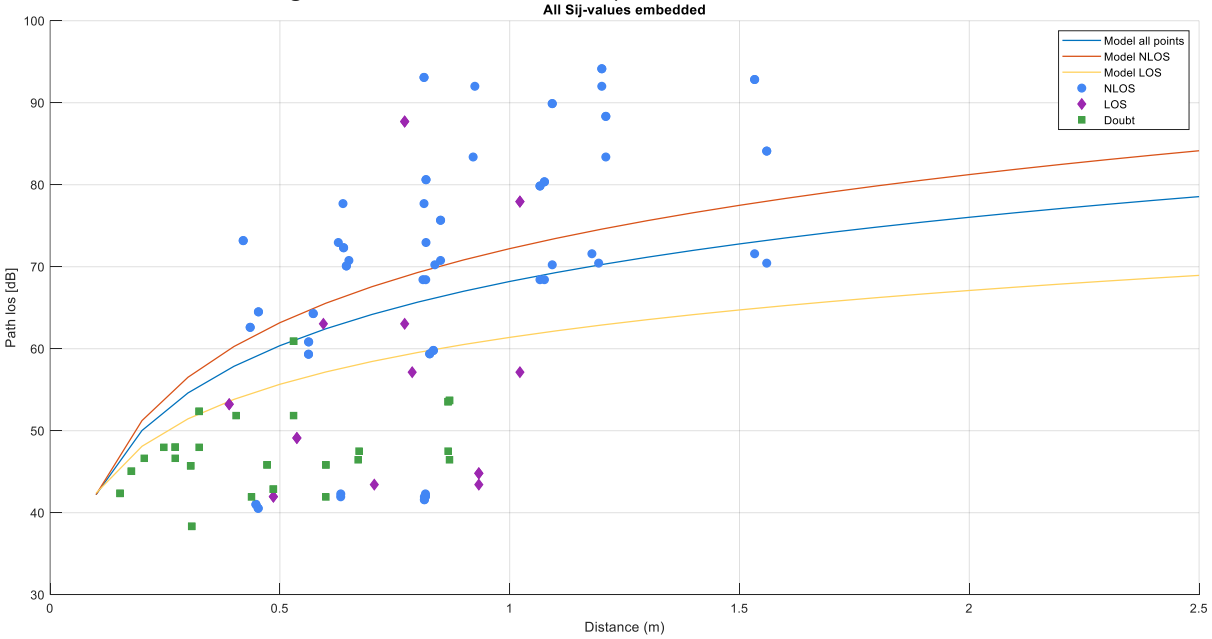

Figure 6-18 Prediction path loss embedded.

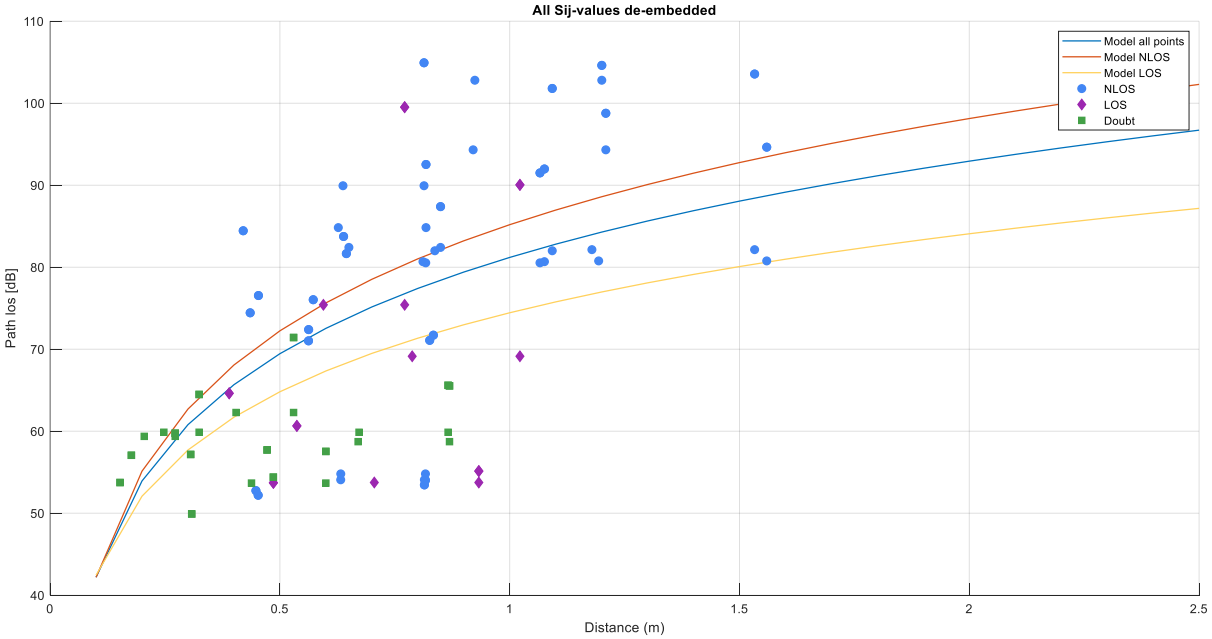

Figure 6-19 Prediction path loss de-embedded

Table 6-8 Results standard deviation en path loss.

		σ	n (path loss exponent)	PL(d_0) (dB)
All points	Embedded	3.63	3.60	28.19
	De-embedded	3.62	3.90	38.56
NLOS	Embedded	3.63	3.00	28.19
	De -embedded	3.62	4.30	38.56
LOS	Embedded	3.81	1.90	28.19
	De -embedded	3.87	3.20	38.26

7 Discussion

The initial focus of the research was on establishing the basis and configuration of WBAN networks, which provided a solid foundation for evaluating simulations. This approach has been effective in identifying errors caused by incorrect configurations or inherent flaws in the simulation technique used.

By utilizing the modelled path, it is now possible to predict path loss for larger horse breeds without the need for time-consuming simulations. In the case of larger horses, where the distance between antennas can reach up to 2 meters, the worst-case modelling scenario (de-embedded NLOS) exhibits a path loss of approximately 100 dB, while for embedded NLOS, it is only around 80 dB. This highlights the importance of carefully selecting suitable antennas. The de-embedded model however does allow to use the same model with a different potentially better antenna. Additionally, the modelled path closely resembles the path achieved in paper [57], where the path loss exponent ranged from 3.06 to 3.12. The highest path loss exponent achieved here is 4.30 for the de-embedded NLOS scenario. When comparing this with Table 2-11, it is not a greater loss than what would be caused by an obstruction in a building. Considering that there may be instances where the horse is obstructing certain connections, it can be assumed that this method is viable.

One effect that was not tested in this simulation but could play a vital role is the influence of multipath. Generally, multipath is seen as undesirable, but in this scenario, it could be beneficial since some antennas may be unreachable due to their location and body shadowing. However, they could become reachable if a multipath allows for a different path to the antenna. This suggests that testing the setup in for example a stable may yield better results. Another aspect of multipath that is consistently present but not considered in the simulation is the floor, as mentioned in reference [57] .This factor could also potentially influence the results.

In cases where certain antennas cannot reach each other due to excessive path loss, a tiered approach can be employed. For example, if antennas 1 and 3 cannot directly communicate, antenna 1 can transmit to antenna 2, and antenna 2 can transmit to antenna 3, making it possible to establish communication with antenna 3. This approach is known as a multi hop approach, as described in references [23], [24], [86], [87].In addition to addressing connectivity, a tiered approach can also help optimize energy consumption, as the physical and MAC layers play a crucial role in this property. Furthermore, a tiered approach may allow nodes on the body to transmit data to a main node, which then relays the data to an off-body system. Since transmitting data off the body is the most power-intensive action, reducing the number of nodes that need to perform this action would be beneficial [86].

However, it is important to note that all the simulations assume a stationary horse. In practice, movement introduces additional challenges. One such challenge is the changing distance between nodes on the body and the nodes at a distant receiving station, which causes the transmitters to continuously adjust their transmitting power. Protocols can also significantly impact this aspect [86] . Another consideration is the Doppler effect, which affects signals when there is movement involved [88].

In conclusion, this model provides a promising starting point for developing a WBAN system for horses, but further work is still required to refine it.

8 Future research

A logical progression for future research would involve conducting measurements on actual horses to validate the accuracy of the model. It is advisable to initially perform tests on Falabella or Shetland horses, as they were the breeds used in the simulations. Subsequently, simulations can be carried out on larger horses such as Quarters or Shires. However, practical considerations must be considered. The physical dimensions of the antenna, measuring 70 mm by 70 mm, may present challenges when fitting it onto the poll region of smaller breeds, making practical measurements in that area more difficult. Moreover, the width of the antenna exceeds the width of the legs of small horses. As a result, only a portion of the antenna would be supported by a horse's leg, while the remaining section would be exposed to the air. Although, in theory, this should not have any impact since the ground plane separates the horse from the antenna, there may be a slight practical influence to consider. However, before these measurements can be conducted, a wireless technology should be selected. This, along with the antenna, can help mitigate the overall path loss.

By comparing the measurements with the simulations, it would be possible to further refine the model. This refinement would enable the implementation of the model across various horse breeds without the need to conduct separate experiments for each breed. Incorporating changes caused by movement into the model would be the next step toward developing a fully functional system.

9 Sustainability reflection

The extensive usage of electrical and electronic equipment contributes significantly to the generation of electronic waste, which has become the fastest-growing waste stream globally [89]. Printed circuit boards (PCBs) are an essential component found in almost all electrical and electronic devices, including WBAN systems. For the application used in this work an antenna printed on PR4 was proposed which is a material used to make PCBs. Improper handling of electronic waste poses serious risks to human health and the environment. Appropriate management strategies encompassing awareness, collection, recycling, and reuse are necessary for the responsible handling of this waste [89]. However, recycling such waste effectively remains a major challenge for societies worldwide. PCBs, the foundation of many electronic industries, contain valuable heavy metals and toxic halogenated organic substances [89]. Paper [89] provides insights into recycling methods for these metals. Alternatively, the use of biodegradable electronics offers the advantage of generating non-toxic and environmentally friendly waste [90]. Additionally, these materials can be safely metabolized within the body without causing adverse physiological reactions. In the context of WBAN, sensors can also be implanted in the body, but not all sensors should remain permanently. Current materials require two operations—one for implantation and another for removal. However, biodegradability addresses these disadvantages by allowing for temporary existence, aiding in medical diagnosis and subsequent removal, thus avoiding the drawbacks of traditional chronic implants [90].
Paper [90] explores different materials that can replace substrates, active layers, electrodes, dielectric layers, adhesives, and encapsulants. It also discusses alternative printing methods that offer ease and cost efficiency compared to traditional semiconductor processing techniques involving lithography and chemical vapor depositions. Semiconductor processing often involves etching away unwanted material, resulting in waste production that can lead to significant wastage if recycling is not performed correctly [90].
Another aspect of sustainability revolves around batteries. WBAN focuses on power consumption to extend the lifespan of sensors. From a sustainable perspective, reducing battery usage is beneficial due to the environmental pollutants generated during various battery processes, such as mining, manufacturing, transportation, collection, storage, treatment, disposal, and recycling. These pollutants include hazardous waste, greenhouse gas emissions, and toxic gases [91]. Energy harvesting emerges as a solution to reduce the reliance on batteries. It involves utilizing sources of non-electric renewable energy to generate electronic energy. Energy harvesting is already implemented on a large scale worldwide but exploring its application in

compact devices like sensor nodes remains a trending topic in research and academia [92]. This self-reliant solution offers nearly green energy supply while reducing system costs and electronic waste in the form of depleted batteries. Energy harvesting also addresses the energy constraints of WBAN, making its usage more practical. Recent advancements have made it possible to scavenge energy from various sources within the human body, which was previously considered impossible or overlooked. Paper [92] lists several of these energy sources. Although batteries will still be necessary for storing energy when other sources are unavailable, energy harvesting has the potential to reduce the number and size of batteries required for WBAN applications. As discussed before a smaller size will also benefit the wearer since it increases comfort. To enable sensors to function indefinitely, they must harvest more energy than they consume. WBAN offers an even greater range of potential energy sources compared to traditional energy harvesting, as depicted in Figure 9-1[92]. The paper [92] delves deeper into this subject, exploring the potential sources that can be harnessed.

It is evident that by embracing bioelectronics or energy harvesting, we can contribute to sustainability. Moreover, these advancements unlock additional applications and energy sources for WBAN, further extending its lifespan.

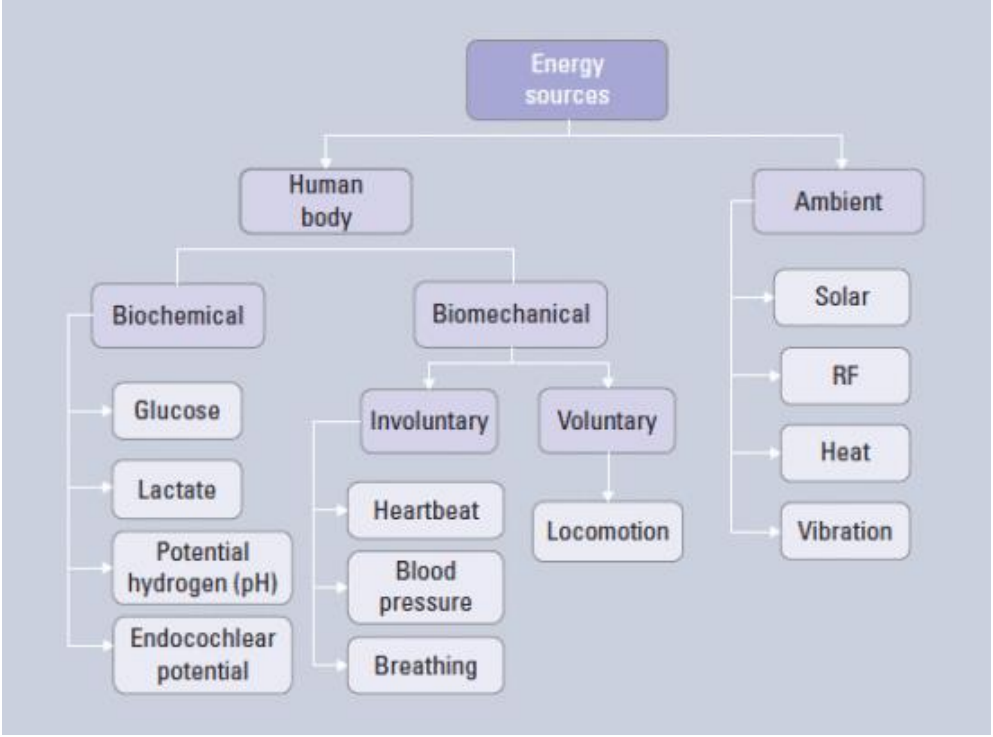

Figure 9-1 Energy sources specific to WBAN

References

[1] R. Cavallari, F. Martelli, R. Rosini, C. Buratti, and R. Verdone, "A survey on wireless body area networks: Technologies and design challenges," *IEEE Communications Surveys and Tutorials*, vol. 16, no. 3, pp. 1635–1657, 2012, doi: 10.1109/SURV.2014.012214.00007.

[2] "View of Innovative technologies of wireless sensor network: The applications of WBAN system and environment." http://sei.ardascience.com/index.php/journal/article/view/69/51 (accessed Apr. 20, 2023).

[3] S. D. Bland, "Equine colic: a review of the equine hindgut and colic," *Veterinary Science Development*, vol. 6, no. 1, Aug. 2016, doi: 10.4081/vsd.2016.6223.

[4] M. M. Sloet van Oldruitenborgh-Oosterbaan, "Laminitis in the horse: A review," *Veterinary Quarterly*, vol. 21, no. 4, pp. 121–127, 1999, doi: 10.1080/01652176.1999.9695006.

[5] S. Benaissa *et al.*, "Characterization of the On-Body Path Loss at 2.45 GHz and Energy Efficient WBAN Design for Dairy Cows," *IEEE Trans Antennas Propag*, vol. 64, no. 11, pp. 4848–4858, Nov. 2016, doi: 10.1109/TAP.2016.2606571.

[6] Ł. Januszkiewicz, "Analysis of Human Body Shadowing Effect on Wireless Sensor Networks Operating in the 2.4 GHz Band," *Sensors 2018, Vol. 18, Page 3412*, vol. 18, no. 10, p. 3412, Oct. 2018, doi: 10.3390/S18103412.

[7] E. Reusens, W. Joseph, G. Vermeeren, and L. Martens, "On-body measurements and characterization of wireless communication channel for arm and torso of human," *IFMBE Proc*, vol. 13, pp. 264–269, 2007, doi: 10.1007/978-3-540-70994-7_44.

[8] Ł. Januszkiewicz, "Analysis of Human Body Shadowing Effect on Wireless Sensor Networks Operating in the 2.4 GHz Band," 2018, doi: 10.3390/s18103412.

[9] S. L. Cotton, A. Mckernan, A. J. Ali, and W. G. Scanlon, "An Experimental Study on the Impact of Human Body Shadowing in Off-Body Communications Channels at 2.45 GHz," *Proceedings of the 5th European Conference on Antennas and Propagation (EUCAP)*, 2011.

[10] S. L. Cotton, "Human Body Shadowing in Cellular Device-to-Device Communications: Channel Modeling Using the Shadowed κ − μ Fading Model," *IEEE JOURNAL ON SELECTED AREAS IN COMMUNICATIONS*, vol. 33, no. 1, p. 111, 2015, doi: 10.1109/JSAC.2014.2369613.

[11] R. Proesmans, K. Deprez, M. Velghe, and A. Thielens, "An on-body antenna for control of a wireless prosthesis in the 2.45 GHz industrial scientific and medical frequency band," *IET Microwaves, Antennas and Propagation*, Dec. 2022, doi: 10.1049/MIA2.12309.

[12] P. S. Hall *et al.*, "Antennas and propagation for on-body communication systems," *IEEE Antennas Propag Mag*, vol. 49, no. 3, pp. 41–58, 2007, doi: 10.1109/MAP.2007.4293935.

[13] S. C. Walpole, D. Prieto-Merino, P. Edwards, J. Cleland, G. Stevens, and I. Roberts, "The weight of nations: an estimation of adult human biomass," *BMC Public Health*, vol. 12, no. 1, p. 439, 2012, doi: 10.1186/1471-2458-12-439.

[14] J. Van Der Heyden *et al.*, "MODE DE VIE ET MALADIES CHRONIQUES ENQUÊTE DE SANTÉ PAR EXAMEN BELGE 2018 Belgian Health Examination Survey (BELHES) _ Projet financé par", Accessed: May 23, 2023. [Online]. Available: www.enquetesante.be

[15] food and agriculture organization of the united nations, "Falabella pony/argentina (horse)." https://fao-dadis-breed-detail.firebaseapp.com/?country=ARG&specie=Horse&breed=Falabella%20Pony&lang=en (accessed May 23, 2023).

[16] "Fokprogramma 2020 EFS; European Falabella Studbook", Accessed: May 23, 2023. [Online]. Available: www.europeanFalabellastudbook.com

[17] "Breed Standard & Points of the Horse – The Shire Horse Society." https://www.shire-horse.org.uk/about-us/the-shire-horse/breed-standard-points-of-the-horse/ (accessed May 23, 2023).

[18] İ. Pala Ercan and Ş. Timur, "Changing Terminology of Definition and Design of Wearable Technology Products," *Online Journal of Art and Design*, vol. 8, no. 3, 2020.

[19] F. Martincic and L. Schwiebert, "Introduction to Wireless Sensor Networking," *Handbook of Sensor Networks: Algorithms and Architectures*, pp. 1–40, Sep. 2005, doi: 10.1002/047174414X.CH1.

[20] "Handbook of Research on Developments in E-Health and Telemedicine," *Handbook of Research on Developments in E-Health and Telemedicine*, May 2010, doi: 10.4018/978-1-61520-670-4.
[21] Guang-Zhong Yang, *Body sensor networks*. springer , 2014.
[22] Md. T. Arefin, M. H. Ali, A. K. M. F. Haque, Md. T. Arefin, M. H. Ali, and A. K. M. F. Haque, "Wireless Body Area Network: An Overview and Various Applications," *Journal of Computer and Communications*, vol. 5, no. 7, pp. 53–64, May 2017, doi: 10.4236/JCC.2017.57006.
[23] H. Taleb, A. Nasser, • Guillaume Andrieux, • Nour Charara, and • Eduardo Motta Cruz, "Wireless technologies, medical applications and future challenges in WBAN: a survey," *Wireless Networks*, vol. 27, doi: 10.1007/s11276-021-02780-2.
[24] F. Touati *et al.*, "An experimental performance evaluation and compatibility study of the bluetooth low energy based platform for ECG monitoring in WBANs," *Int J Distrib Sens Netw*, vol. 2015, 2015, doi: 10.1155/2015/645781.
[25] "802.15.6-2012 - IEEE Standard for Local and metropolitan area networks - Part 15.6 : Wireless Body Area Networks.," 2012.
[26] N. Todtenberg and R. Kraemer, "A survey on Bluetooth multi-hop networks," *Ad Hoc Networks*, vol. 93, p. 101922, Oct. 2019, doi: 10.1016/J.ADHOC.2019.101922.
[27] E. Georgakakis, S. A. Nikolidakis, D. D. Vergados, and C. Douligeris, "An analysis of bluetooth, Zigbee and bluetooth low energy and their use in WBANs," in *Lecture Notes of the Institute for Computer Sciences, Social-Informatics and Telecommunications Engineering*, 2011, pp. 168–175. doi: 10.1007/978-3-642-20865-2_22.
[28] J. Verhaevert, *Draadloze en mobiele communicatie*. UGhent, 2022.
[29] L. Wang, S. Hao, P. Yu, and Z. Huang, "Low-power Wireless Sensor Network protocol of Mobile Health based on IPv6," in *Chinese Control Conference, CCC*, IEEE Computer Society, Aug. 2016, pp. 8479–8484. doi: 10.1109/ChiCC.2016.7554710.
[30] Z. Yang and C. H. Chang, "6LoWPAN Overview and Implementations," 2019.
[31] "EN 302 502 - V1.2.1 - Broadband Radio Access Networks (BRAN); 5,8 GHz fixed broadband data transmitting systems; Harmonized EN covering the essential requirements of article 3.2 of the R&TTE Directive | Enhanced Reader."
[32] Bran, "EN 301 893 - V1.7.1 - Broadband Radio Access Networks (BRAN); 5 GHz high performance RLAN; Harmonized EN covering the essential requirements of article 3.2 of the R&TTE Directive," 2012, Accessed: May 23, 2023. [Online]. Available: http://portal.etsi.org/chaircor/ETSI_support.asp
[33] Erm, "EN 300 328 - V1.8.1 - Electromagnetic compatibility and Radio spectrum Matters (ERM); Wideband transmission systems; Data transmission equipment operating in the 2,4 GHz ISM band and using wide band modulation techniques; Harmonized EN covering the essential requirements of article 3.2 of the R&TTE Directive," 2012, Accessed: May 23, 2023. [Online]. Available: http://portal.etsi.org/chaircor/ETSI_support.asp
[34] Y. Kim, S. Lee, and S. Lee, "Coexistence of ZigBee-Based WBAN and WiFi for Health Telemonitoring Systems; Coexistence of ZigBee-Based WBAN and WiFi for Health Telemonitoring Systems," *IEEE J Biomed Health Inform*, vol. 20, no. 1, 2016, doi: 10.1109/JBHI.2014.2387867.
[35] S. Kharche and S. Pawar, "Optimizing network lifetime and QoS in 6LoWPANs using deep neural networks," *Computers and Electrical Engineering*, vol. 87, Oct. 2020, doi: 10.1016/J.COMPELECENG.2020.106775.
[36] "Paarden | Landbouw & Visserij." https://landbouwcijfers.vlaanderen.be/landbouw/paarden (accessed Apr. 20, 2023).
[37] D. Landbouw en Visserij, "De paardensector in Vlaanderen 2020", Accessed: Apr. 20, 2023. [Online]. Available: www.vlaanderen.be/landbouwcijfers
[38] "Google Trends." https://trends.google.com/trends?geo=BE&hl=nl (accessed May 23, 2023).
[39] S peter and Hao Yang, "Antennas and Propagation for Body-Centric Wireless Communications."
[40] "Cell Phones and Cancer Risk Fact Sheet - NCI." https://www.cancer.gov/about-cancer/causes-prevention/risk/radiation/cell-phones-fact-sheet (accessed May 23, 2023).
[41] M. I. Hossain, M. R. I. Faruque, and M. T. Islam, "Analysis on the effect of the distances and inclination angles between human head and mobile phone on SAR," *Prog Biophys Mol Biol*, vol. 119, no. 2, pp. 103–110, Nov. 2015, doi: 10.1016/J.PBIOMOLBIO.2015.03.008.

[42] V. G. Khurana, C. Teo, M. Kundi, L. Hardell, and M. Carlberg, “Cell phones and brain tumors: a review including the long-term epidemiologic data,” *Surg Neurol*, vol. 72, no. 3, pp. 205–214, Sep. 2009, doi: 10.1016/J.SURNEU.2009.01.019.
[43] “(PDF) A Review on SAR Reduction Methods Used For Mobile Application.” https://www.researchgate.net/publication/285591408_A_Review_on_SAR_Reduction_Methods_Used_For_Mobile_Application (accessed May 23, 2023).
[44] “The Antenna Theory Website.” https://www.antenna-theory.com/ (accessed Mar. 09, 2023).
[45] “Wearable Antennas – Applications, Technologies, and their Impact on Human Body - Mistral Solutions.” https://www.mistralsolutions.com/blog/wearable-antennas-applications-technologies-impact-human-body/ (accessed Mar. 09, 2023).
[46] Y. Fan, X. Liu, J. Li, and T. Chang, “A Miniaturized Circularly-Polarized Antenna for In-Body Wireless Communications,” *Micromachines 2019, Vol. 10, Page 70*, vol. 10, no. 1, p. 70, Jan. 2019, doi: 10.3390/MI10010070.
[47] “Frequentieplan | BIPT.” https://www.bipt.be/operatoren/frequentieplan (accessed Mar. 09, 2023).
[48] R. Mavaddat, “Network Scattering Parameters,” vol. 2, Mar. 1996, doi: 10.1142/2791.
[49] N. Ha-Van and C. Seo, “A Single-Feeding Port HF-UHF Dual-Band RFID Tag Antenna,” *Journal of Electromagnetic Engineering and Science*, vol. 17, no. 4, pp. 233–237, Oct. 2017, doi: 10.26866/JEES.2017.17.4.233.
[50] “The Mysterious 50 Ohm Impedance: Where It Came From and Why We Use It | Blog | Altium Designer.” https://resources.altium.com/p/mysterious-50-ohm-impedance-where-it-came-and-why-we-use-it (accessed Mar. 28, 2023).
[51] J. Verhaevert, *Draadloze en mobiele communicatie*. UGhent, 2022.
[52] N. Atina *et al.*, “The Distribution of Path Loss Exponent in 3D Indoor Environment,” *International Journal of Applied Engineering Research*, vol. 12, pp. 7154–7161, 2017, Accessed: Mar. 06, 2023. [Online]. Available: http://www.ripublication.com
[53] Andrea Goldsmith, *Wireless communications* . 2012.
[54] S. Kaur and J. Malhotra, “Survey on Empirical Channel Models for WBAN,” *International Journal of Future Generation Communication and Networking*, vol. 8, no. 2, pp. 399–410, 2015, doi: 10.14257/ijfgcn.2015.8.2.34.
[55] P. Van Torre *et al.*, “Characterization of Measured Indoor Off-Body MIMO Channels with Correlated Fading, Correlated Shadowing and Constant Path Loss,” *IEEE Trans Wirel Commun*, vol. 11, no. 2, 2012, doi: 10.1109/TWC.2011.111611.110298.
[56] L. Roelens and L. Martens, “Path loss model for wireless narrowband communication near biological tissue,” *6th UGent-FirW Doctoraatssymposium, Interactive poster session, paper nr. 120 (proceedings available on CD-Rom)*, 2005, doi: 1854/4782.
[57] S. Benaissa *et al.*, “Internet of animals: On-and off-body propagation analysis for energy efficient WBAN design for dairy cows,” *2017 11th European Conference on Antennas and Propagation, EUCAP 2017*, pp. 298–302, May 2017, doi: 10.23919/EUCAP.2017.7928112.
[58] M. M. Khan, Q. H. Abbasi, A. Alomainy, and C. Parini, “Experimental Investigation of Subject-Specific On-Body Radio Propagation Channels for Body-Centric Wireless Communications,” *Electronics 2014, Vol. 3, Pages 26-42*, vol. 3, no. 1, pp. 26–42, Jan. 2014, doi: 10.3390/ELECTRONICS3010026.
[59] “Beard” “Cory” and “William” “Stallings,” *wireless communication and networks and systems*. 2016.
[60] T. Kumpuniemi, T. Tuovinen, M. Hämäläinen, K. Yekeh Yazdandoost, R. Vuohtoniemi, and J. Iinatti, “Measurement-Based On-Body Path Loss Modelling for UWB WBAN Communications”.
[61] A. Nahali, A. Hamdi, and R. Braham, “Body Area Networks: Path Loss Modeling and Antenna Design,” *2018 14th International Wireless Communications and Mobile Computing Conference, IWCMC 2018*, pp. 174–179, Aug. 2018, doi: 10.1109/IWCMC.2018.8450400.
[62] A. Nahali, A. Hamdi, M. Gautier, A. Courtay, and R. Braham, “Energy Modeling of Wireless Body Area Networks with On-Body Communication Channel Characterization”.
[63] J. C. Wang, E. G. Lim, M.Leach, Z.Wang, and K.L. Man, “Review of wearable antennas for WBAN application”.
[64] “FR4 Dielectric Constant and Material Properties.” https://resources.altium.com/p/fr4 (accessed Mar. 28, 2023).

[65] H. Darbandi *et al.*, "Using different combinations of body-mounted IMU sensors to estimate speed of horses-A machine learning approach," *Sensors (Switzerland)*, vol. 21, no. 3, pp. 1–12, Feb. 2021, doi: 10.3390/S21030798.
[66] "How it works - EquiMoves." https://equimoves.nl/system-overview/how-it-works/ (accessed Mar. 28, 2023).
[67] C. J. Thompson, L. M. Luck, J. Keshwani, S. K. Pitla, and L. K. Karr, "Location on the Body of a Wearable Accelerometer Affects Accuracy of Data for Identifying Equine Gaits," *J Equine Vet Sci*, vol. 63, pp. 1–7, Apr. 2018, doi: 10.1016/J.JEVS.2017.12.002.
[68] A. Eerdekens *et al.*, "A framework for energy-efficient equine activity recognition with leg accelerometers," *Comput Electron Agric*, vol. 183, p. 106020, Apr. 2021, doi: 10.1016/J.COMPAG.2021.106020.
[69] C. Hartmann, L. Lidauer, J. Aurich, C. Aurich, and C. Nagel, "Detection of the time of foaling by accelerometer technique in horses (Equus caballus)—a pilot study," *Reproduction in Domestic Animals*, vol. 53, no. 6, pp. 1279–1286, Dec. 2018, doi: 10.1111/RDA.13250.
[70] S. Bosch *et al.*, "EquiMoves: A Wireless Networked Inertial Measurement System for Objective Examination of Horse Gait," 2018, doi: 10.3390/s18030850.
[71] J. W. Kamminga, L. M. Janßen, N. Meratnia, and P. J. M. Havinga, "Horsing Around-A Dataset Comprising Horse Movement," 2019, doi: 10.4121/uuid:2e08745c-4178-4183-8551-f248c992cb14.
[72] J. B. Burla, A. Ostertag, H. Schulze Westerath, and E. Hillmann, "Gait determination and activity measurement in horses using an accelerometer," *Comput Electron Agric*, vol. 102, pp. 127–133, Mar. 2014, doi: 10.1016/J.COMPAG.2014.01.001.
[73] "What are the Most Popular Horse Breeds?" https://www.saddlebox.net/what-are-the-most-popular-horse-breeds/ (accessed Mar. 28, 2023).
[74] "Horse Height & Weight: A Guide." https://horseandcountry.tv/horse-height-and-weight-guide (accessed Mar. 28, 2023).
[75] "Typische Kenmerken - Belgisch Studbook van de Shetlandpony." http://www.shetlandstudbook.be/typische-kenmerken.html (accessed May 24, 2023).
[76] C. F. Kearns, K. H. McKeever, and T. Abe, "Overview of Horse Body Composition and Muscle Architecture: Implications for Performance," *The Veterinary Journal*, vol. 164, no. 3, pp. 224–234, Nov. 2002, doi: 10.1053/TVJL.2001.0702.
[77] "Determining Horses' body Weight and Ideal Condition | Three Steps." https://three-steps.nl/determining-horses-body-weight-and-ideal-condition/ (accessed Mar. 28, 2023).
[78] "Percheron." https://horse-canada.com/breeds/percheron/ (accessed Mar. 28, 2023).
[79] "Horse free 3D model | CGTrader." https://www.cgtrader.com/free-3d-models/animals/other/horse-6a800de8-6f28-4404-945e-7d784d58ac13 (accessed Mar. 09, 2023).
[80] "3D mesh-triangles with different resolution (3D Modelling for... | Download Scientific Diagram." https://www.researchgate.net/figure/3D-mesh-triangles-with-different-resolution-3D-Modelling-for-programmers-Available-at_fig2_322096576 (accessed May 08, 2023).
[81] J. Tirapu Azpiroz, G. W. Burr, A. E. Rosenbluth, and M. Hibbs, "Massively-parallel FDTD simulations to address mask electromagnetic effects in hyper-NA immersion lithography," *Optical Microlithography XXI*, vol. 6924, p. 69240Y, Mar. 2008, doi: 10.1117/12.774443.
[82] S. Prepeliță *et al.*, "Influence of voxelization on finite difference time domain simulations of head-related transfer functions," *J Acoust Soc Am*, vol. 139, no. 5, pp. 2489–2504, May 2016, doi: 10.1121/1.4947546.
[83] "Tissue Frequency Chart » IT'IS Foundation." https://itis.swiss/virtual-population/tissue-properties/database/tissue-frequency-chart/ (accessed Apr. 17, 2023).
[84] N. Huda, A. Rahman, Y. Yamada, M. Shakir, and A. Nordin, "materials Analysis on the Effects of the Human Body on the Performance of Electro-Textile Antennas for Wearable Monitoring and Tracking Application," 2019, doi: 10.3390/ma12101636.
[85] R. Salvado, C. Loss, Gon, and P. Pinho, "Textile Materials for the Design of Wearable Antennas: A Survey," *Sensors (Basel)*, vol. 12, no. 11, p. 15841, Nov. 2012, doi: 10.3390/S121115841.

[86] K. Hasan, K. Biswas, K. Ahmed, N. S. Nafi, and M. S. Islam, “A comprehensive review of wireless body area network,” *Journal of Network and Computer Applications*, vol. 143, pp. 178–198, Oct. 2019, doi: 10.1016/J.JNCA.2019.06.016.

[87] E. Reusens *et al.*, “Characterization of on-body communication channel and energy efficient topology design for wireless body area networks,” *IEEE Transactions on Information Technology in Biomedicine*, vol. 13, no. 6, pp. 933–945, Nov. 2009, doi: 10.1109/TITB.2009.2033054.

[88] M. O. Munoz, R. Foster, and Y. Hao, “Exploring physiological parameters in dynamic WBAN channels,” *IEEE Trans Antennas Propag*, vol. 62, no. 10, pp. 5268–5281, Oct. 2014, doi: 10.1109/TAP.2014.2342751.

[89] S. M. Abdelbasir, S. S. M. Hassan, A. H. Kamel, and R. S. El-Nasr, “Status of electronic waste recycling techniques: a review,” *Environmental Science and Pollution Research*, vol. 25, no. 17, pp. 16533–16547, Jun. 2018, doi: 10.1007/S11356-018-2136-6/FIGURES/2.

[90] M. J. Tan, C. Owh, P. L. Chee, A. K. K. Kyaw, D. Kai, and X. J. Loh, “Biodegradable electronics: cornerstone for sustainable electronics and transient applications,” *J Mater Chem C Mater*, vol. 4, no. 24, pp. 5531–5558, Jun. 2016, doi: 10.1039/C6TC00678G.

[91] A. R. Dehghani-Sanij, E. Tharumalingam, M. B. Dusseault, and R. Fraser, “Study of energy storage systems and environmental challenges of batteries,” *Renewable and Sustainable Energy Reviews*, vol. 104, pp. 192–208, Apr. 2019, doi: 10.1016/J.RSER.2019.01.023.

[92] F. Akhtar and M. H. Rehmani, “Energy Harvesting for Self-Sustainable Wireless Body Area Networks,” *IT Prof*, vol. 19, no. 2, pp. 32–40, Mar. 2017, doi: 10.1109/MITP.2017.34.

A. Appendix

I. Gain on horse

Table 1 Gain with or without Selveryne

	Poll	Sacrum	Withers	LF	LH	RF	RH
Horse	5.81	5.94	5.64	5.76	5.90	5.63	6.11
No horse	5.91	6.06	6.02	6.11	5.76	6.16	5.72
Difference between no horse and horse	0.11	0.12	0.38	0.35	-0.13	0.54	-0.39

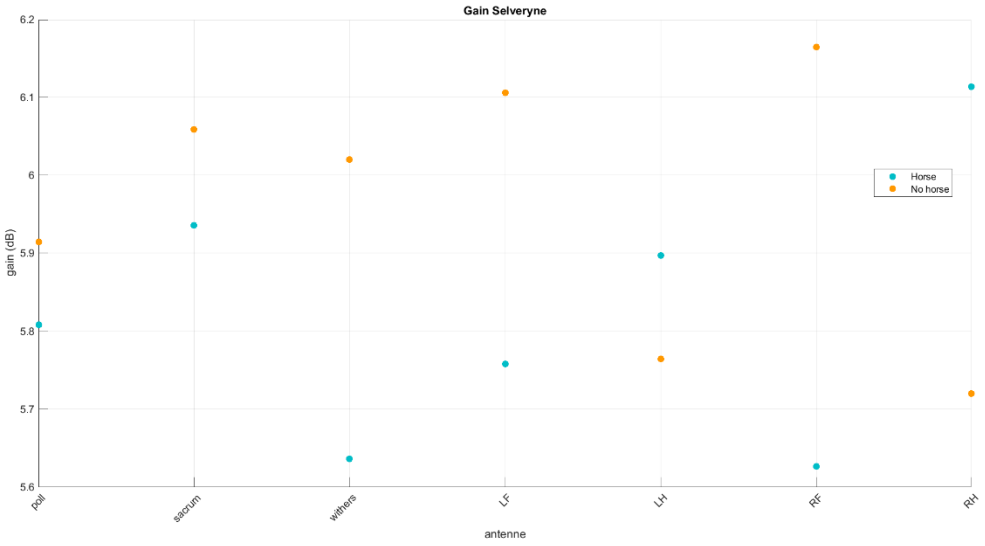

Figure 1 Gain with or without Selveryne

Table 2 Gain with or without Falabella

	Poll	Sacrum	Withers	LF	LH	RF	RH
Horse	4.50	5.82	5.94	6.44	6.06	6.30	5.84
No horse	5.79	5.95	5.85	5.75	5.62	5.78	5.65
Difference between no horse and horse	1.29	0.13	-0.09	-0.69	-0.45	-0.51	-0.19

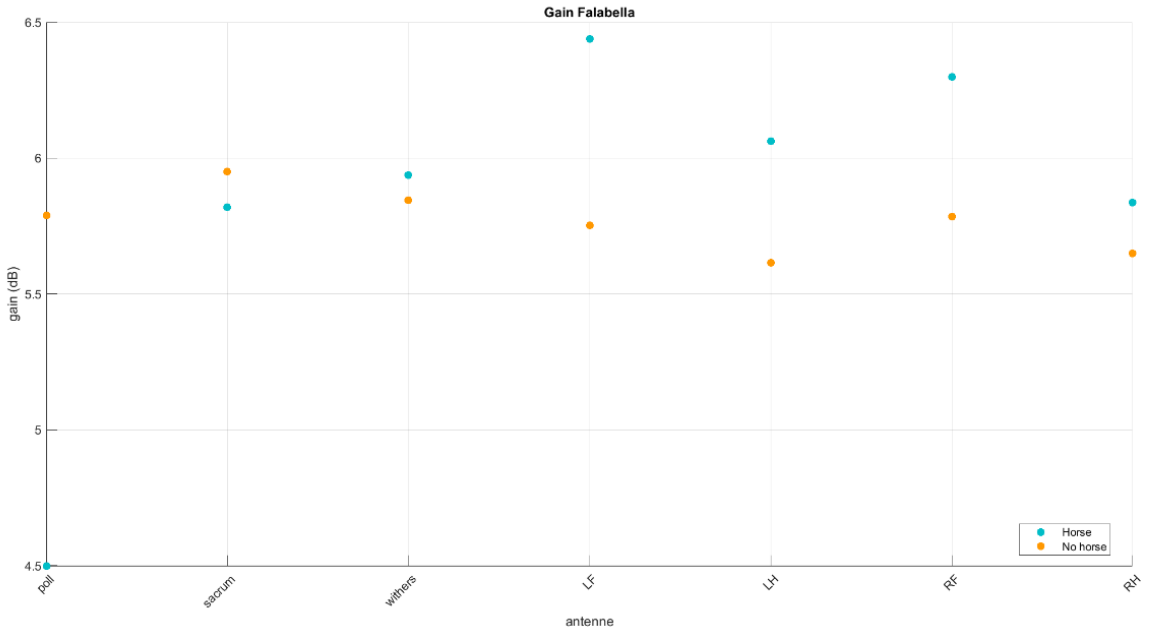

Figure 2 Gain with or without Falabella

Table 3 Gain with or without Shetland

	Poll	Sacrum	Withers	LF	LH	RF	RH
Horse	4.57	5.76	5.94	5.87	6.16	5.90	5.96
No horse	5.79	5.90	5.89	5.88	5.64	5.81	5.65
Difference between no horse and horse	1.21	0.14	-0.05	0.01	-0.51	-0.09	-0.32

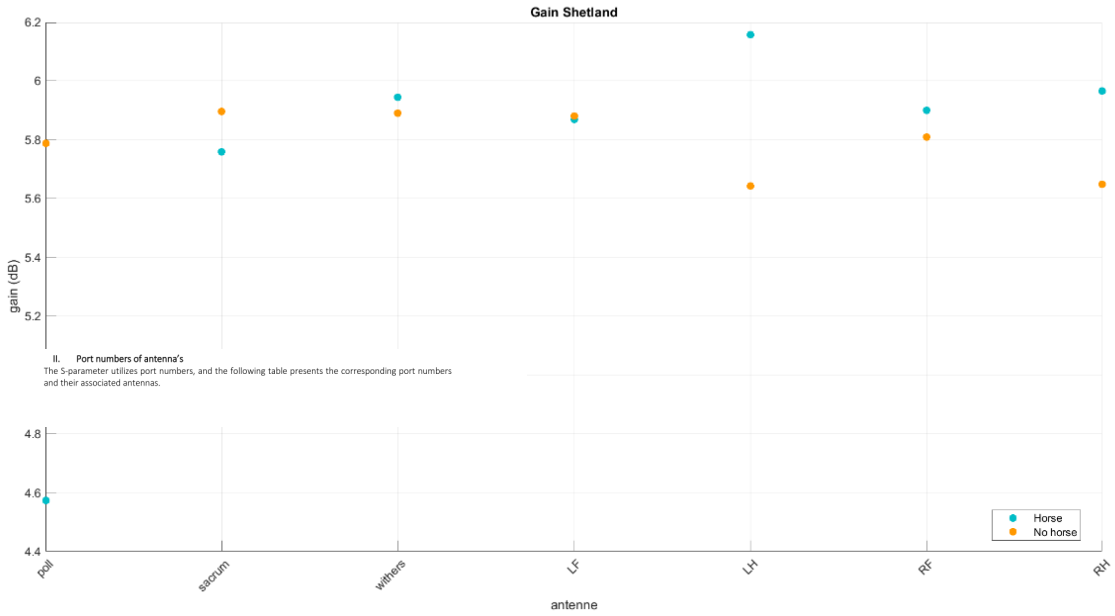

Figure 3 Gain with or without Shetland

II. Port numbers of antenna's

The S-parameter utilizes port numbers, and the following table presents the corresponding port numbers and their associated antennas.

Table 4 Port number and antenna name

Port number	Antenna
1	poll
2	sacrum
3	withers
4	LF
5	LH
6	RH
7	RF

III. LOS and NLOS points

These tables show which connections have been considered LOS and NLOS. The numbers are once as shown in section II.

Table 5 (N)LOS paths

Sij		LOS	NLOS	Doubt
12	21	x		
13	31			x
14	41		x	
15	51		x	
16	61		x	
17	71		x	
23	32			x
24	42		x	
25	52		x	
26	62		x	
27	72		x	
34	43	x		
35	53	x		
36	63		x	
37	73		x	
45	54		x	
46	64			x
47	74			x
56	65			x
57	75			x
67	76		x	

IV. S-parameters

The s parameters are simulated wo times. First time with the horse and a second time without the horse but at the same distance as if they were on the horse. This gives the opportunity to compare the impact of the horse on the S parameters.

Selveryne

Table 6 S-parameters Selveryne

port	poll	sacrum	withers	LF	LH	RH	RF
poll	-21.7867	-41.9631	-45.7262	-70.0969	-59.3803	-59.7933	-72.317
sacrum	-41.9632	-21.0714	-38.3384	-59.33	-62.6097	-64.4987	-60.833
withers	-45.7261	-38.3383	-22.2374	-53.2319	-49.1161	-64.2887	-73.1857
LF	-70.0968	-59.3299	-53.2319	-21.0763	-40.5402	-45.8415	-42.3603
LH	-59.3802	-62.6096	-49.116	-40.5402	-23.0648	-45.0553	-42.8768
RH	-59.7932	-64.4985	-64.2887	-45.8415	-45.0554	-21.578	-41.0153
RF	-72.3169	-60.8329	-73.1857	-42.3603	-42.8768	-41.0154	-21.8971

Table 7 S-parameters Selveryne no horse

port	poll	sacrum	withers	LF	LH	RH	RF
poll	-20.596	-46.0889	-56.9252	-55.9341	-57.7608	-56.0875	-54.0837
sacrum	-46.089	-20.6421	-48.3651	-58.8565	-52.681	-53.8638	-56.1718
withers	-56.9251	-48.365	-22.1796	-43.9183	-50.2795	-48.8552	-53.2068
LF	-55.9339	-58.8563	-43.9182	-21.126	-38.4246	-54.8719	-51.9495
LH	-57.7607	-52.6807	-50.2794	-38.4246	-23.2394	-52.9665	-48.7793
RH	-56.0873	-53.8636	-48.8551	-54.872	-52.9665	-20.8062	-38.0747
RF	-54.0836	-56.1717	-53.2069	-51.9497	-48.7794	-38.0748	-22.2142

Falabella

Table 8 S-parameter Falabella

port		poll	sacrum	withers	LF	LH	RH	RF
poll		-18.60	-43.43	-51.85	-83.38	-71.58	-70.44	-92.01
sacrum		-43.43	-22.64	-41.92	-68.42	-72.95	-70.76	-68.42
withers		-51.85	-41.92	-23.82	-63.04	-57.14	-70.24	-77.70
LF		-83.38	-68.42	-63.04	-23.63	-42.30	-46.45	-46.64
LH		-71.58	-72.95	-57.14	-42.30	-22.80	-47.98	-47.51
RH		-70.44	-70.76	-70.24	-46.45	-47.98	-23.55	-41.95
RF		-92.01	-68.42	-77.70	-46.64	-47.51	-41.95	-23.23
port		poll	sacrum	withers	LF	LH	RH	RF

Table 9 S-parameter Falabella no horse

port	poll	sacrum	withers	LF	LH	RH	RF
poll	-22.64	-49.69	-57.71	-56.44	-62.99	-59.82	-56.89
sacrum	-49.69	-22.79	-51.46	-62.57	-57.63	-55.45	-58.66
withers	-57.71	-51.46	-21.93	-50.92	-52.71	-50.68	-53.47
LF	-56.44	-62.57	-50.92	-23.38	-40.15	-60.50	-52.02
LH	-62.99	-57.63	-52.71	-40.15	-22.53	-54.88	-51.91
RH	-59.82	-55.45	-50.68	-60.50	-54.88	-23.25	-41.10
RF	-56.89	-58.66	-53.47	-52.02	-51.91	-41.10	-22.71

Shetland

Table 10 S-parameter Shetland

port	poll	sacrum	withers	LF	LH	RH	RF
poll	-18.9733	-44.8083	-60.9119	-88.3373	-92.8322	-84.1041	-94.1448
sacrum	-44.8079	-21.9366	-45.8351	-80.3576	-80.6174	-75.6692	-79.846
withers	-60.9115	-45.8351	-23.2429	-87.7088	-77.9441	-89.8939	-93.0889
LF	-88.3368	-80.3575	-87.7087	-23.353	-42.0015	-53.6962	-47.9945
LH	-92.8319	-80.6175	-77.9441	-42.0016	-22.345	-52.3639	-53.5455
RH	-84.1036	-75.6692	-89.8938	-53.6963	-52.3637	-23.1477	-41.5897
RF	-94.1443	-79.8459	-93.0889	-47.9946	-53.5455	-41.5898	-23.1962
port	poll	sacrum	withers	LF	LH	RH	RF

Table 11 S-parameter Shetland no horse

port	poll	sacrum	withers	LF	LH	RH	RF
poll	-22.4168	-52.7278	-59.4557	-60.0441	-66.0431	-62.5961	-60.3912
sacrum	-52.7278	-22.4993	-55.996	-61.2651	-59.8905	-59.5577	-63.494
withers	-59.4559	-55.9961	-20.949	-54.5237	-53.119	-52.4043	-54.9468
LF	-60.0441	-61.265	-54.5235	-23.1083	-41.9783	-63.7027	-54.2862
LH	-66.0431	-59.8905	-53.1189	-41.9784	-22.5742	-56.4561	-54.253
RH	-62.5961	-59.5577	-52.4041	-63.7027	-56.456	-22.5652	-42.8656
RF	-60.3913	-63.4941	-54.9467	-54.2863	-54.253	-42.8657	-22.3989

V. Distances between antennas

Table 12 Distance between antenna's Selveryne

Port number		distance (mm)	distance (m)
12	21	485.819	0.485819
13	31	305.857	0.305857
14	41	644.624	0.644624
15	51	825.928	0.825928
16	61	833.972	0.833972
17	71	638.571	0.638571
23	32	308.104	0.308104
24	42	562.276	0.562276
25	52	435.362	0.435362
26	62	453.323	0.453323
27	72	562.517	0.562517
34	43	389.667	0.389667
35	53	536.935	0.536935
36	63	572.548	0.572548
37	73	420.195	0.420195
45	54	452.758	0.452758
46	64	472.064	0.472064
47	74	152.153	0.152153
56	65	176.837	0.176837
57	75	485.748	0.485748

Table 13 Distance between antenna's Falabella

Port number		distance (mm)	distance (m)
12	21	705.434	0.705434
13	31	404.565	0.404565
14	41	920.479	0.920479
15	51	1178.878	1.178878
16	61	1193.565	1.193565
17	71	924.161	0.924161
23	32	438.236	0.438236
24	42	811.283	0.811283
25	52	627.109	0.627109
26	62	650.11	0.65011
27	72	817.306	0.817306
34	43	594.647	0.594647
35	53	787.893	0.787893
36	63	837.102	0.837102
37	73	637.259	0.637259
45	54	632.454	0.632454
46	64	670.216	0.670216
47	74	204.873	0.204873
56	65	247.513	0.247513
57	75	672.201	0.672201
67	76	632.318	0.632318

Table 14 Distance between antenna's Shetland

Port number		distance (mm)	distance (m)
12	21	932.836	0.932836
13	31	529.769	0.529769
14	41	1209.132	1.209132
15	51	1532.901	1.532901
16	61	1559.256	1.559256
17	71	1200.372	1.200372
23	32	599.994	0.599994
24	42	1075.563	1.075563
25	52	817.888	0.817888
26	62	849.58	0.84958
27	72	1065.898	1.065898
34	43	771.468	0.771468
35	53	1022.25	1.02225
36	63	1092.607	1.092607
37	73	813.595	0.813595
45	54	816.709	0.816709
46	64	869.022	0.869022
47	74	272.195	0.272195
56	65	324.254	0.324254
57	75	865.951	0.865951
67	76	814.4	0.8144

Table 15 Distance between antenna's Quarter

Port number		distance (mm)	distance (m)
12	21	1382.562	1.382562
13	31	862.712	0.862712
14	41	1918.495	1.918495
15	51	2460.657	2.460657
16	61	2458.139	2.458139
17	71	1916.182	1.916182
23	32	846.31	0.84631
24	42	1667.251	1.667251
25	52	1363.563	1.363563
26	62	1366.068	1.366068
27	72	1674.284	1.674284
34	43	1207.773	1.207773
35	53	1625.491	1.625491
36	63	1029.275	1.029275
37	73	1282.899	1.282899
45	54	1222.888	1.222888
46	64	1389.748	1.389748
47	74	406.08	0.40608
56	65	512.084	0.512084
57	75	1401.151	1.401151
67	76	1321.799	1.321799

Table 16 Distance antenna's Shire

Port number		distance (mm)	distance (m)
12	21	1614.824	1.614824
13	31	1016.256	1.016256
14	41	2251.239	2.251239
15	51	2883.426	2.883426
16	61	2881.006	2.881006
17	71	2252.173	2.252173
23	32	990.713	0.990713
24	42	1956.126	1.956126
25	52	1602.699	1.602699
26	62	1602.609	1.602609
27	72	1959.144	1.959144
34	43	1413.541	1.413541
35	53	1901.179	1.901179
36	63	1982.509	1.982509
37	73	1503.49	1.50349
45	54	1540.716	1.540716
46	64	1630.148	1.630148
47	74	474.932	0.474932
56	65	593.645	0.593645
57	75	1629.868	1.629868
67	76	1541.488	1.541488